

WRDC-TR-89-2139

AD-A221 673



DEVELOPMENT OF A MATHEMATICAL MODEL FOR THE
THERMAL DECOMPOSITION OF AVIATION FUELS

John L. Krazinski and S. P. Vanka
Materials and Components Technology Division
Argonne National Laboratory
9700 South Cass Avenue
Argonne, Illinois 60439

DECEMBER 1989

FINAL REPORT for period Sept 88 - Dec 89

Approved for public release; distribution unlimited.

AERO PROPULSION AND POWER LABORATORY
WRIGHT RESEARCH DEVELOPMENT CENTER
AIR FORCE SYSTEMS COMMAND
WRIGHT-PATTERSON AIR FORCE BASE, OHIO 45433-6563

NOTICE

When Government drawings, specifications, or other data are used for any purpose other than in connection with a definitely Government-related procurement, the United States Government incurs no responsibility or any obligation whatsoever. The fact that the government may have formulated or in any way supplied the said drawings, specifications, or other data, is not to be regarded by implication, or otherwise in any manner construed, as licensing the holder, or any other person or corporation; or as conveying any rights or permission to manufacture, use, or sell any patented invention that may in any way be related thereto.

This report is releasable to the National Technical Information Service (NTIS). At NTIS, it will be available to the general public, including foreign nations.

This technical report has been reviewed and is approved for publication.

WILLIAM E. HARRISON III

WILLIAM E. HARRISON III
Fuels Branch
Fuels and Lubrication Division
Aero Propulsion and Power Laboratory

FOR THE COMMANDER

CHARLES L. DELANEY

CHARLES L. DELANEY, Chief
Fuels Branch
Fuels and Lubrication Division
Aero Propulsion and Power Laboratory



LEO S. HAROOTYAN, JR., Assistant Chief
Fuels and Lubrication Division
Aero Propulsion and Power Laboratory

If your address has changed, if you wish to be removed from our mailing list, or if the addressee is no longer employed by your organization please notify WRAC/POSH WPAFB, OH 45433-6563 to help us maintain a current mailing list.

Copies of this report should not be returned unless return is required by security considerations, contractual obligations, or notice on a specific document.

DISCLAIMER

This report was prepared as an account of work sponsored by the United States Government. Neither the United States nor any agency thereof, nor any of their employees, makes any warranty, expressed or implied, or assumes any legal liability or responsibility for accuracy, completeness, or usefulness of any information, apparatus, product, or process disclosed, or represents that its use would not infringe privately owned rights. References herein to any specific commercial product, process or service by trade name, mark, manufacturer, or otherwise, does not necessarily constitute or imply its endorsement, recommendation, or favoring by the United States Government or any agency thereof. The views and opinions of the authors expressed herein do not necessarily state or reflect those of the United States Government or any agency thereof.

Accession For	
NTIS GRA&I	<input checked="" type="checkbox"/>
DTIC TAB	<input type="checkbox"/>
Unannounced	<input type="checkbox"/>
Justification	
By _____	
Distribution/	
Availability Codes	
Dist	1
A-1	



Unclassified

SECURITY CLASSIFICATION OF THIS PAGE

Form Approved
OMB No 0704-0188

REPORT DOCUMENTATION PAGE

1a REPORT SECURITY CLASSIFICATION Unclassified		1b RESTRICTIVE MARKINGS None	
2a SECURITY CLASSIFICATION AUTHORITY N/A		3 DISTRIBUTION/AVAILABILITY OF REPORT Approved for Public Release; Distribution Unlimited	
2b DECLASSIFICATION/DOWNGRADING SCHEDULE N/A		4 PERFORMING ORGANIZATION REPORT NUMBER(S) N/A	
5 MONITORING ORGANIZATION REPORT NUMBER(S) WRDC-TR-89-2139		6a NAME OF PERFORMING ORGANIZATION Argonne National Laboratory	
6b OFFICE SYMBOL (If applicable) N/A		7a NAME OF MONITORING ORGANIZATION Wright Research and Development Center Aero Propulsion and Power Laboratory (WRDC/POSL)	
6c ADDRESS (City, State, and ZIP Code) 9700 South Cass Avenue Argonne, IL 60439		7b ADDRESS (City, State, and ZIP Code) Wright-Patterson AFB, OH 45433-6563	
8a NAME OF FUNDING/SPONSORING ORGANIZATION		8b OFFICE SYMBOL (If applicable)	
8c ADDRESS (City, State, and ZIP Code)		9 PROCUREMENT INSTRUMENT IDENTIFICATION NUMBER FY 1455-86-N0657	
10 SOURCE OF FUNDING NUMBERS		11 TITLE (Include Security Classification) Development of a Mathematical Model for the Thermal Decomposition of Aviation Fuels	
12 PERSONAL AUTHOR(S) J. L. Krazinski, S. P. Vanka		13a TYPE OF REPORT Final	
13b TIME COVERED FROM Sept. 88 TO Dec. 89		14. DATE OF REPORT (Year, Month, Day) 1989 December	
15. PAGE COUNT 126		16. SUPPLEMENTARY NOTATION <i>Deposit Removal Mechanism (JC)</i>	
17. COSATI CODES		18. SUBJECT TERMS (Continue on reverse if necessary and identify by block number) Aviation Fuels, Computational Fluid Dynamics, Deposit Formation, Fouling, JP-5, Mathematical Model, Thermal Decomposition, Thermal Stability,	
19. ABSTRACT (Continue on reverse if necessary and identify by block number) This report describes the development of a mathematical model for predicting the rate of thermal decomposition of aviation fuels. The model provides a global description of the chemical and physical processes of fuel autoxidation, precursor formation, and deposition at a solid surface. The model contains several unknown parameters that must be determined for a particular fuel. Calibration of the model involves the determination of these parameters from experimental data. This report describes the calibration procedure and presents sample calculations from the calibrated model for both laminar and turbulent flows.			
20. DISTRIBUTION/AVAILABILITY OF ABSTRACT <input checked="" type="checkbox"/> UNCLASSIFIED/UNLIMITED <input type="checkbox"/> SAME AS RPT <input type="checkbox"/> DTIC USERS		21. ABSTRACT SECURITY CLASSIFICATION Unclassified	
22a NAME OF RESPONSIBLE INDIVIDUAL William E. Harrison III		22b TELEPHONE (Include Area Code) 513-255-6601	
22c OFFICE SYMBOL WRDC/POSL		23. SECURITY CLASSIFICATION OF THIS PAGE Unclassified	

Block 19. ABSTRACT (Contd.)

The model described in the report assumes that deposits are formed as a result of two types of reactions: a heterogeneous wall reaction that occurs only at the fuel/solid interface, and homogeneous reactions that occur in the bulk fluid. The heterogeneous reaction is assumed to produce deposits directly on the solid surface. The homogeneous reaction is assumed to be a one-step, autoxidation reaction that produces deposit-forming species which are then transported to the wall by convection and diffusion. Transport equations were developed for both dissolved oxygen and the deposit-forming species (deposit precursors) formed from the bulk fuel reaction. These equations were incorporated into an existing computer code originally developed for the calculation of multidimensional, reactive fluid flows. The two-dimensional code solves the transport equations simultaneously with the continuity, momentum, and energy equations.

An accurate determination of the unknown parameters in the model requires a series of well-controlled experiments that can effectively isolate the fuel chemistry, transport processes, and surface phenomena occurring in the overall decomposition/ deposition process. Since such data were not found in the literature, results from heated-tube experiments were used to calibrate the model. The report describes the calibration procedure for JP-5 fuel and presents several parametric studies that illustrate the sensitivity of the calculations to the model parameters. The predictive capabilities of the calibrated model are examined by a comparison with different sets of data for JP-5. The report also discusses additional experiments that are recommended to better understand the mechanisms of fuel decomposition and provide further input into the model.

TABLE OF CONTENTS

<u>Section</u>		<u>Page</u>
	FOREWORD	vii
	ACKNOWLEDGMENTS	viii
1.0	INTRODUCTION	1
2.0	REVIEW OF THE LITERATURE	4
2.1	Fuel Chemistry	4
2.2	Transport Processes	7
2.3	Surface Adhesion	9
2.4	Deposit-Removal Mechanisms	11
3.0	DEVELOPMENT OF A MATHEMATICAL FRAMEWORK FOR FUEL DECOMPOSITION AND WALL DEPOSITION	17
4.0	CURRENT DATA BASE FOR AVIATION FUEL DECOMPOSITION	32
5.0	SOLUTION APPROACH AND RESULTS FROM THE PRESENT STUDY ...	50
5.1	Calibration of the Model for JP-5 Fuel	50
5.2	Sample Calculations With the Calibrated Model	73
5.3	Sample Variable Profiles for Pipe Flow	86
5.4	Modification of the Chemical Kinetics Model	96
6.0	PROPOSED EXPERIMENTS TO SUPPORT FURTHER MODEL DEVELOPMENT	108
7.0	CONCLUSIONS AND RECOMMENDATIONS	112
8.0	REFERENCES	114

LIST OF FIGURES

No		Page
2.1	Characteristic Fouling Curves.....	13
3.1	JP-5 Enthalpy.....	25
3.2	JP-5 Density.....	26
3.3	JP-5 Viscosity	27
3.4	JP-5 Prandtl number.....	28
3.5	Self-Diffusion Coefficients for n-Paraffins.....	31
4.1	Average Deposition Rates of Four Test Fuels.....	40
5.1	Comparison of Predicted Temperature Profiles With Data for a Fuel Velocity of 2.1 m/s and Max T _{wall} = 589 K.....	55
5.2	Comparison of Predicted Temperature Profiles With Data for a Fuel Velocity of 2.1 m/s and Max T _{wall} = 672 K.....	56
5.3	Arrhenius Plot of JP-5 Deposition Rates for a Fuel Velocity of 2.1 m/s.....	57
5.4	Initial Calibration of the Chemistry Model.....	58
5.5	Effect of the Diffusion Coefficient on the Predicted Deposition Rates.....	64
5.6	Effect of the Wall Parameter K on the Predicted Deposition Rates.....	67
5.7	Comparison of the Parameters K and DPFRAC on the Predicted Deposition Rates.....	69
5.8	Effect of the Parameter DPFRAC on the Predicted Deposition Rates.....	71
5.9	Effect of the Preexponential Constant for the Bulk Reaction on the Predicted Deposition Rates.....	72
5.10	Comparison of Predicted Temperature Profiles With Data for a Fuel Velocity of 0.3 m/s and Max T _{wall} = 589 K.....	75
5.11	Comparison of the Calibrated Model With the Data of Marteney and Spadaccini for a Fuel Velocity of 0.3 m/s.....	76
5.12	Comparison of the Calibrated Model With Deposition Data for a Fuel Velocity of 0.076 m/s.....	78
5.13	Prediction of the Dissolved-Oxygen Concentration in Heated-Tube Tests.....	79

LIST OF FIGURES (Continued)

<u>No</u>		<u>Page</u>
5.14	Comparison of Enthalpy Curve-Fits for JP-5	81
5.15	Comparison of Density Curve-Fits for JP-5.....	82
5.16	Comparison of Predicted Temperature Profiles With the Data of TeVelde and Glickstein.....	84
5.17	Comparison of the Calibrated Model With the Data of TeVelde and Glickstein for a Fuel Velocity of 2.57 m/s.....	85
5.18	Predicted Temperature Profiles for Laminar Flow.....	87
5.19	Predicted Oxygen Profiles for Laminar Flow.....	88
5.20	Predicted Deposit Precursor Profiles for Laminar Flow.....	89
5.21	Predicted Temperature Profiles.....	91
5.22	Predicted Oxygen Profiles	92
5.23	Predicted Deposit Precursor Profiles.....	93
5.24	Predicted Axial Wall and Bulk Fuel Temperatures	94
5.25	Predicted Deposition Rates	95
5.26	Calibration of the Autoxidation Reaction for a Fuel Velocity of 0.076 m/s.....	99
5.27	Prediction of the Dissolved-Oxygen Concentration With the Modified Model for a Fuel Velocity of 0.076 m/s.....	100
5.28	Calibration of the Precursor Decomposition Reaction for a Fuel Velocity of 0.076 m/s	102
5.29	Calibration of the Precursor Decomposition Reaction for a Fuel Velocity of 2.1 m/s	103
5.30	Effect of the Wall and Bulk Reactions on the Predicted Deposition Rates for a Fuel Velocity of 2.1 m/s.....	104
5.31	Comparison of the Modified Calibrated Model With Deposition Data for a Fuel Velocity of 0.3 m/s.....	105
5.32	Comparison of the Modified Calibrated Model With Deposition Data for a Fuel Velocity of 2.57 m/s.....	107

LIST OF TABLES

<u>No</u>		<u>Page</u>
4.1	Some Thermal Stability Tests Performed With Aviation Fuels.....	35
4.2	Global Activation Energies for Deposit Formation.....	42
5.1	Test Matrix for JP-5 Fuel.....	51
5.2	Selected Properties of JP-5 Test Fuel	52
5.3	Comparison of Code Results With Mass Transfer Correlation of Harriott and Hamilton.....	61
5.4	Comparison of Diffusion Coefficients for Molecules and Particles.....	63

FOREWORD

In September 1986, the Fuels Branch of the Aero Propulsion and Power Laboratory at Wright-Patterson Air Force Base, Ohio, commenced an investigation of the potential for production of jet fuels from the liquid by-product streams produced by the gasification of lignite at the Great Plains Gasification Plant located in Beulah, North Dakota. Funding was provided to the U.S. Department of Energy (DOE), Pittsburgh Energy Technology Center (PETC), to administer the experimental portion of this effort. This report details the efforts of Argonne National Laboratory (ANL), which as a contractor to DOE (DOE Contract Number FWP 49444), developed and tested computational fluid dynamic models which incorporate preliminary fuel thermal degradation chemistry models. DOE/PETC was funded through Military Interdepartmental Purchase Request (MIPR) FY1455-86-NO657. Mr. William E. Harrison III was the Air Force program manager, Mr. Nand Narain was the DOE/PETC program manager, and Mr. John Krazinski was the Argonne program manager. The effort ended December 1989.

ACKNOWLEDGMENTS

This project was jointly supported by the U.S. Department of Energy, Pittsburgh Energy Technology Center, and the WRDC/Aero Propulsion and Power Laboratory, Wright-Patterson AFB. The authors wish to express their appreciation to Messrs. G. J. Stiegel and N. K. Narain (Pittsburgh Energy Technology Center) and Mr. W. E. Harrison III (WRDC/Aero Propulsion and Power Laboratory) for their support of this effort. The authors would also like to acknowledge Messrs. W. M. Roquemore and J. A. Pearce (WRDC/Aero Propulsion and Power Laboratory) for their technical input and guidance throughout the course of this study. The authors wish to thank Dr. A. S. Nejad (Advanced Propulsion Division of the WRDC/Aero Propulsion and Power Laboratory) for providing the source code of FLANELS-2D, an unreleased computational fluid dynamics computer code that served as the base for the thermal decomposition model. In addition, the authors would like to express their gratitude to Messrs. P. J. Marteney and L. J. Spadaccini (United Technologies Research Center) for providing the data used in the model calibration and for their many useful discussions. The authors also appreciate the assistance of Ms. Verna M. Stainback in the preparation of the manuscript.

1.0 INTRODUCTION

The stability of an aviation fuel is a key consideration in the design of aircraft fuel systems. Aviation fuels can decompose both during storage and during exposure to elevated temperatures in the fuel system. The decomposition products include soluble gums as well as insoluble materials that can deposit on heat-transfer surfaces, obstruct valves and filters in the fuel line, and degrade the performance of injection nozzles. The expected increase in the thermal loadings of high-performance aircraft, in which some surfaces are cooled by the fuel, will require a careful design of the fuel system to prevent exposure of the fuel to excessively high temperatures. Because of uncertainty over the quality and composition of future aircraft fuels, including alternative fuels such as coal-derived liquids, a better understanding is needed of those fuel constituents that contribute to fuel breakdown. For example, fuel impurities such as sulfur or metals, whose concentration tends to be higher in alternative, lower-quality fuels than in currently available fuels such as JP-5, can often enhance the degradation process.

Although the thermal stability of hydrocarbon fuels has been studied over a long period of time, the degradation process is complex and not well understood. Some factors that affect the fuel decomposition rate include the temperature-time history, the system pressure and flow field, the fuel composition, the concentration of dissolved air and contaminants, and the nature of the solid surfaces in the fuel system. Various tests have been conducted in an effort to quantify the rate of thermal decomposition for selected fuels. These tests typically subject the fuel to a constant heat flux for a specified period of time. The fuel and the test apparatus are then examined to assess the rate of decomposition. Such tests provide global information on fuel decomposition rates, rather than more detailed data on the fundamental mechanisms of the decomposition process. In addition, aircraft fuel systems are quite complicated with both fuel flows and heat fluxes varying over time. Consequently, it is difficult to extrapolate the available experimental results to the actual operating environment of an aircraft fuel system.

Fuel decomposition and deposit formation are complex physicochemical processes that include the individual steps of precursor or gum formation, transport of precursor materials to solid surfaces, adhesion to either a solid (metal) surface or to an existing deposit layer, and possible deposit removal followed by convection to downstream components in the fuel system. Each of these steps, in turn, can occur by a number of different mechanisms. The chemical reactions leading to gum formation depend on temperature, pressure, concentration of air dissolved in the fuel, and the concentration of fuel impurities (e.g., sulfur, metals, etc.). Although aviation fuel undergoes autoxidation reactions at lower temperatures, the fuel can also decompose by pyrolysis if the temperature becomes sufficiently high. Very small

concentrations of impurities such as copper, when present at the parts-per-million level or less, can accelerate the rate of decomposition by orders of magnitude.

The possible modes of transport of deposit precursors or particles to a surface include diffusion (laminar or turbulent), impaction, sedimentation, and thermophoresis. Once transported to a surface, a particle may or may not adhere depending upon the surface geometry (smooth wall or irregular deposit), surface stickiness, and the electrochemical forces between the particle and the surface. The surface material can play a role in any chemical reactions that occur on the surface. Sections of a deposited layer may also be removed by erosion (shear) or turbulent bursts, for example, resulting in possible redeposition or clogging at other locations in the fuel system.

Our current understanding of the overall fuel decomposition problem is limited by a lack of clear experimental data on the fundamental mechanisms of the process. The available mathematical models of thermal decomposition and particle deposition typically contain unknown parameters whose values are adjusted by a comparison with specific sets of data. The applicability of these models to different fuels under various flow conditions remains unknown. There is a need for further experiments to isolate the individual processes of fuel decomposition and deposition and to provide information on the underlying mechanisms involved.

The objective of the present investigation is to initiate the development of a mathematical model that combines fluid mechanics, heat transfer, chemical kinetics, and the deposition mechanisms. It is intended that such a model will help provide a better understanding of the interaction between these individual elements of the fuel decomposition and surface deposition processes. In order to develop and validate the model, however, it is necessary to have data from carefully instrumented experiments that have isolated the different mechanisms in the overall process. To determine the adequacy of the available data, a literature search was initially conducted for this study. Section 2.0 contains a brief review of the literature on decomposition, fouling, fuel chemistry, and other related aspects of the overall problem. This section is followed by a description in Section 3.0 of a proposed mathematical model that attempts to combine these various aspects of fuel decomposition. The model contains several unknown parameters that must be determined by experiments. Section 4.0 describes the results from a number of thermal decomposition tests conducted with aviation fuels. These tests form the existing data base that was used to initially calibrate and

validate the model. Some calculated results from the model are presented and compared with experimental data in Section 5.0.

Although the current model is two-dimensional in nature, the existing data base consists primarily of results from one-dimensional flows in tubes and annuli. Before the model can be applied to more complicated geometries, initial calibration of the model in these one-dimensional flows is needed. However, the data base for flows even in these simple geometries is inadequate for validating and testing the proposed model of fuel decomposition. Therefore, Section 6.0 outlines a series of experiments that are needed to provide further input into the model beyond that available from current experimental data.

Finally, Section 7.0 provides a summary of the key conclusions from the present study.

2.0 REVIEW OF THE LITERATURE

The thermal decomposition of aviation fuel is a complex process involving a wide variety of both physical and chemical phenomena. Because of the multidisciplinary nature of the problem, literature from a variety of areas was reviewed to assess the relevance of existing analytical techniques and experimental data to fuel decomposition. The literature review included references on heat exchanger fouling, fuel chemistry, deposition of particles and aerosols, and the electrical interaction forces between particles and solid surfaces. References dealing directly with the thermal stability of jet fuels were also examined; this information is discussed in more detail in Section 4.0.

Because the existing literature on these subjects is quite extensive, a complete review was beyond the scope of the present study. The number of references on heat exchanger fouling alone is too vast to cover here [1] and earlier reviews on the subject are available [2]. The Coordinating Research Council reviewed the available literature on the thermal stability of jet fuel in 1979 [3]. Although additional work on the subject has been conducted during the past 10 years, much uncertainty about the problem still remains. The objective of this review is to obtain pertinent information from the literature to (1) provide a foundation for an initial mathematical model and (2) identify additional experiments that are needed to supplement the existing data base. For the purposes of this discussion, thermal decomposition and deposition will be divided into four areas: fuel chemistry, transport processes, surface adhesion, and deposit-removal mechanisms. These areas are discussed in the following subsections.

2.1 Fuel Chemistry

Thermal decomposition of aviation fuels involves a complex series of chemical reactions. Some of the earlier work investigating the chemistry of fuel decomposition and deposit formation was performed by Taylor [4-6] and Hazlett [7,8]. Taylor and his co-workers conducted a series of experiments to identify the key factors affecting the rate of deposit formation. A series of experimental devices were constructed in which fuels were passed over heated surfaces for periods of up to 4 h. Upon completion of a test run, the apparatus was disassembled and the rate of deposition on the heated surface was determined for the test period. The variables investigated by Taylor included temperature, pressure, dissolved-oxygen content, and the levels of trace impurities such as sulfur compounds. The experiments were conducted with various jet fuels and with individual hydrocarbons (e.g., n-dodecane).

The jet fuel results showed that the exclusion of oxygen generally resulted in a dramatic reduction in deposit formation [4], although with one lower-quality fuel the reduction was

minimal [6]. The deposits appeared to form as a result of a complex, free radical autoxidation process that produced insoluble compounds that eventually formed solid deposits. Compared to the oxygen concentration, the rate of deposit formation was much less sensitive to the nature of the surface material (glass vs. stainless steel), although trace levels of sulfur compounds played an important role in initiating or catalyzing the deposition process.

Kinetic studies on pure hydrocarbons and hydrocarbon mixtures were also performed by Taylor [5]. The deposition behavior observed with the hydrocarbon mixtures was quite complex, compared with that of the individual hydrocarbon components. These differences lead to difficulties in extrapolating pure hydrocarbon data to the behavior of actual jet fuels. The effect of pressure on the deposition rates was also complex, lowering the amount of deposits for one fuel and having very little effect on another fuel [6]. For tests conducted at 7.0 MPa (69 atm), a pressure significantly above the critical pressure of 2.2 MPa (22 atm), the deposition rates exhibited a sharp drop above a certain temperature. This was attributed to the transition between the liquid phase and a supercritical vapor phase in which the deposition rates were presumed to be much lower.

Additional experiments on the thermal decomposition of jet fuels have been conducted by Hazlett and his co-workers [7,8]. A series of tests were performed with the normal alkane, n-dodecane. This compound was selected for study because it is a major component of JP-5 and Jet A fuels and, being a pure hydrocarbon, it simplifies the chemical analysis of the decomposition products. As discussed above, however, actual jet fuels are complex mixtures and the results from pure compound tests should be extrapolated cautiously.

The n-dodecane tests were conducted in the Jet Fuel Thermal Oxidation Tester (JFTOT) at a pressure of 5.52 MPa (800 psi) gage and tube temperatures between 464 K (375°F) and 811 K (1000°F). Three different heater materials were used: 316 stainless steel, 304 stainless steel, and 6061 aluminum. Tests were conducted with both aerated n-dodecane and oxygen-free liquid.

The initial decomposition product, dodecyl hydroperoxide, was stable up to 561 K (550°F), but decomposed into a variety of products at higher temperatures, reacting completely at 672 K (750°F). Dissolved oxygen significantly increased the rate of reaction at lower temperatures. At higher temperatures, the influence of oxygen was less significant, although at 811 K the decomposition product yields at the low oxygen level (0.04 mmol/L) were still only

~60% of the levels for air saturated dodecane (1.80 $\mu\text{mol/L}$ of oxygen). The type of metal did not significantly control either the type or the amount of product formation.

The reaction patterns observed in the tests were interpreted on the basis of two schemes: autoxidation and pyrolysis [7,8]. The autoxidation reactions controlled the decomposition rates below 533 K (500°F), whereas pyrolysis reactions predominated above 755 K (900°F). In the intermediate temperature regime 533–755 K, oxygenated products played an important role in deposit formation, but the reaction pathways were more complex. The Fabuss, Smith, and Satterfield one-step decomposition model for n-paraffins [9] applied very well to the n-dodecane pyrolysis results from Hazlett's experiments [8].

More recent work on the thermal stability of aviation fuels has also been reported [10–12]. Kendall and Mills found that additions of either copper or iron at levels of 20–40 $\mu\text{g/L}$ increased the oxidation rates of jet fuels, with copper having the greatest effect [10]. However, iron inhibited the effect of copper, lowering the oxidation rate obtained for copper alone. The dissolved copper appeared to increase the oxidation rate by increasing the rate of radical initiation.

Mayo and Lan investigated gum and deposit formation in both jet turbine and diesel fuels at 100°C and 130°C [11,12]. Their results provide good evidence that hard deposits on hot engine parts arise mainly from soluble gums in the fuel. Several mechanisms were proposed for the formation of soluble gums in air at temperatures up to 130°C [11]. However, the manner in which such gums are converted to hard deposits is still uncertain.

Although the major factors affecting the rate of fuel decomposition have been reasonably well identified, the detailed chemical reaction mechanism is not completely understood. Slight variations in the composition of a fuel can dramatically change its decomposition rate. The expected rate of decomposition of a new fuel under different conditions cannot be predicted *a priori* from its chemical composition. The ability to make such predictions will probably not be available in the foreseeable future. From a modeling perspective, a series of well-controlled chemistry experiments are needed whose data will allow the construction of relatively simple kinetic models that represent the decomposition process with reasonable accuracy. Models with a complexity on the order of the two-step [13] or four-step [14] reaction schemes for gaseous hydrocarbons would be appropriate as an initial description of the process. Such a simplified model could be readily incorporated into a

complex fluid mechanics computer code for analyzing both fuel decomposition and the precursor transport/deposition processes.

2.2 Transport Processes

Once deposit-forming species or deposit precursors have formed in the bulk fluid, they may be transported to a solid surface and accumulate as a layer of deposits. If the fuel decomposes in the tubes of a heat exchanger, for example, some of the precursors formed within the tubes may deposit on the tube walls. The remaining precursors would be carried out of the heat exchanger and could eventually form deposits in other components of the fuel system, such as the fuel nozzles. In order to predict where deposits will form in a fuel system, it is necessary to understand the mechanisms by which deposit precursors can be transported from the bulk fluid to a solid surface.

Particles in a fluid can be transported to a solid surface by a number of different mechanisms, including diffusion, electrostatic or thermal forces, inertial impaction, and gravitational settling [15]. For pipe flow, gravitational settling becomes more important as the particle size increases and/or the flow velocity decreases. Inertial impaction can occur with larger particles which may not follow the fluid streamlines when the flow changes direction. An example would be flow of a dust-laden gas stream around a cylinder, where some of the dust particles may diverge from the gas streamlines near the cylinder and impact on the solid surface [16]. Particles can also deposit by thermophoretic forces resulting from a temperature gradient in the fluid [17]. This force is in the direction of decreasing temperature and results from the fact that molecules colliding with the particle from opposite directions have different average velocities because of the temperature gradient. Thermophoresis plays an important role in the deposition of particles on cooled turbine blades [18]. In addition to the above effects, electrical interaction forces become more important as particles approach a solid surface [19,20].

Deposit precursors can also be transported to the walls by diffusion. The mechanism of diffusional transport depends upon whether the flow is laminar or turbulent. In fully developed laminar pipe flow, particles would be transported to a wall by molecular or Brownian diffusion. In turbulent flow, this process would be augmented by turbulent diffusion. The effective diffusion coefficient then becomes the sum of the molecular diffusion coefficient (D) and an eddy diffusion coefficient (ϵ). For fully developed turbulent pipe flow, Davies developed an empirical expression for ϵ/v (where v is the kinematic viscosity) as a function of

the pipe Reynolds number and the distance from the pipe wall [21]. Except for the region very close to the wall, ϵ is typically much larger than D [16].

Particle deposition onto a surface is often described in terms of a deposition velocity or a deposition coefficient, defined as [22,23]

$$K = \frac{\text{Particle flux deposited onto the solid surface}}{\text{Particle concentration above the surface}}.$$

Sehmel, who examined the turbulent deposition of aerosol particles from an air stream, used the particle concentration located at 1 cm above the surface in the above expression for K [22]. This reference height was selected since it was the closest position to the surface at which the particle concentration was measured. For channel or pipe flow, Beal used the average (bulk) particle concentration [23]. The parameter K includes the net effect of all the interaction forces between a wall (or deposited layer) and an approaching particle.

Beal developed equations for predicting particle deposition in turbulent pipe or channel flows, including the effects of molecular (Brownian) diffusion, turbulent diffusion, and particle inertia [23]. Beal used expressions from Lin et al. [24] for the turbulent diffusivity, ϵ , and incorporated the stopping distance concept of Friedlander and Johnstone [25] into his model. This concept presumes that particles need only diffuse to within a certain distance from the wall (the stopping distance), at which point they will coast to the wall by virtue of their momentum. The particle's momentum at the stopping distance is thus large enough to overcome the drag force exerted by the surrounding fluid.

By including both diffusional and inertial effects, Beal's model predicts a particle size at which the deposition coefficient will be a minimum. This particle diameter varies from ~ 2.0 μm at an average fluid velocity of 0.3 m/s to ~ 0.2 μm at an average fluid velocity of 10.0 m/s. For particle sizes below these critical values, the rate of deposition is diffusion controlled and thus decreases with increasing particle sizes. For particles larger than the critical value, momentum effects become more important and the deposition rate increases with increasing particle size. When the particle size becomes large enough that the stopping distance exceeds the boundary layer thickness, the particle size no longer has any effect on the transport rate and the model predicts a constant deposition coefficient for a given average fluid velocity.

Beal compared his model with experimental data covering a wide range of conditions, including particle diameters from $\sim 10^{-3}$ μm (benzoic acid molecules) to 30 μm (lycopodium

spheres), velocities from 0.3–61.0 m/s (1–200 ft/s), and Reynolds numbers from 3×10^3 to 1×10^5 [23]. In all cases it was assumed that every particle reaching the stopping distance adhered to the wall. Fairly good agreement was achieved in most cases, although scatter in some of the data made comparisons with the model difficult. In other cases the agreement was not as good. The reasons for this were not clear, although particle re-entrainment (which was not included in the model) was cited as a possible cause.

If the deposit precursors that formed during the decomposition of aviation fuel are presumed to be molecular in size, then the primary mode of transport from the bulk fluid to the tube wall would be by laminar or turbulent diffusion. In order to model this process, values for the diffusion coefficient (D) and the eddy diffusivity (ϵ) are needed. The diffusion coefficients for liquids are much smaller than the values for low-pressure gases, since molecules in a liquid are in closer proximity and thus more strongly influenced by the force fields from their neighbors. For example, diffusion coefficients for organic liquids at infinite dilution are typically on the order of $10^{-8} - 10^{-9}$ m²/s at room temperature [26], compared with values of $10^{-4} - 10^{-5}$ m²/s for gases at low pressures. These small diffusivities result in very thin concentration boundary layers, even for laminar flow. The ability to resolve these thin boundary layers near a solid surface may be very important in the development of an analytical model for predicting deposition rates.

2.3 Surface Adhesion

After a particle has been transported to a surface, it may adhere to that surface and form a deposit. The mechanisms of particle adhesion will depend upon the characteristics of the surface, as well as the interaction forces between the surface and the approaching particle. These forces can also change with time as a deposited layer builds up, so that approaching particles no longer encounter a bare wall but rather an established layer of deposits. Once a particle has reached the wall, it may or may not stick. Chemical reactions could also be occurring in conjunction with the adhesion process, possibly changing the deposit characteristics over time (e.g., increasing the strength of the deposit).

Most previous research on particle deposition has focused on transport processes, with less attention being given to the actual adhesion process. One approach to analyzing adhesion involves modeling the interaction forces between a solid surface and an approaching particle [27,28]. Such a model treats particle deposition as a combination of mass transfer in the bulk fluid with a first-order reaction at the walls. The surface interactions are assumed to be limited to a very narrow region near the wall and include the effects of London-van der Waals,

electrical double-layer, and hydrodynamic interaction forces. These forces are included in a surface rate constant, K_1 , which has units of velocity [27]. The limit $K_1 \rightarrow \infty$ corresponds to an infinite sink wall boundary condition, in which the rate of deposition is controlled by mass transfer in the fluid. As K_1 becomes smaller, the deposition rate is increasingly controlled by surface interactions. The model presented in Refs. 27 and 28 is only applicable to the initial rate of deposition, when surface coverage by the deposited particles is negligible.

The above model was compared with deposition data for laminar flow in a smooth parallel-plate channel [28]. In the experiment, a suspension containing silica spheres with an average particle diameter of $\sim 0.5 \mu\text{m}$ flowed through a channel in which the particles could deposit on the walls but did not chemically interact. The particles were radioactively tagged and their accumulation on the wall was monitored by a collimated detector. The test section was constructed of plastic-coated glass plates, whereas most of the loop components were Teflon, a surface on which the particles showed little tendency to deposit. Two sets of experiments were conducted. In the first set, negatively charged particles were deposited onto a positively charged substrate. In this case the deposition rate was controlled by mass transfer and the model predictions with $K_1 = \infty$ showed good agreement with the data. In the second set of experiments, negatively charged particles were deposited onto a negatively charged substrate. Here the deposition rate was controlled by surface interactions (a finite value of K_1). Although the model provided a qualitative description of the experimental results, the quantitative agreement was poor, with the predicted deposition rates being orders of magnitude lower than the measured values [28]. The discrepancy was attributed to uncertainties in the values of K_1 , the surface reaction rate constant. In particular, the model did not account for small-scale heterogeneities on the surface where preferential deposition might occur much more rapidly than predicted, because of locally favorable conditions not considered in the model. Other experiments have shown that a range of forces was required to remove deposited particles from a surface, providing some evidence for the existence of such local surface heterogeneities [29].

Because of uncertainties in the mechanisms of surface adhesion, global parameters have previously been used to account for the interaction between a surface and an approaching particle. One such parameter is the sticking probability or the probability that a particle approaching a solid surface will actually adhere to that surface. Beal attributed the discrepancies between his predicted deposition coefficients and the observed values for turbulent flow as being largely due to the failure of some particles to stick to the wall [30]. His model, which originally assumed that all particles stuck to the wall (sticking probability of

100%), overpredicted the deposition coefficients for cases involving larger particles and higher fluid velocities. Beal used the differences between the predicted and observed deposition coefficients to calculate values for the sticking probability. The magnitudes of the sticking probabilities ranged from below 10^{-4} to greater than 1. Since sticking probabilities of greater than 1 are physically unrealistic, a maximum value of 1 was imposed on the calculated values. It was unclear whether the unrealistically high calculated sticking probabilities resulted from inadequacies in the model, experimental uncertainties, or both.

The effect of surface roughness on particle deposition has also been investigated. For turbulent flow the predicted deposition rates were found to be very sensitive to the surface roughness, even for roughness values that were too small to produce aerodynamically rough flow [31]. In initially comparing his model predictions for smooth tubes with the experimental results of Montgomery and Corn [32], Browne found that his predicted deposition rates were too low by a factor of 1000 [31]. For a pipe of diameter D , equivalent surface roughness κ , and roughness ratio κ/D of 0.0001, however, reasonable agreement was obtained, even though there are very small differences between the Fanning friction factors for $\kappa/D = 0.0$ (smooth pipe) and $\kappa/D = 0.0001$ over the Reynolds number range of 5.0×10^4 to 4.0×10^5 covered in the experiments. For particle diameters less than about $5 \mu\text{m}$, such as those used by Montgomery and Corn [32], the higher deposition velocities obtained for slightly rough surfaces were presumed to result from the larger capture distances compared with those for smooth surfaces.

The above results indicate that although some models have been developed for particle adhesion, much uncertainty about the process still remains. Although the models have achieved reasonable agreement with some limited sets of data, poor agreement is obtained in other cases. The adhesion process involves complex physical and possibly chemical interactions between a surface and an approaching particle. The nature of these interactions may also change with time as a deposited layer builds up. A surface which is initially very smooth, for example, could become quite rough as deposits accumulate with time, thereby possibly changing the deposition rate. If deposition rates are very sensitive to changes in the surface conditions, the development of a reliable model that can adequately predict these effects will be very difficult.

2.4 Deposit-Removal Mechanisms

As deposits accumulate on a solid surface, parts of the deposited layer may be removed and convected downstream. This material can then redeposit at another location in the fuel system or possibly clog small passages such as fuel nozzles. The ease of removal of an existing

deposit will depend upon the strength of adherence of the deposited layer and the characteristics of the flow field. Much less work has been done on deposit-removal mechanisms than on the processes of deposit formation. Deposit removal could involve either re-entrainment of individual particles or fragmentation and removal of large chunks of material. Possible deposit-removal mechanisms are briefly discussed in this section.

The existing body of literature on the fouling of heat exchangers is considerable [1]. Typical fouling curves are shown in Fig. 2.1. After an initiation or delay period in which little fouling occurs, deposits start to accumulate on the wall and the resistance to heat transfer increases. Heat exchangers in the chemical process industry have typically been designed by using a global parameter called the fouling factor, which accounts for the added resistance to heat transfer caused by the accumulated deposits [33]. Fouling curves have often been observed to follow the asymptotic path shown in Fig. 2.1, in which the heat-transfer resistance of the deposited layer reaches a maximum value and then levels off. This behavior has typically been described by postulating the existence of a removal mechanism whose rate eventually balances the rate of deposition. During the initial build-up of the deposited layer, the deposition rate exceeds the removal rate and thus the fouling resistance increases.

The earliest mathematical model of heat exchanger fouling cited in the literature [2] is that of McCabe and Robinson [34]. Many years later, Kern and Seaton developed a second fouling model, including terms for both deposit formation and its rate of removal [35]. They based their removal model on the observation that fouled heat exchangers could at least be partially cleaned by temporarily increasing the fluid velocity. This suggested the influence of fluid shear as a deposit-removal mechanism, since the shear stress is nearly proportional to the square of the fluid velocity in turbulent flow. In arriving at an expression for the average rate of removal, Kern and Seaton made the following additional assumptions: (1) the deposit is sheared off in chunks at random planes of weakness, instead of being removed particle-by-particle, and (2) these planes of weakness are likely to occur at any depth [35]. The average removal rate over a heat exchanger tube was taken to be roughly proportional to the product of the surface shear stress and the thickness of the deposited layer. The rate of deposition was assumed to be a constant, depending only on the flow rate and the dirt content of the flow. By using these functional forms for the deposition and removal rates, Kern and Seaton were able to reproduce the asymptotic fouling curves often observed in heat exchangers employed in the chemical process industry.

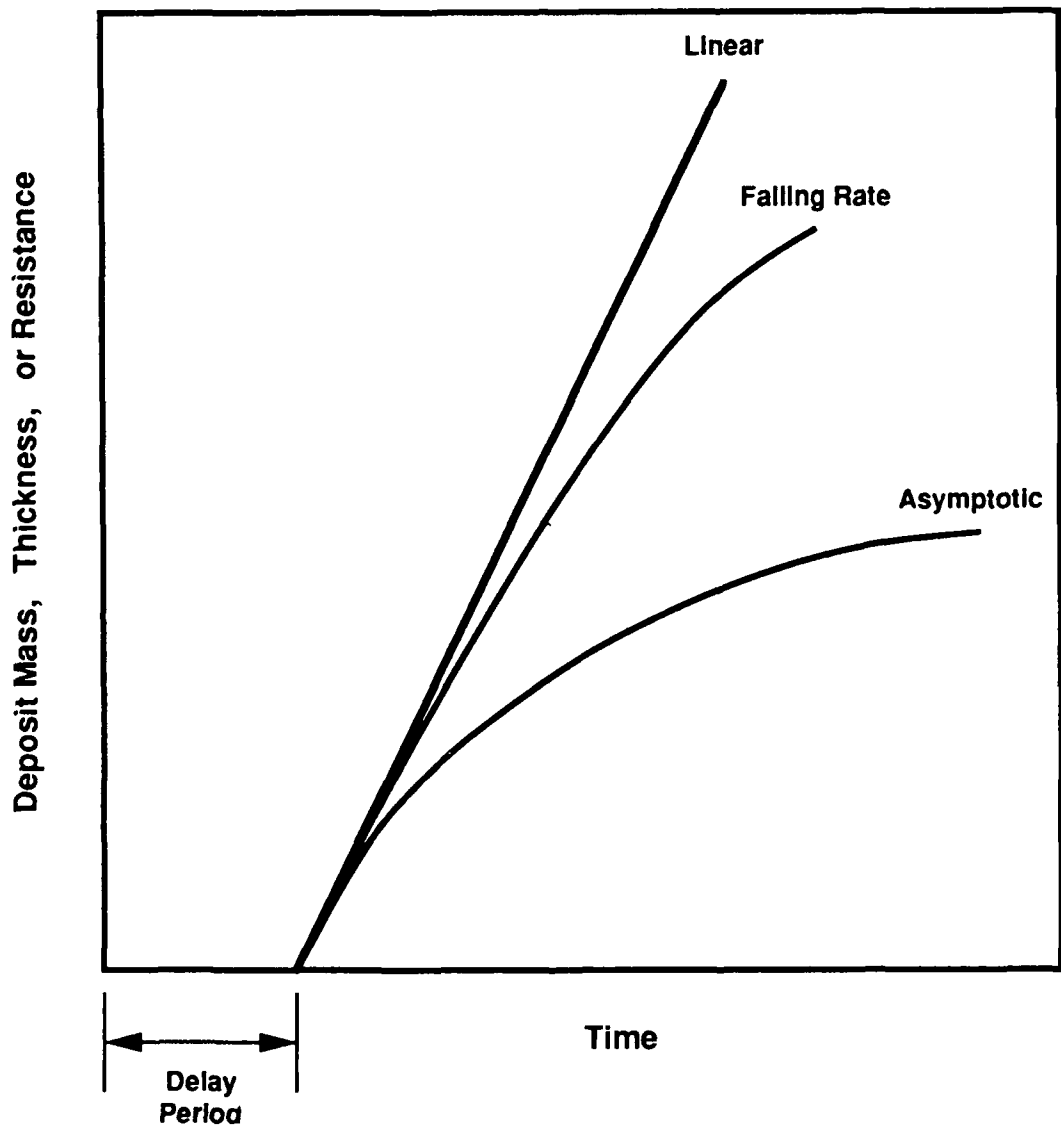


Fig. 2.1 Characteristic Fouling Curves [Ref. 2]

Taborek et al. developed a model for predicting the fouling rate of cooling tower water [36,37]. This model also assumed that the net fouling rate was based on the difference between a deposition rate and a removal rate. The deposit removal rate, ϕ_r , was taken to be proportional to the ratio of the shear stress at the fluid/deposit interface, τ_s , to the deposit bond resistance, R_b , i.e.,

$$\phi_r \approx \tau_s / R_b \quad (2.1)$$

The bond resistance is basically the adhesive strength of the deposit per unit area at the plane of weakest adhesion. The following assumptions were made regarding the deposit bond resistance: (1) R_b increases with the uniformity of the deposit structure, (2) R_b may decrease with deposit thickness because of an increase in the number of planes with a potential weakness, and (3) R_b is only a function of the clean wall characteristics if the deposit/wall interface adhesion is weaker than the internal adhesive forces within the deposit. Based on these assumptions, R_b was postulated to have the form

$$R_b = \psi \left(\frac{1}{x_f} \right)^m \quad (2.2)$$

where x_f is the deposit-layer thickness, ψ is a parameter describing the deposit structure, and m is a constant. The value of ψ will change depending on whether the deposit strongly adheres to the solid surface or is a loosely packed structure that can be readily removed. Since R_b is inversely proportional to the deposit-layer thickness, the removal rate becomes proportional to the product of the surface shear stress and the deposit-layer thickness, as was the case with the Kern and Seaton model [35].

The model of Kern and Seaton assumes that fluid shear is the mechanism responsible for deposit removal [35]. However, Epstein has pointed out a conceptual problem with the assumption that such a removal mechanism co-exists with particle deposition [2]. If a re-entrainment mechanism resulting from fluid shear is operative at the fluid/surface interface, the question arises as to how a particle can ever be deposited in the first place. In other words, if the forces responsible for re-entrainment acted on all the particles approaching a solid surface, a layer of deposits would never form. This raises the possibility that other mechanisms could be responsible for the removal of an existing deposit.

Particle re-entrainment in heat exchanger fouling is primarily a turbulent flow phenomenon [2]. The laminar flow experiments conducted by Bowen and Epstein with radioactively tagged particles have shown no evidence of the re-entrainment of previously deposited particles [28]. For turbulent flow, Cleaver and Yates have proposed a detachment mechanism that appears to resolve the above dilemma [38-40]. Examining the available data, Cleaver and Yates concluded that the flow adjacent to a surface has to be turbulent before significant (if any) removal is observed. Furthermore, they argue that fluid shear alone is incapable of providing sufficient lift forces to dislodge particles attached to a surface. Previous investigations of turbulent boundary layers have shown that the viscous sublayer is not steady, but rather is disrupted by randomly periodic and randomly distributed turbulent "bursts." These turbulent bursts are eruptions of the fluid normal to the wall that can carry fluid away from the wall into the mean flow. The bursts can be thought of as miniature, three-dimensional tornadoes randomly distributed throughout the surface. It is the turbulent bursts, according to Cleaver and Yates, that are responsible for particle re-entrainment in turbulent flow.

At any instant of time, turbulent bursts are estimated to cover less than 1/2% of the solid surface. These violent updrafts are compensated by gentler fluid downsweeps over the much larger surface area not covered by the bursts. Particle deposition occurs via these gentle backsweeps toward the surface. For a particle with diameter d , the model of Cleaver and Yates predicts that detachment will only occur when

$$\tau_w d^{4/3} > \beta \quad (2.3)$$

where τ_w is the wall shear stress and β is a factor that depends on the particle shape, fluid characteristics, and the adhesive forces between the particle and the surface [38]. Unfortunately, values for β are very difficult to determine. Comparisons of the model with the limited available data gave values for β on the order of 3×10^{-4} . An estimate of β from the theory of attractive forces gave a value of $\sim 5 \times 10^{-3}$. Detailed experiments will be required to obtain reliable values of this parameter and to further test the turbulent-burst model.

As noted earlier, very few models have been proposed for particle re-entrainment compared with particle deposition. The evidence discussed above indicates that the rate of deposit removal is negligible in laminar flows. In turbulent flows, turbulent bursts have been postulated as being responsible for particle detachment from a solid surface. It will be difficult to distinguish the various possible interaction modes between a solid surface and a particle.

For example, will particles that initially adhere to a surface and then become re-entrained need to be differentiated from particles that approach and possibly touch the surface but do not adhere (a sticking probability of less than 100%)? An understanding of these mechanisms is important in formulating mathematical models that can adequately describe the deposition behavior of aviation fuels under a variety of flow conditions.

3.0 DEVELOPMENT OF A MATHEMATICAL FRAMEWORK FOR FUEL DECOMPOSITION AND WALL DEPOSITION

The formation and surface deposition of the decomposition products from aviation fuels are governed by a number of fluid dynamic and chemical processes. The fundamental process responsible for the thermal degradation of the fuel is the convective heat transfer from the wall to the fluid. With dissolved oxygen in the fuel, the increase in fuel temperature in layers adjacent to the wall can result in an autoxidation reaction and the formation of free radical species. The resulting series of chemical reactions eventually produces insoluble species which can deposit onto solid surfaces. Thus, determination of the near-wall temperature distribution is essential for predicting the rate of fuel decomposition.

Once the decomposition products are formed, they may or may not deposit onto the walls, depending on a number of complex physicochemical processes. The products not immediately deposited on the walls may be convected downstream and deposited elsewhere. The rate of deposition can be a function of the wall roughness, flow turbulence, sticking characteristics of the gums, and turbulence levels in the fluid. Currently, there is no clear understanding of the role and significance of these processes on the deposition rate. The deposition rate is also influenced by the surface chemistry at the walls [28].

Construction of a comprehensive mathematical model describing each of these processes is a very difficult task. Currently, there have been no systematic studies (experimental or analytical) identifying the role of the various mechanisms responsible for the overall deposition rate. Even if such information were available, the mathematical model would be very complex if it were to integrate the dynamics of all the individual processes.

A simplified way to mathematically represent the formation, transport, and deposition of decomposition products onto a surface is to solve a transport equation for the concentration of the product species or deposit precursors. This concentration equation will represent the convection and diffusional processes of transport, as well as the generation and loss of the product species through formation and deposition, respectively. The concentration equation may be written as

$$\text{div}(\mathbf{G} C_1) = \text{div}(\Gamma_c \text{grad} C_1) + S_f - S_d \quad (3.1)$$

where \mathbf{G} is the mass flux, C_1 is the concentration of the species (i.e., deposit precursors), Γ_c is the effective diffusion coefficient, and S_f , S_d are the rates of formation and deposition of the

precursors. The mass flux \mathbf{G} is a three-dimensional vector field describing the convection of species from the bulk fluid to the walls. Γ_c represents the effective diffusion coefficient and includes molecular as well as turbulent diffusion. Models for the eddy-diffusivity in turbulent pipe flows have been proposed earlier by Davies [21], but they are restricted to fully developed flow. For the heated-tube experiments discussed in Sec. 4.0, the small tube diameters result in fully developed flow throughout most of the tube length, so such a model could be used in these cases.

When the flow field is very simple and can be determined analytically, the convective term is easy to evaluate. However, in many instances the flow may not be fully developed and one-dimensional. In such cases, the Navier-Stokes equations with the appropriate boundary conditions must be solved to determine the velocity field. When the flow is turbulent, the turbulent viscosity can be calculated in a number of ways, ranging from an empirical prescription of the viscosity field to its calculation through the solution of additional partial differential equations. Turbulence models of varying degrees of sophistication can be employed to characterize the flow [41].

The source terms S_f and S_d representing the formation and deposition of the precursors are more difficult to evaluate, because of the various processes contributing to the total rate. The rate of formation of deposits can be lumped into a single Arrhenius expression involving the local temperature and the concentrations of oxygen and other species. At this time, such relations are not well known for the various aviation fuels.

The thermal decomposition model also includes a transport equation of the form of Eqn. 3.1 for the dissolved oxygen in the fuel. In this case C_l is the concentration of dissolved oxygen, Γ_c is the effective oxygen diffusion coefficient (assumed to be the same as that for the deposit precursors), and S_d is a sink term for the rate of autoxidative reactions in the fuel. The initial concentration of dissolved oxygen is a required input value for the model. The source term S_f in Eqn. 3.1 is zero for the dissolved oxygen.

Marteney and Spadaccini have conducted a series of thermal decomposition experiments in electrically heated tubes using JP-5 and several alternate fuels [42,43]. When plotted against the reciprocal of the initial wall temperature, the deposition data could be fitted with Arrhenius expressions throughout most of the temperature range. The low-temperature data below 533 K (500°F) were well fitted by a line representing an activation energy of 8–10 kcal/mole. These low activation energies suggested a heterogeneous or wall-catalyzed reaction

[43]. Above 533 K, the data were fitted with a line corresponding to an activation energy of 40 kcal/mole. This higher value suggested a homogeneous reaction in the bulk liquid. It was presumed that both types of reactions occurred at all times, but each was more important in a different temperature regime [43].

Based on the above results, the present model includes both a wall reaction term and a homogeneous reaction term for the bulk fuel. Since the detailed chemical kinetics of fuel decomposition and deposit formation are unknown, these initial reactions are modeled as global, one-step Arrhenius reactions. Both reactions are assumed to occur throughout the entire range of temperatures encountered by the heated fuel. The wall reaction is included in the model as a boundary condition in the oxygen equation. This boundary condition has the form

$$\mathcal{D}_{O_2} \frac{\partial [O_2]}{\partial r} \Big|_{\text{wall}} = - A_w \exp(-E_w/RT_w) [Fu]_w^{a_w} [O_2]_w^{b_w}. \quad (3.2)$$

Here \mathcal{D}_{O_2} is the diffusion coefficient for dissolved oxygen in aviation fuel, E_w is the activation energy for the wall reaction, A_w is the preexponential constant for the wall reaction, $[O_2]_w$ is the oxygen concentration at the fuel/wall interface, and $[Fu]_w$ is the fuel concentration at the fuel/wall interface. A value of 1.0 is currently used for a_w and b_w . Values of A_w and E_w for a particular fuel must be determined from experiments.

For the homogeneous reaction in the bulk fuel, the initial model assumes a global reaction of the form



The model assumes that the fuel has a molecular weight of 170 kg/kmol, which is equivalent to that of n-dodecane ($C_{12}H_{26}$), a hydrocarbon that is a significant component of JP-5 and Jet A fuels [7]. The source term for the homogeneous autoxidation reaction, S_f , is thus written as

$$S_f = A_b \exp(-E_b/RT_b) [Fu]_b^{a_b} [O_2]_b^{b_b} \quad (3.3)$$

where E_b is the activation energy for the bulk liquid reaction, A_b is the preexponential constant for the bulk liquid reaction, $[O_2]$ is the oxygen concentration, and $[Fu]$ is the

concentration of the fuel. A value of 1.0 is currently used for a_b and b_b . For a given fuel the values of A_b and E_b , in addition to A_w and E_w , must be determined from experiments.

The current chemistry models are restricted to temperatures where autoxidation reactions control the rate of fuel decomposition. Autoxidation reactions were found to control the decomposition rates below 533 K (500°F), whereas oxygenated products played an important role in the intermediate temperature regime of 533–755 K (500–900°F) [8]. At temperatures above 755 K, pyrolysis reactions become significant and result in fuel cracking without the presence of oxygen. In order to predict the rate of fuel pyrolysis, an additional source term would be required in Eqn. 3.1 to account for the formation of precursors from pyrolysis reactions. A pyrolysis model such as that of Fabuss, Smith, and Satterfield [9] would then be needed.

The term S_d in Eqn. 3.1 represents the net loss of precursors from deposition processes at the wall. The mass transfer resulting from concentration gradients within the fluid has already been taken into account in the diffusion term. S_d represents the rate of deposition from flow impaction, sticking, sedimentation, etc. This term also includes the rate of erosion of previously deposited products because of flaking, wall shear, etc. At this time, the modeling of the source term S_d is very difficult because of a lack of understanding of these processes and the absence of data from clearly defined experiments.

Deposits at a fuel/wall interface are assumed to form as a result of two different mechanisms. The first mechanism involves the formation of deposits directly on the solid surface from the heterogeneous reaction described by Eqn. 3.2. The second mechanism involves the transport of deposit precursors produced in the bulk fluid to the wall, where they are assumed to adhere and form a solid deposit. The total deposition rate is the sum of the deposition rates from these two processes.

The deposition rate resulting from the heterogeneous reaction is assumed to be proportional to the rate of transport of oxygen molecules to the surface, i.e., proportional to

$$\mathcal{D}_{O_2} \frac{\partial [O_2]}{\partial r} \bigg|_{\text{wall}}$$

As shown in Eqn. 3.2, the magnitude of this term will depend on the values of A_w and E_w . For a fixed value of the activation energy E_w , calibration of the model involves adjusting

the preexponential constant A_w until the predicted deposition rates match the experimental data. This calibration procedure is illustrated in Section 5.0 for JP-5 fuel.

The deposition rate resulting from the homogeneous, bulk fuel reaction is assumed to be proportional to the mass flux of deposit precursors at the solid surface. The model currently accounts for mass transport of deposit precursors to the wall by laminar or turbulent diffusion only. The rate of deposition at the wall is described by the boundary condition

$$\mathcal{D}_{C_1} \left. \frac{\partial C_1}{\partial r} \right|_{\text{wall}} = - K C_w^n \quad (3.4)$$

where C_w is the concentration of deposit precursors at the wall. The negative sign is needed on the right hand side of Eqn. 3.4 since the gradient $\partial C / \partial r$ is less than zero because of deposition at the wall. For lack of better information, the precursor/wall interaction was assumed to be first-order with respect to the wall concentration, i.e., $n = 1$. The parameter K thus has units of velocity and may be interpreted as a deposition coefficient as described by Beal [23]. The net effect of the complex physicochemical processes occurring at the fuel/wall interface (or the fuel/deposit interface for an established deposit layer) are lumped together into this parameter. These processes include the transport processes in the near-wall region, possible chemical reactions of the precursors at the deposit layer, deposit sticking mechanisms, and the detailed interaction forces occurring between a surface and an approaching precursor molecule or particle. Thus K can be a function of the flow field, the surface conditions, and the temperature, as well as other factors. Because of this complex dependence, K cannot be accurately predicted from first principles and needs to be determined experimentally for each fuel.

The magnitude of K can also be considered as a measure of the relative rates of diffusion and surface reaction of the deposit precursors. For a diffusional boundary layer of thickness δ with a linear variation of C_1 , Eqn. 3.4 becomes

$$\frac{\mathcal{D}_{C_1} (C_0 - C_w)}{\delta} = K C_w \quad (3.5)$$

where C_0 is the concentration at the edge of the boundary layer. Equation 3.5 can be rearranged as

$$C_w = \left(\frac{D_{C_1} / \delta}{D_{C_1} / \delta + K} \right) C_0 . \quad (3.6)$$

In the limit $K \rightarrow 0$, $C_w \rightarrow C_0$ and the overall rate of deposition is increasingly controlled by the rate of reaction of precursors at the surface. As $K \rightarrow \infty$, $C_w \rightarrow 0$ and the overall rate of deposition is controlled by the rate of diffusion of precursors to the surface. In this case the deposit precursors instantaneously adhere when they reach the wall or deposit layer (a sticking probability of 100%). Some initial order-of-magnitude values of K for turbulent flow are presented in Ref. 23. More accurate values of K will require carefully controlled deposition experiments under conditions characteristic of those encountered by aviation fuels.

The baseline model assumes that all of the precursor species arriving at the wall adhere and form a deposit. This boundary condition is enforced by setting K equal to a very large number (10^{20}). This ensures that C_w is effectively zero at the solid surface. The effect of variations in K on the predicted model results is examined in Section 5.0.

Based on initial attempts at calibrating the baseline model with the deposition data of Marteney and Spadaccini for JP-5 fuel [42,43], it was necessary to introduce an additional parameter into the model. The initial calibration procedure consisted of varying the preexponential constants in the wall and bulk reactions in order to match the calculated deposition rates with the data. By varying the preexponential constants, a good match could be obtained between the code results and the deposition data throughout most of the temperature range in the heated tube. However, the peak predicted deposition rates near the end of the tube, where the fuel and wall temperatures were the highest, were significantly higher (by factors of 50–100) than the data. As is discussed more fully in Section 5.0, these differences could not be adequately explained by uncertainties in the diffusion coefficients or inaccuracies in the precursor transport model. Consequently, the simplified chemistry model used in the code was further examined in an attempt to account for the high predicted deposition rates.

The initial decomposition model assumed that the deposit precursors produced from the bulk reaction would be transported directly to the wall, where they would form a deposit. Based on deposition experiments conducted in heated tubes, however, Hazlett concluded that the deposit chemistry did not appear to be in the main reaction sequence involving the formation and decomposition of the oxygenated products (i.e., hydroperoxides)[8]. Although hydroperoxides were identified as precursors to the formation of deposits, the actual deposit-

forming chemistry appeared to be a closely related side branch to the primary sequence of chemical reactions. For example, the maximum hydroperoxide concentration measured in decomposition experiments with n-dodecane was approximately 200 mg/L [8]. The typical deposit mass from a liter of fuel, however, was only 0.01 to 0.1 mg. By assuming that the deposit precursors were directly transported to the wall, where they adhered to the solid surface and formed a deposit, the initial model could have substantially overestimated the deposition rates.

The deposition rates resulting from the transport of precursors to the wall were therefore modified with an additional factor, DPFRAC, which varies between 0 and 1. The original model assumed that the precursors formed by the autoxidation reaction in the bulk fuel would be transported to the wall and form a deposit, i.e., DPFRAC = 1. A DPFRAC value of less than 1 corresponds to the case in which only a fraction of the product species resulting from the thermal decomposition reactions become insoluble and form a solid deposit. This additional factor, along with the preexponential constants for the bulk and wall reactions, needs to be determined in calibrating the model. This calibration procedure is described in Section 5.0.

Based on a survey of the literature, it appeared that more thermal decomposition data were available for JP-5 than for other aviation fuels. Consequently, the initial calibration and testing of the model were conducted for JP-5. Most of the deposition data were obtained from heated-tube experiments in which the fuel was exposed to a constant heat flux. Because of the large temperature variations within the tubes, there is a significant variation in the fuel properties. The viscosity of JP-5, for example, changes by a factor of more than 10 over the temperature range of 293–593 K (68–608°F). In order to account for variable fluid properties, curve-fits of the liquid fuel properties as a function of temperature were included in the model.

Properties for liquid JP-5 fuel have been compiled by the Shell Development Company over a temperature range of 273–673 K (32–752°F)[44]. Curve-fits for these properties were developed in SI units by J. A. Pearce, WRDC/Aero Propulsion and Power Laboratory, Wright-Patterson AFB, and supplied to ANL [45]. These curve-fits were generalized to include additional options for the functional dependence of the properties on the fuel temperature. Curve-fit equations for the fuel enthalpy, density, viscosity, and Prandtl number were included in the model. The generalized curve-fit equations have the following forms, where the temperature T is given in degrees Kelvin:

Enthalpy:

$$h \text{ (J/kg)} = AHFU + BHFU \cdot T + CHFU \cdot T^2 + DHFU \cdot T^3 \quad (3.7)$$

Density:

$$\rho \text{ (kg/m}^3\text{)} = ARHO + BRHO \cdot T + CRHO \cdot T^2 + DRHO \cdot T^3 \quad (3.8)$$

Viscosity:

$$\mu \text{ (kg/m-s)} = AMU + \frac{BMU}{T^{DMU}} + CMU \cdot \exp(DMU/T) \quad (3.9)$$

Prandtl number:

$$Pr = APR + \frac{BPR}{T^{DPR}} + CPR \cdot \exp(DPR/T) \quad (3.10)$$

The specific values of these constants used for JP-5 are shown in Figs. 3.1-3.4, along with a comparison of the curve-fits to the fuel properties from Ref. 44.

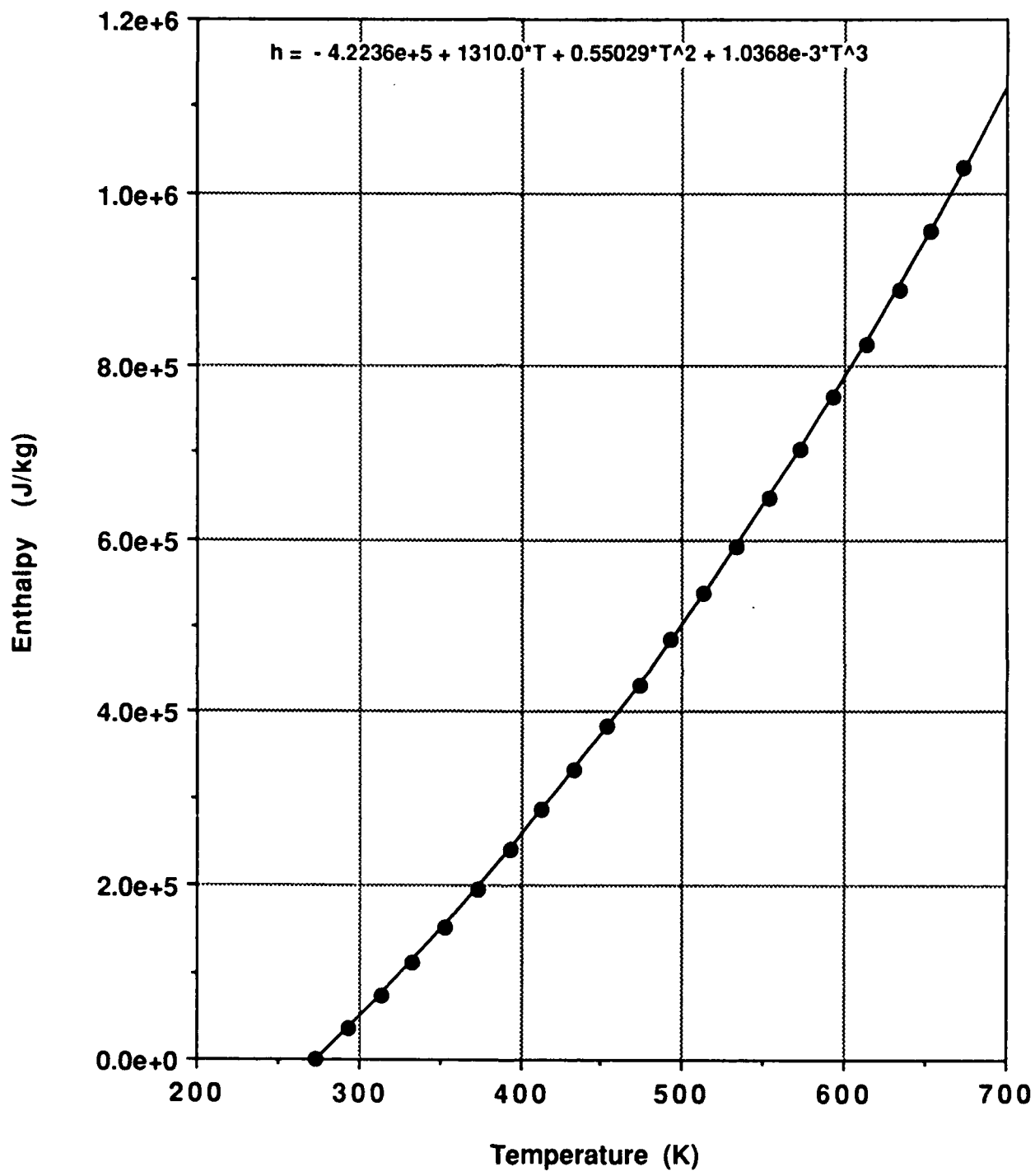


Fig. 3.1 JP-5 Enthalpy

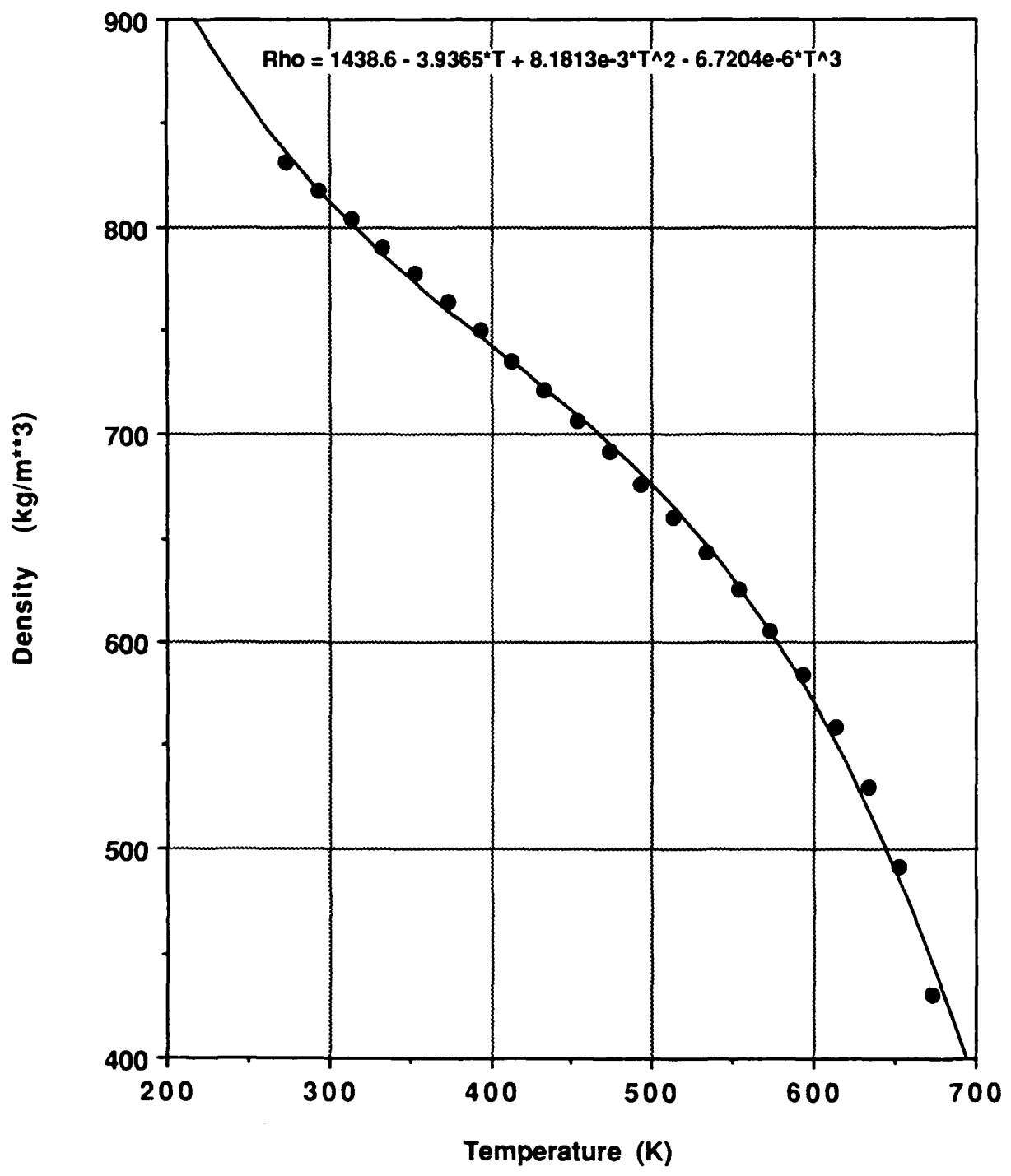


Fig. 3.2 JP-5 Density

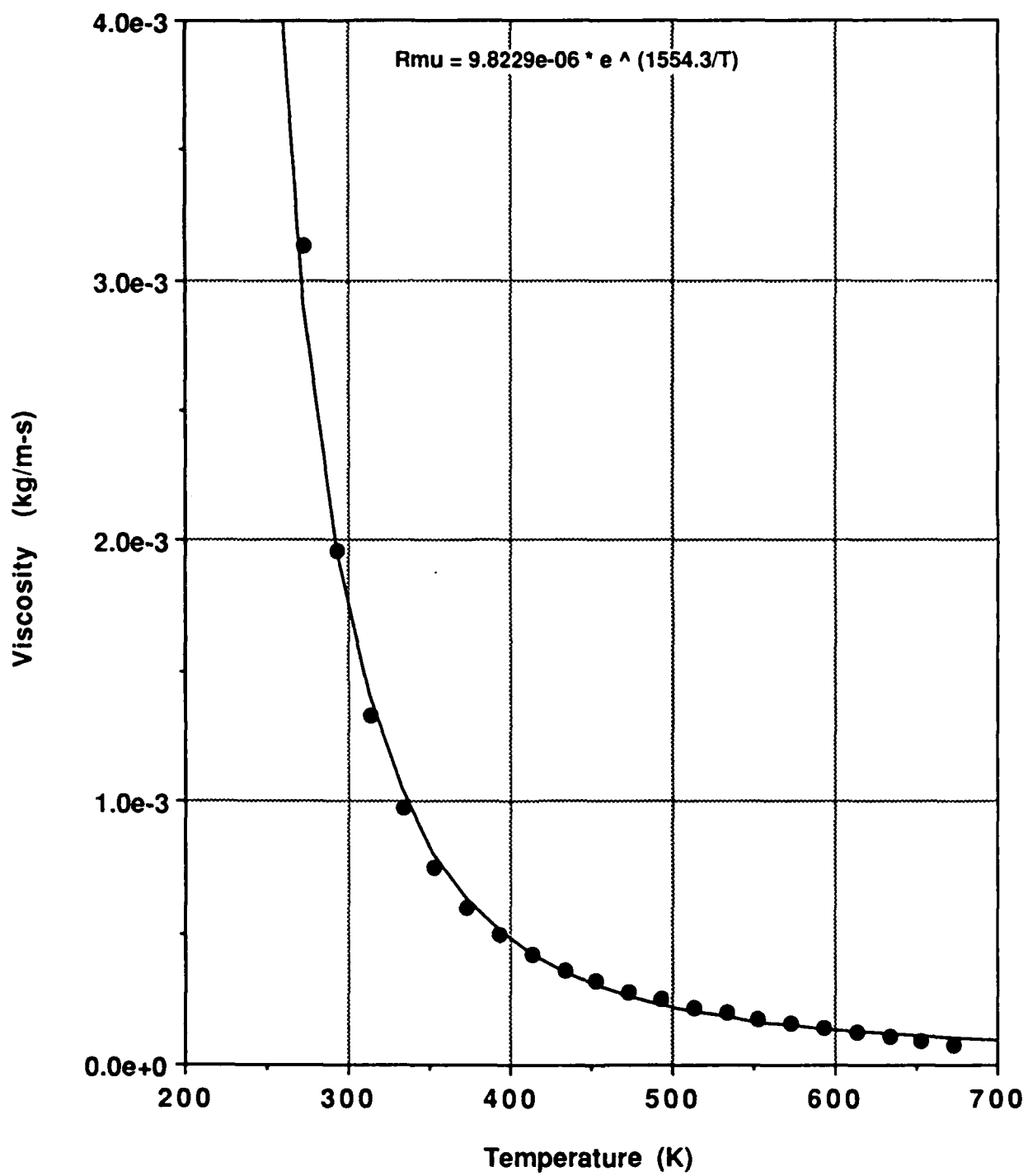


Fig. 3.3 JP-5 Viscosity

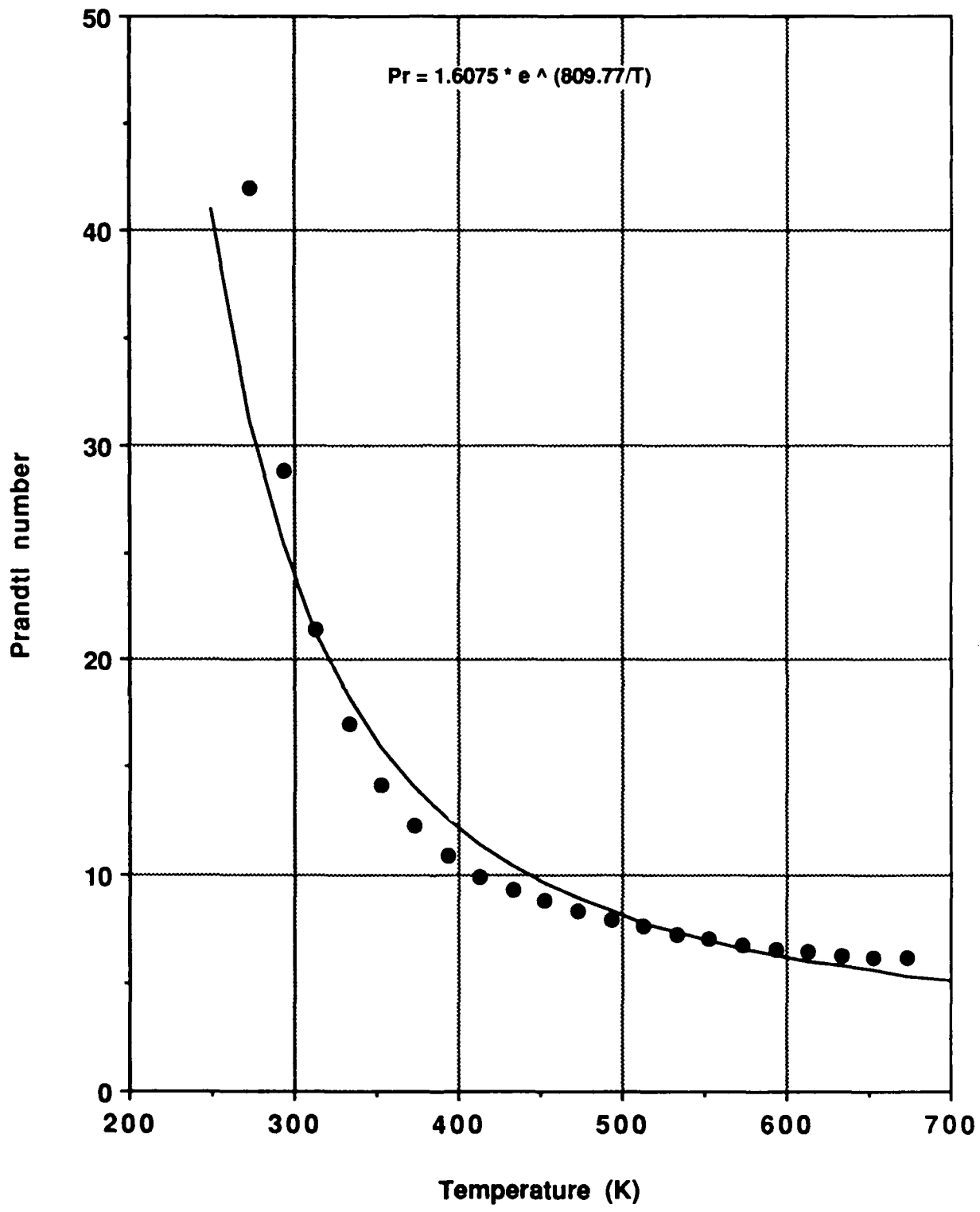


Fig. 3.4 JP-5 Prandtl number

In addition to the above fuel properties, the transport equations for dissolved oxygen and the deposit precursors require values for the Schmidt numbers

$$Sc = \frac{\mu}{\rho D} \quad (3.11)$$

In order to calculate Sc for a particular species, corresponding values of the diffusion coefficient must be known. Accurate values of diffusion coefficients are important for the precursor transport equation, since they directly affect the predicted deposition rates. The rate of transport of dissolved oxygen from the bulk fuel to the higher-temperature region near the tube wall depends on the magnitude of the oxygen diffusion coefficient. The theory for liquid-phase diffusion is not as well developed as the theory for diffusion in gas systems [26]. Those diffusion coefficients that have been tabulated typically cover only a narrow range of temperatures near room temperature. Moreover, the actual species that are transported to the wall and subsequently form a deposit have not been identified. The value of the diffusion coefficient will vary significantly, depending on whether these deposit-forming species are molecular species or larger-sized particles or agglomerates. There is thus much more uncertainty in the value of the diffusion coefficients than in the values of the other fluid properties.

In order to obtain an initial estimate of the diffusion coefficients, a literature search was conducted to identify the available property data. Ertl and Dullien measured self-diffusion coefficients for n-paraffins over a temperature range of 185-439 K (-127-330°F) [46]. Over this temperature range, a good fit to the data was obtained by assuming an exponential dependence of the diffusion coefficient on the temperature. A more generalized correlation of self-diffusivity for the complete fluid region, including the compressed liquid state, was developed by Lee and Thodos [47]. This generalized correlation is more complicated than the exponential expression of Ertl and Dullien and, given the many uncertainties in the nature of the deposit-forming species, does not appear to be warranted at this time. Consequently, the exponential expression of Ertl and Dullien was used to calculate the variation of the diffusion coefficients with temperature.

Ertl and Dullien measured diffusivities of n-paraffins ranging from n-heptane (n-C₇H₁₆) to n-octadecane (n-C₁₈H₃₈). Higher diffusion coefficients were measured for the lower molecular weight hydrocarbons. At 373 K, for example, the self-diffusion coefficient of n-C₁₈H₃₈ was approximately 1 x 10⁻⁹ m²/s, whereas that for n-C₇H₁₆ was about 7 x 10⁻⁹ m²/s [46]. The diffusion coefficients for n-dodecane (n-C₁₂H₂₆) were in the middle of the values

measured for the seven *n*-paraffins. Since the present model considers *n*-dodecane to be representative of a fuel molecule, the equation obtained by Ertl and Dullien for *n*-dodecane self-diffusion coefficients was used as the baseline correlation for this property. For lack of better information, the diffusion coefficients (and Schmidt numbers) for dissolved oxygen were taken to be the same as those for the deposit precursors. Section 5.0 discusses the sensitivity of the predicted deposition rates to variations in the diffusion coefficient.

The generalized correlation for the diffusion coefficient included in the model is of the form

$$D(m^2/s) = ADF + \frac{BDF \cdot T}{\mu} + CDF \cdot \exp(-DDF/T). \quad (3.12)$$

The second term on the right-hand side of Eqn. 3.12 is in the form of the Wilke-Chang correlation [26], which is widely used to predict liquid diffusion coefficients for dilute mixtures, i.e., maximum solute concentrations of 5 or possibly 10 mole %. The variable μ in Eqn. 3.12 is the dynamic viscosity of the solvent, which is aviation fuel in the present application. The specific values of the constants in Eqn. 3.12, along with several diffusivity correlations from Ertl and Dullien, are shown in Fig. 3.5. The correlations were found to fit the data to within 4%. The solid curves in Fig. 3.5 cover the temperature range of the data. The dashed sections of the curves represent extrapolations of the correlations beyond the range of the measurements. These results illustrate the need for additional data on liquid diffusion coefficients at the higher temperatures characteristic of the heated-tube experiments.

The thermal decomposition model described above has been incorporated into an existing computer code originally developed for the calculation of multidimensional, reactive fluid flows. The code uses an efficient multigrid algorithm to solve the two-dimensional, Reynolds-averaged mass, momentum, and energy conservation equations. The code also includes the $k-\epsilon$ model for turbulent flows. A description of the solution algorithm and the various models in the original code is given in Ref. 48 and will not be included here. Transport equations for dissolved oxygen and the deposit precursors have been integrated into the code and are solved simultaneously with the conservation equations. The gas property equations in the original code were supplemented with the property correlations for liquid fuels as described in this section. The initial results obtained with the modified code are presented in Section 5.0.

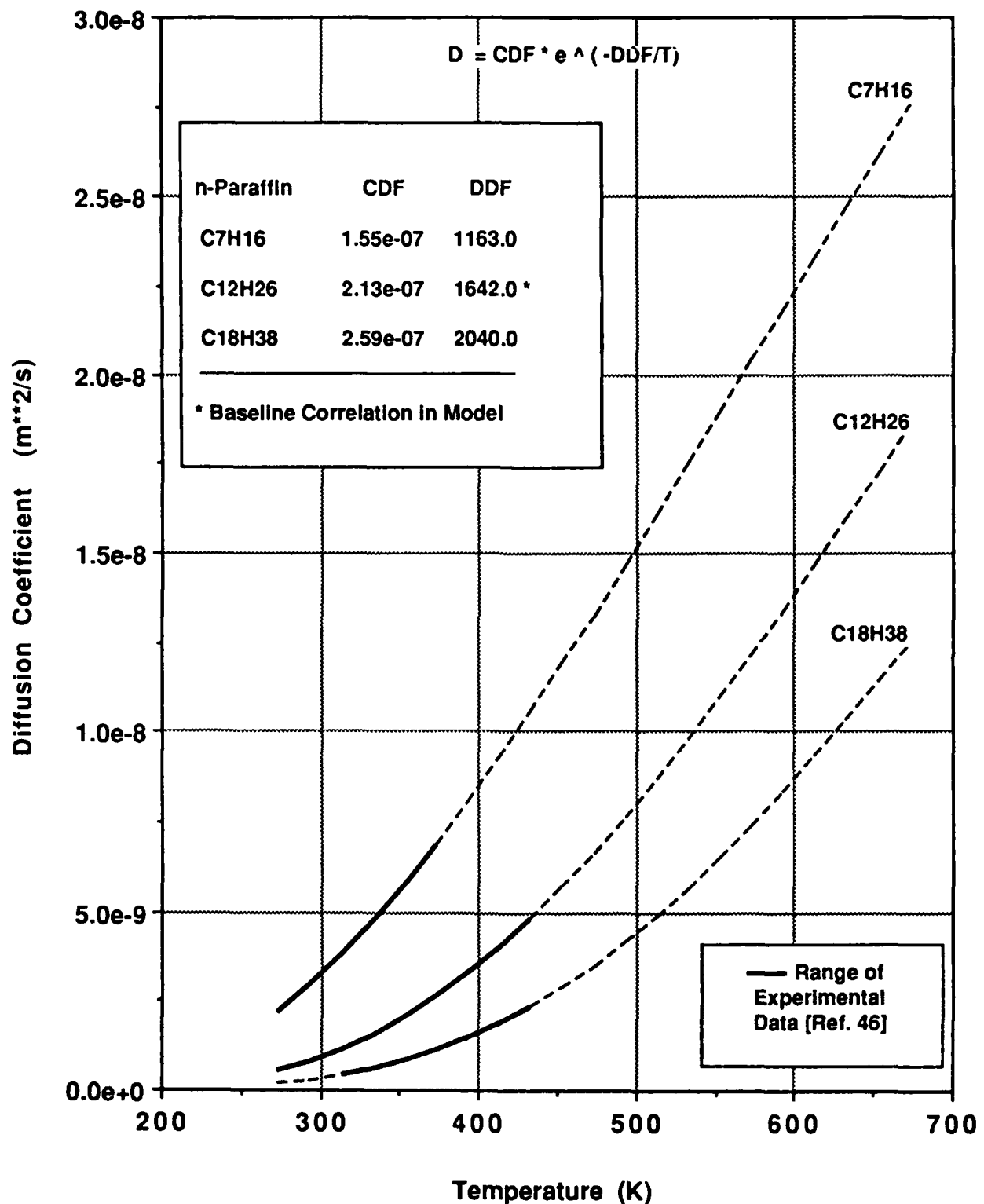


Fig. 3.5 Self - Diffusion Coefficients for n-Paraffins

4.0 CURRENT DATA BASE FOR AVIATION FUEL DECOMPOSITION

The thermal decomposition model discussed in Section 3.0 contains a number of input parameters that must be determined from experimental data. These parameters are associated with both the decomposition chemistry and the fluid mechanics of the deposition process. The chemistry parameters include the activation energies and preexponential constants for the wall and bulk autoxidation reactions, as well as the order of the reactions. The initial concentration of oxygen dissolved in the fuel (in wppm, for example) is a required input value. Information is also needed that relates the local concentration of oxygenated reaction products (e.g., hydroperoxides) to the concentration of the species that actually forms the deposit. This is the DPFRAC factor in the current model. The input parameters needed for the transport models include the diffusion coefficients, sticking probabilities (value of K), and rates of deposit removal. The existing data base for the thermal decomposition of aviation fuels was examined in order to ascertain whether available data could be used to determine the required input parameters.

Section 2.0 contains a brief review of the general literature on thermal decomposition, particle deposition, particle/surface interactions, and deposit-removal mechanisms. Although some of these references dealt specifically with aviation fuels, much of the work involved research from different technical areas, such as the aerosol deposition problem in gas flows. Although the quantitative information from such sources is not directly applicable to the thermal decomposition of aviation fuels, the analytical approaches and models used to interpret the experimental data can be useful in developing an initial mathematical model of fuel decomposition and wall deposition. In addition to this more general work, research has also been conducted specifically on the thermal stability of aviation fuels. These experiments form the data base used in the present study to guide the development and testing of the initial fuel decomposition model. The experimental approaches and the available data from these aviation fuel experiments are discussed in this section.

In 1979 the Coordinating Research Council (CRC) published Report No. 509, which contained a review of the available literature on the thermal stability of jet fuels [3]. Although much information on the problem had already been accumulated by that time, the available data base was largely empirical with little understanding of the fundamental mechanisms of fuel decomposition. The state of the art was summarized by the CRC as follows [3]:

- Aircraft fuel-system simulators exhibit qualitative agreement with laboratory test devices.
- The fuel injector nozzles, fuel/oil heat exchangers, and fuel controls were identified as critical engine components where deposit formation can cause serious problems.
- The removal of oxygen usually improves the fuel thermal stability.
- Compounds containing the heteroatoms oxygen, nitrogen, and sulfur are major deposit precursors, and
- Metals, especially copper, catalyze the formation of deposits.

Since the publication of the CRC report, additional information has been acquired on fuel decomposition and deposit formation, although the physicochemical mechanisms of the processes are still not well understood. More details on the results from earlier work on thermal stability are contained in the CRC report [3]; data from several of the more recent test programs on fuel stability are summarized below.

In an effort to quantify the thermal stability of aviation fuels, various test methods have been developed throughout the years. When the initial static tests were found to be inadequate, a dynamic test device known as the ASTM-CRC Fuel Coker was developed and eventually standardized as ASTM D 1660 [49,50]. In the coker, the test fuel flows across a heated tube and then passes through a heated filter used to simulate the atomizer nozzle. The increased pressure drop across the filter and the visual appearance and color of deposits on the preheater tube were used to rate the stability of a particular fuel [3].

The CRC later initiated the development of an improved dynamic testing device, resulting in the development of the Jet Fuel Thermal Oxidation Tester or JFTOT. The JFTOT is basically a smaller, automated version of the Fuel Coker that requires less test time, less fuel, and less manpower [49]. In addition, the JFTOT procedure uses the maximum heater-tube temperature as the controlling variable, rather than the maximum fuel temperature as was used in the Fuel Coker. Controlling the maximum fuel temperature was a recognized shortcoming of the Fuel Coker, since the flow was laminar and there were large temperature gradients across the heater tube. Thus, the fuel temperature at the tube wall could be

significantly higher than that of the bulk fluid and more representative of the maximum rate of fuel decomposition. The JFTOT procedure has been standardized as ASTM D 3241 [51].

In the JFTOT test method, test fuel flows over a heated aluminum tube and then through a 17- μm nominal porosity precision filter [51]. The fuel flow rate is 3.0 mL/min and the fuel system pressure is maintained at 3.45 MPa (500 psi) gage. The flow in the test section is laminar with the inlet Reynolds numbers being less than 10. Prior to the 2 1/2-hour test, the maximum heater-tube temperature is preset as specified. The result of a JFTOT test is the breakpoint temperature of a fuel, which corresponds to the maximum heater-tube temperature at which the amount of deposits on the wall or the measured filter pressure drop do not exceed specified limits. The maximum specified pressure drop for JP-5 fuel is 3.3 kPa (25 mm Hg) during a 2 1/2-hour test. The amount of deposits on the aluminum heater tube is either rated visually, by comparison with the ASTM Color Standard, or by a Tube Deposit Rater (TDR) that measures changes in the surface reflectivity of the tube resulting from the accumulated deposits [49].

The JFTOT was basically established as a pass/fail type of test for rating fuels at maximum specified heater temperatures. No information is provided regarding the wall deposition rate or the amount of decomposition products formed within the heater section but carried downstream. The deposit rating techniques also have shortcomings. The test is of short duration and the amount of deposits formed on the tube walls is usually very small. Since the fuel temperature varies throughout the test section, the decomposition rates differ from point to point within the tube. The flow is also laminar, so that transport processes occurring in turbulent flow may not be accurately represented. Although the JFTOT tests provide a useful way to rank the thermal stability characteristics of aviation fuels, more detailed information will be needed to develop mathematical models for fuel decomposition and deposit formation.

Many of the more recent experiments on thermal stability involve flowing a fuel through a heated test section and measuring the rate of deposit accumulation on various surfaces. These tests provide more quantitative information than is obtained from the JFTOT. As shown in Table 4.1, the experiments are also of longer duration than the JFTOT tests. The results obtained from the tests listed in Table 4.1 are discussed in the remainder of this section.

Vranos and Marteney investigated the thermal stability of Jet A and No. 2 Home Heating oil as a function of temperature, pressure, flow rate, and fuel pretreatment (preheating

Table 4.1 Some Thermal Stability Tests Performed With Aviation Fuels

Investigators [Ref.]	Experimental Apparatus	Fuels	Test Time (h)
Vranos/Martency [52]	Fuel System Simulator	Jet A No. 2 Oil	—
Vranos et al. [53]	Electrically Heated Tube	Jet A	1-24
TeVelde/Glickstein [54]	Electrically Heated Tube	JP-5, NAPC-7 NAPC-11, NAPC-14	1-20
Purvis [56]	Experimental Coking Apparatus	JP-7, JP-8, JP-4 (10%, 25%, 35% Aromatics by Vol.), Light Diesel Oil	1-4
Giovannetti/Szetzela [57]	Electrically Heated Tube	Jet A Sun Tech A	3-730
Martency/Spadaccini [42,43]	Electrically Heated Tube	JP-5, Sun Tech A, Sun Tech B, Naval Distillate Fuel, Sulfur-Doped JP-5	8-32
Martency [60]	Electrically Heated Tube	JP-5	2-500

and deoxygenation) [52]. No. 2 Home Heating oil was selected as being both commercially available and representative of a possible, next-generation jet fuel or ERBS (Experimental Reference Broad Specification) fuel. The ERBS fuel could come from modified refinery techniques developed for lower quality crude oils or coal-derived liquids. The most important differences between Jet A and ERBS fuels are the increased aromatic and naphthenic contents of the latter. Increases in these fuel constituents are generally expected to result in higher thermal decomposition rates and thus lower breakpoint temperatures [52].

The deposition rates were measured on four stainless steel discs mounted within a test assembly along the flow direction. The test assembly was fabricated from a copper-beryllium alloy and the surfaces were plated with gold and nickel to minimize the catalytic effects of the walls. Chromalox heaters were used to maintain the temperature of the test assembly and thermocouples mounted along the length of the flow channel were used to determine the temperature uniformity. Pressure-atomizing nozzles were used to obtain the desired flow rate; a cylindrical chamber equipped with optical windows was used to view the spray pattern. After each test run, the stainless steel discs were removed and washed in a 1/1 mixture of benzene and hexane to remove residual fuel. The discs were then dried in a vacuum oven and weighed on a microbalance to determine the quantity of accumulated deposits.

Tests were run with Jet A fuel over a range of wall temperatures from 533–672 K (500–750°F) and flow rates of 2.14×10^{-3} to 2.14×10^{-2} kg/s (2.5–25.0 gal/h). The inlet fuel temperature was 294 K (70°F) and the baseline pressure was 2.07 MPa (300 psi) gage. It was found that the deposition rates were sensitive to both flow rate and temperature. At the lowest wall temperature (533 K) and flow rate (2.14×10^{-3} kg/s), a maximum deposition rate was observed in the flow direction at the location of the second stainless steel disc. This maximum was attributed to the combined effects of the rising bulk fluid temperature, which would increase the fuel/oxygen reaction rate, and the depletion of liquid phase deposit precursors further downstream. At a somewhat higher temperature (589 K) and flow rate (6.78×10^{-3} kg/s), the deposition curve showed the same qualitative shape. In this case, however, the maximum deposition rate was higher (~55 $\mu\text{g}/\text{cm}^2\text{-h}$ vs. ~35 $\mu\text{g}/\text{cm}^2\text{-h}$ for the first case) and was shifted downstream to the location of the third disc. The higher deposition rate was attributed to the higher wall temperature. The downstream shift in the peak deposition rate resulted from a slower fluid temperature rise because of the higher flow rate. At the lowest flow rate (2.14×10^{-3} kg/s) and maximum wall temperature (672 K) condition, the peak deposition rate occurred upstream of the location of the first disc. In this case the value measured at the

first disc ($140 \mu\text{g}/\text{cm}^2\text{-h}$) was approximately four times greater than that for the lower-temperature case ($35 \mu\text{g}/\text{cm}^2\text{-h}$).

The effects of deoxygenation and system pressure on the deposition rates were also examined. Deoxygenation of the fuel resulted in very low deposition rates. At a flow rate of $2.14 \times 10^{-3} \text{ kg/s}$, for example, the average deposition rate (average of the measured values for the four discs) for deoxygenated fuel was less than one-third of that for the oxygenated fuel, despite the higher wall temperatures for the deoxygenated fuel tests (603 K vs. 533 K). Increasing the pressure from 0.69–2.07 MPa (100–300 psi) gage increased the average deposition rate for Jet A fuel by a factor of four. The reason for this effect was not clear, although it was suggested that dissolved oxygen may have come out of solution at the lower pressures, thereby lowering the rate of the liquid phase fuel/oxygen reactions [52].

Deposition data were also obtained by Vranos and Marteney for No. 2 heating oil [52]. As with Jet A, the results were found to depend on both the flow rate and the temperature. At a maximum wall temperature of 603 K, increasing the flow rate from $2.22 \times 10^{-3} \text{ kg/s}$ to $7.11 \times 10^{-3} \text{ kg/s}$ reduced the maximum deposition rate. The peak location was also shifted further downstream, as was observed with Jet A. At a lower wall temperature (533 K), however, increasing the flow rate resulted in higher maximum deposition rates. It was postulated that these increased deposition rates at higher flow rates could have resulted from either a transition in the flow regime (laminar to turbulent) or a change in the fuel decomposition mechanism.

The above results indicate that both the fuel temperature and the flow rate are important variables affecting deposition rates. The surface temperature encountered by the fuel is also an important parameter. Higher flow rates can result in either higher or lower deposition rates, depending on the test conditions. Data from well-defined experiments that isolate the effects of these variables are not currently available, but are needed to further understand the mechanisms of fuel decomposition and wall deposition. From a modeling perspective, the capability to accurately predict the flow field and temperature distribution in the fuel is needed to reliably predict deposition rates under a variety of different conditions.

Using a somewhat different apparatus, Vranos et al. obtained additional deposition data for Jet A fuel [53]. The variables investigated here included time, temperature, tube diameter, fuel flow rate, and surface roughness. In these experiments, deposits were accumulated on thin metal strips of 302 stainless steel that were held within circular tubes by

the tube wall. Thin strips were used to minimize the fluid/wall temperature differences. Two tube sizes were used in the experiments: 1.80 and 4.77 mm (0.071 and 0.188 in.) ID. The fuel flow was varied from 1.13×10^{-3} to 3.65×10^{-3} kg/s (9–29 lb/h) and the temperature range for the experiments was 394–630 K (250–675°F). To investigate the effect of surface roughness on the results, the roughness of the test strips was varied from 0.06–5.08 μm (2.3–200 μin). The corresponding roughness ratios for the two tube sizes thus ranged from 1.2×10^{-5} to 2.8×10^{-3} . The test pressure was maintained at 4.14 MPa (600 psi) gage to prevent a phase change of the liquid fuel.

The dependence of the deposition rate upon time was found to be minor, although the maximum specified run time was only 24 h. At test temperatures of 422 K (300°F) and 533 K (500°F), the deposition rate increased with Reynolds number over the range of 600 to 10,000. However, there was no obvious dependence on the flow regime (laminar vs. turbulent). The Reynolds number dependence of the results seems to indicate the importance of diffusion in the formation of surface deposits. At a given Reynolds number, the deposition rates at 533 K were an order of magnitude greater than those measured at 422 K. However, the deposition rate was independent of the surface roughness up to a maximum Reynolds number of 1.0×10^4 . By contrast, for higher Reynolds numbers in the range of 5.0×10^4 to 4.0×10^5 , the initial discrepancies found between a particle deposition model [31] and a set of experimental data [32] were attributed to the neglect of surface roughness in the model. By using a roughness ratio of 1.0×10^{-4} , reasonable agreement with the data was obtained [31].

Using data at a Reynolds number of 1130, an activation energy was obtained for the overall deposition rate. The resulting value was approximately 10 kcal/mole. This relatively low value suggested that the fuel/oxygen reaction was catalyzed by the solid surface [53]. The surface deposits themselves were not uniform and sections of fresh metal surface were observed. The deposits consisted of clusters of particles about 15 Å in diameter. The deposit structure and its nonuniformity indicated that the deposits formed because of the precipitation of insoluble, liquid-phase particulates or precursors. The existence of such particulates in the liquid, however, could not be confirmed by direct measurement. The overall conclusion of Vranos et al. was that the oxidative decomposition of Jet A fuel was catalyzed by the surface, but was also dependent on mass transfer [53].

TeVelde and Glickstein conducted a series of thermal stability experiments on NAPC-5 fuel (JP-5) and three additional Navy aircraft fuels [54]. The primary objectives for the initial phase of their program were (1) the establishment of a thermal stability data base for the

selected fuels and (2) the development of a model for correlating deposit accumulations with measured heat-transfer effects. The experiments were conducted in thin-walled, electrically heated tubes constructed of 316 stainless steel and Inconel 600. The tubes were either 1.22 m or 2.44 m (4 ft or 8 ft) in length, with an OD of 3.17 mm (1/8 in.) and a wall thickness of 0.5 mm (20 mil). Wall temperatures, fuel temperatures, and pressure drops were measured along the test section. The variables investigated include inlet pressures of 2.76 MPa and 5.52 MPa (400 psi and 800 psi) gage, flow rates from 5.67×10^{-3} to 1.51×10^{-2} kg/s (45–120 lb/h), resulting in tube entrance Reynolds numbers of 2250–6000, fuel exit temperatures of 533–755 K (500–900°F), and test durations of 1–20 h. The deposit mass was measured by cutting the tube into 5-cm sections, placing the sections in a heated furnace, reacting the deposit with air, and using the resultant CO and CO₂ concentrations in the effluent gas stream to determine the amount of carbon in the deposit. Two batches of NAPC-5 fuel were used for the experiments: 400 gal obtained from the Naval Air Propulsion Center (NAPC) and 750 gal transferred from Pratt and Whitney Aircraft (P&WA) as residual Government property. Although laboratory analyses indicated no dissimilarities between the fuels, the P&WA fuel failed the JFTOT pressure drop criterion at 522 K (480°F), whereas the reported breakpoint temperature for the NAPC fuel was 544 K (520°F). The fuel batches were kept separate for the thermal stability tests.

Deposit formation rates for the four test fuels were measured over the ranges of parameters outlined above. Typical results for the fuels are presented in Fig. 4.1. Since the initial wall temperature increased along the length of the tube (constant heat flux boundary condition), the abscissa in Fig. 4.1 also represents the axial distance along the tube. The data shown in the figure indicate that the peak deposition rates occurred in the center of the tube, not at the maximum temperature location. This behavior was generally characteristic of the deposition data for the other fuels that were tested and is consistent with earlier data for three batches of Jet A fuel heated to 644 K (700°F) in Nichrome V tubing [55]. In those earlier tests, two maxima in the data were sometimes observed. The lower-temperature peak occurred only in the presence of oxygen. The higher-temperature peak occurred at the same wall temperature (for a given pressure) both with and without oxygen and thus appeared to result primarily from a thermal process [55].

In addition to the wall temperature, TeVelde and Glickstein investigated the effect of other variables on the deposition rates for JP-5 [54]. The flow velocity appeared to affect the rate of deposition of the NAPC fuel, but not the P&WA fuel. The effect of surface material was examined by conducting a test with an Inconel 600 tube. The resulting temperature profile in the fully developed flow regime (where entrance effects are negligible) was nearly the same as

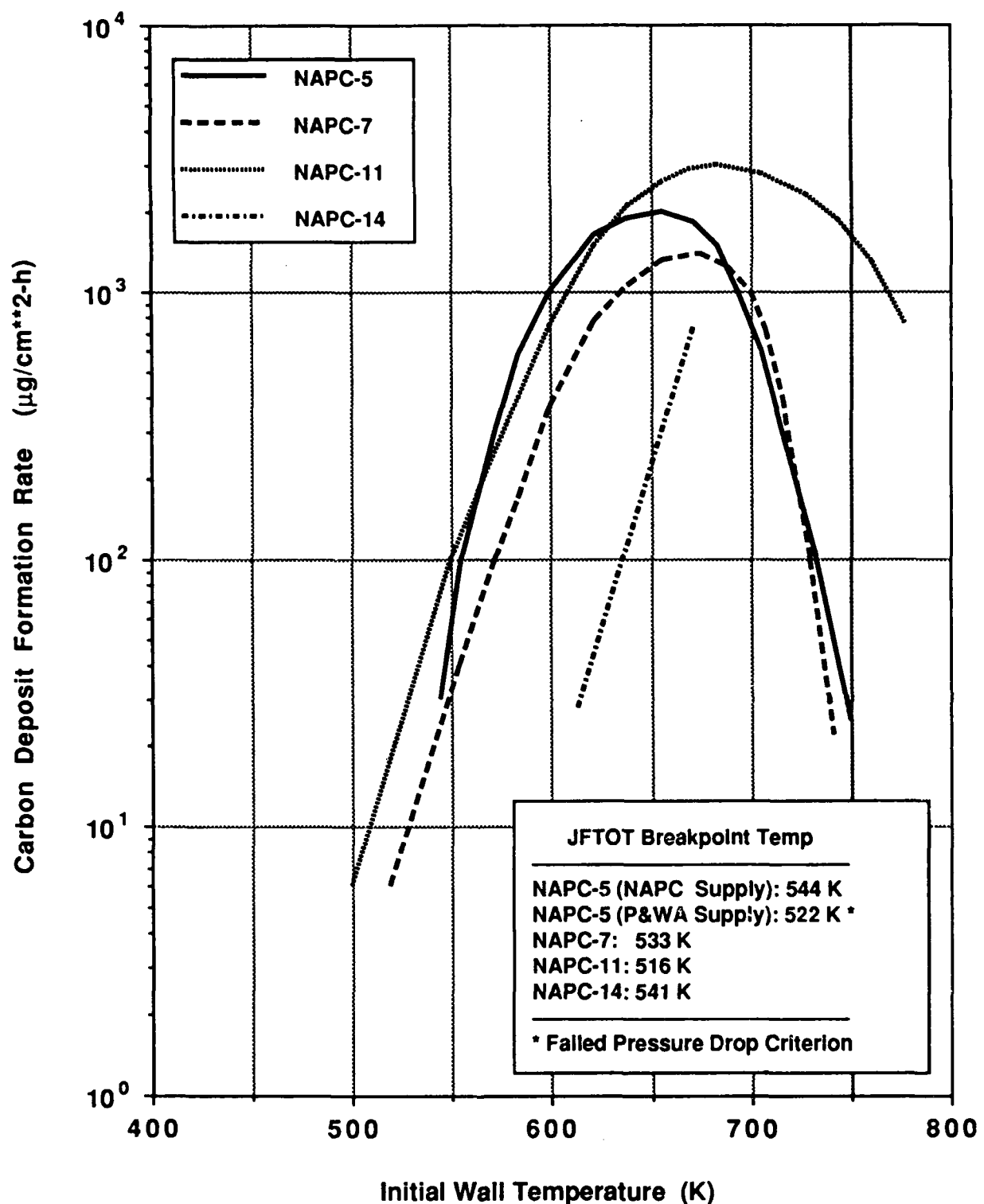


Fig. 4.1 Average Deposition Rates of Four Test Fuels [Ref. 54]

that for the 316 stainless steel tube. In addition, neither the pressure (changed from 2.76 MPa to 5.52 MPa gage) nor the test duration (varied from 1–18 h for the P&WA fuel) had a significant effect on the deposition rates.

Stability tests were also conducted with NAPC-7 fuel, which was a mixture of 80% JP-5 and 20% hydrocracked gas oil. Based on the JP-5 results, the test matrix for the NAPC-7 fuel incorporated a wider range of flow rates (up to 1.51×10^{-2} kg/s), a shorter test tube (1.22 m vs. 2.44 m for the JP-5 tests), and a lower fuel exit temperature (644 K (700°F) compared with 755 K (900°F) for JP-5). Increasing the flow rate from 7.56×10^{-3} to 1.51×10^{-2} kg/s had no noticeable effect on the deposition rate. Deposition rates for the 1.22-m tube were consistently higher than those for the 2.44-m tube. Since the flow rates and fuel exit temperatures were the same for the two tests, the fuel residence time was shorter for the 1.22-m tube but the heat flux was higher. Based on the shorter residence times for the 1.22-m tube, however, lower deposition rates would have been expected. The deposition rates obtained at the lower fuel exit temperature agreed with those obtained at the higher exit temperature over the region where the temperature profiles overlapped.

Stability tests were conducted by TeVelde and Glickstein with two additional fuels: NAPC-11 (a mixture of 50% JP-5 and 50% No. 2 heating oil) and NAPC-14 (an acid-treated, shale-derived JP-5 with the stripped nitrogen compounds partially replaced). The NAPC-11 data showed a peak deposition rate at an intermediate tube location, similar to that in the JP-5 and NAPC-7 results. Unlike the NAPC-7 results, however, the deposition rates for the 1.22-m tube were similar to those for the 2.44-m tube. Tests with the NAPC-14 fuel were conducted at lower fuel exit temperatures, from 533–644 K (500–700°F). Because of the unexpectedly high thermal stability of this fuel, the deposition rates did not exhibit a peak at an intermediate tube location. Rather, the maximum deposition rates occurred at the tube exit. Like the other fuels, the NAPC-14 deposition rates showed a strong dependence on the initial wall temperature.

The average deposition rates for the four fuels are compared in Fig. 4.1. By approximating these data as straight lines over the temperature ranges shown in Table 4.2, activation energies were obtained for the deposit formation rates. The activation energies shown in Table 4.2 are global values representing all of the chemical and physical processes occurring during fuel decomposition and wall deposition. These activation energies are higher than the global values of 9–10 kcal/mole reported for Jet A fuel in the temperature range of 422–672 K (300–750°F) [52,53].

Using a different experimental apparatus, Purvis investigated the thermal stability of various jet fuels [56]. His device, termed an Experimental Coking Apparatus (ECA), contained a cylindrical reaction chamber in which jet fuels were maintained at maximum temperatures up to 561 K (550°F) for periods ranging from 1–4 h. The test chamber was heated with a 15-kW Tocco

Table 4.2 Global Activation Energies for Deposit Formation [Ref. 54]

Fuel	Activation Energy (kcal/mole)	Initial Wall Temperature Range (K)
NAPC-5	44.2	544–594
NAPC-7	32.3	527–616
NAPC-11	28.9	505–633
NAPC-14	50.5	616–672

induction heater. Compressed air cylinders supplied a steady, continuous flow of oxygen to the test chamber. For each fuel, the test pressure was set at 10% above the pseudocritical pressure to ensure that the fuel remained in the liquid state. Deposits were collected on 4-square-inch stainless steel coupons. After each test, the coupons were weighed, cleaned, and then reweighed to determine the amount of material deposited during the test period. Peroxide analyses of the fuel samples were also conducted upon removal from the test chamber.

The six fuels tested were JP-7, JP-8, JP-4 with 10% aromatics, JP-4 with 25% aromatics, JP-4 with 35% aromatics, and light diesel oil. Prior to testing, all fuels were clay-treated, severely, to eliminate polar compounds (e.g., nitrogen, oxygen, and sulfur compounds) and fuel additives (e.g., antioxidants). In addition to the deposit data obtained for the baseline fuels, five currently used fuel additives were blended with four of the fuels to determine their effects on the deposition rates.

The measured peroxide levels were generally in agreement with the deposition rates, i.e., higher peroxide levels corresponded to higher rates of deposition. For the JP-4 fuels, the deposition rates increased with the aromatic content. Over the temperature range of 408–561 K (275–550°F), the deposition rates for the JP-4 fuel with 35% aromatics were approximately 50% greater than those for the JP-4 fuel with 10% aromatics. The effects of the fuel additives were as follows: the antioxidant decreased the deposition rates from those of the baseline fuel,

the metal deactivator and conductivity additives increased the deposition rates, and the icing and corrosion inhibitors had little effect on the deposition rates.

Assuming a pseudo-first-order reaction, the data were used to determine activation energies for the rates of deposit and peroxide formation. For the baseline fuels, the activation energies for the rate of deposit formation varied from 7.8–8.8 kcal/mole. The activation energies for the peroxide formation were somewhat higher, 8.1–9.7 kcal/mole. Fuels treated with the antioxidant had lower peroxide levels, whereas fuels treated with the metal deactivator or conductivity additive had higher peroxide levels than the baseline fuel. These results further support the key role of hydroperoxides in the fuel decomposition and deposit formation processes, a role that was also shown in earlier work [7,8].

Long-term fuel deposition experiments were conducted by Giovanetti and Szetela with both Jet A fuel and an alternative fuel, Sun Tech A [57]. The tests were conducted for periods of time ranging from 3–730 h. The test section consisted of three electrically heated tubes connected to three isothermal tubes downstream. Multiple tubes were used to allow different tests of varying duration to be run concurrently. The heated tubes were constructed of 316 stainless steel and were 0.91 m long with an ID of 0.22 cm. The isothermal tubes were 0.30 m long and were enclosed in ceramic ovens to maintain a constant temperature. Stainless steel wafer specimens were inserted into the flow both upstream and downstream of the isothermal tubes to provide additional deposit data under constant-temperature conditions.

Deposit data were obtained at flow velocities of 0.07 m/s and 1.3 m/s. With Jet A fuel, the deposition rate for the low-velocity case exhibited a maximum at an intermediate tube location corresponding to an initial wall temperature of about 550 K. This behavior in heated-tube experiments was also observed by other investigators [52,54] and has been postulated as being related to the formation and depletion of active oxygenated precursors such as hydroperoxides [57]. As the test duration was increased the rate of deposition also increased, indicating a possible role of the deposit surface in enhancing the deposition rate.

The deposition rates obtained for Jet A at the higher-velocity case also initially increased with increasing wall temperature. At an initial wall temperature of 550 K, the deposition rates for both the high- and low-velocity cases were approximately $150 \mu\text{g}/\text{cm}^2\text{-h}$. At higher wall temperatures, however, the deposition rates for the high-velocity case did not decrease like those for the low-velocity case. This result suggested that the active oxygenated

species were not depleted in the high-velocity test because of the shorter residence time (less than 1 s) in the heated tube.

The deposit structure also differed between the low- and high-velocity tests. The deposits formed in the low-velocity test were cellular with an irregular structure. The deposit density was estimated to be $\sim 0.08 \text{ g/cm}^3$. The high-velocity deposits were more uniform and densely packed, with an average density of $\sim 0.8 \text{ g/cm}^3$. (By comparison, the density of graphite is in the range of $1.6\text{--}2.7 \text{ g/cm}^3$ [58].) It was proposed that the greater wall shear of the high-velocity tests may have suppressed the growth of a cellular deposit, resulting in a more compact, denser structure.

Deposition tests were also conducted with Sun Tech A, chosen by the Navy as an example of an alternative, lower quality fuel. Relative to Jet A, Sun Tech A had higher concentrations of sulfur (0.24% vs. 0.05%), nitrogen (250 ppm vs. 12 ppm), and aromatics (40% by volume vs. 21%). However, the reported JFTOT breakpoint temperature for Sun Tech A was 538 K, compared with 529 K for Jet A [57]. The low-velocity deposition rates for Sun Tech A showed the same trends as those for Jet A, with a maximum deposition rate occurring at a wall temperature of approximately 560 K. Despite the higher reported thermal breakpoint temperature for Sun Tech A, however, its peak deposition rate exceeded that for Jet A by a factor of ten.

Marteney and Spadaccini conducted their thermal decomposition experiments using a test section that also consisted of an electrically heated, thin-walled tube [42,43]. The tube was constructed of 316 stainless steel with a length of 2.44 m (8 ft), an OD of 3.17 mm (1/8 in.), and a wall thickness of 0.4 mm (16 mil). Several tests were also conducted with 1.22 m-long (4 ft) tubes. The tests investigated the effects of temperature, pressure, flow rate, and test duration on the wall deposition rates for JP-5 and three alternate fuels. The test matrix for JP-5 fuel included fuel exit temperatures of 475, 535, and 615 K, wall temperatures of 420–675 K, pressures of 1.72, 2.76, and 5.52 MPa gage, fluid velocities of 0.3, 2.1, and 15.0 m/s (corresponding to inlet Reynolds numbers in the laminar (400), transitional (3000), and turbulent (21,000) ranges), and test times of 8, 16, and 32 h. The fuels were air-saturated prior to being heated in the test section.

In addition to JP-5, tests were conducted with Sun Tech A, Sun Tech B, and Naval Distillate Fuel (NDF). These latter three fuels all had higher percentages of sulfur, nitrogen, and aromatics than JP-5. Two of the fuels, Sun Tech A and Sun Tech B, had higher reported

thermal breakpoint temperatures (538 K and 536 K, respectively) than JP-5 (531 K). The breakpoint temperature for Sun Tech A varied during storage. The reported breakpoint temperature for NDF was 517 K.

The data for JP-5 indicated that pressures above the critical point (2.28 MPa [44]) had little effect on the deposition rates. The data showed the characteristic maximum in the deposition rate at an intermediate tube location, which in this case corresponded to an initial wall temperature of approximately 645 K. It was unclear as to whether this behavior resulted from oxygen depletion, decomposition of hydroperoxides at elevated temperatures, changes in the rate-limiting reaction steps, or some other factor [42].

The deposition data for JP-5 were used to obtain a global activation energy for the overall process as a function of the initial wall temperature. Two separate regimes were identified: below 535 K the data were fitted by assuming an activation energy of 10 kcal/mole, whereas the activation energy determined for the higher-temperature data was 40 kcal/mole [42]. The value of 10 kcal/mole was consistent with the value found for Jet A fuel in the temperature range of 422–533 K [53]. Since activation energies for gas-phase reactions are typically in the range of 20–60 kcal/mole [59], the low-temperature activation energy suggested a surface-catalyzed process [53], whereas the high-temperature activation energy suggested a homogeneous liquid-phase reaction [42]. These changes in the activation energy may be the result of different reaction mechanisms which become rate-controlling over different temperature regimes.

Over test times of 8–32 h, the rates of deposition progressively increased with test duration. Similar behavior was observed for longer-duration tests (up to 730 h) conducted with Jet A fuel [57]. To investigate the effect of flow rate, tests were run at three velocities corresponding to laminar, transitional, and turbulent flow, while maintaining a constant fluid outlet temperature. The deposition rates for the laminar and transitional flows were basically the same at wall temperatures up to 560 K, but the peak deposition rate for the laminar-flow case occurred at a lower temperature. The turbulent-flow case exhibited higher deposition rates below 535 K and appeared to merge with the transitional-flow data at higher temperatures. The occurrence of the peak deposition rate at a lower temperature in laminar flow suggested that either the reaction became mixing-limited at higher temperatures (governed by the transport of reactive species from the bulk fluid to the walls) or the increased residence time at the lower velocity resulted in a more rapid depletion of oxygenated species [42]. The data did not, however, permit the exact cause of this behavior to be identified.

Deposition rates were also obtained for the three alternate fuels in order to investigate the correspondence between the JFTOT breakpoint temperatures and the observed deposition rates. Although NDF had the lowest breakpoint temperature, Sun Tech A had a higher deposition rate in the range of 500–600 K. Deposition rates for Sun Tech A were consistently higher than those for Sun Tech B (e.g., by a factor of five at their breakpoint temperatures), even though their thermal breakpoint temperatures were virtually identical (538 K vs. 536 K). The Sun Tech A and B fuels both showed maxima in their deposition rates at interior locations in the test tube. The NDF data did not show such a maximum, although the highest initial wall temperature was less than 600 K, compared to peak initial wall temperatures of ~675 K for the other three fuels.

For their heated-tube experiments in which the maximum fuel temperatures occur at the tube walls, Marteney and Spadaccini found that the local surface temperature was the key variable affecting the fuel deposition rates. The fuel velocity and test duration were also found to play an important role. The fuel pressure (above the critical value) and bulk fuel temperature were both found to have a secondary effect on the deposition rates.

Results from longer-term deposition tests with JP-5 fuel were recently reported by Marteney [60]. The objective of these experiments was to extend the thermal stability data base for JP-5 to longer test durations and lower flow velocities than those covered in the earlier experiments of Marteney and Spadaccini [42]. The effect of dissolved copper on deposit formation was also examined. For these tests, Marteney used the same multiple-tube apparatus previously used for the long-term stability experiments with Jet A and Sun Tech A fuels [57]. To maintain continuity with the earlier tests using JP-5 [42], a fuel with a thermal breakpoint temperature of approximately 533 K (500°F) was desired. The available JP-5 for these tests was initially found to have a breakpoint temperature above 533 K. The fuel was subsequently blended with 3% No. 2 heating oil to obtain a breakpoint temperature in the range of 530–533 K (495–500°F). This was consistent with the breakpoint temperature of 531 K reported by Marteney and Spadaccini for the lot of JP-5 fuel (Lot I) used in their earlier tests [42].

The initial series of JP-5 deposition tests were conducted by Marteney and Spadaccini at a minimum flow velocity of 0.3 m/s [42]. For the current tests, the flow velocity was reduced to 0.076 m/s (0.25 ft/s), which corresponded to an inlet Reynolds number of 70. In addition, the earlier test at 0.3 m/s was repeated with the second lot of JP-5 fuel, although the test period was

extended to 25 h from the 8 h used for the original test. The deposition rates for the Lot II fuel were about 50% higher than those for the Lot I fuel. This difference was attributed to variations in fuel composition and test times. The two tests at the different flow rates were conducted at approximately the same wall temperatures, with the maximum wall temperature being 589 K (600°F). The low-velocity data exhibited a maximum in the deposition rate of \sim 150 $\mu\text{g}/\text{cm}^2\text{-h}$. This corresponded to an interior tube location with an initial wall temperature of 519–533 K (475–500°F). The peak deposition rate for the higher-velocity test, 200 $\mu\text{g}/\text{cm}^2\text{-h}$, occurred at the tube exit where the wall temperature was 589 K. The corresponding deposition rate for the low-velocity test had fallen to \sim 10–20 $\mu\text{g}/\text{cm}^2\text{-h}$ at the tube exit. The lower-velocity test thus showed substantially higher deposition rates at lower wall temperatures. This could have resulted from the longer residence time at the lower flow rate, resulting in a greater extent of autoxidation reactions and a subsequent increase in the deposition rates. Measurements of dissolved-oxygen concentrations along the heated tube did show a greater reduction in oxygen concentration for the lower-velocity test [60].

Extended duration tests were also carried out by Marteney beyond the maximum time of 32 h reported for the first series of experiments by Marteney and Spadaccini. The test durations ranged up to 150 h at a velocity of 0.076 m/s (0.25 ft/s) and 500 h at a velocity of 0.3 m/s (1 ft/s). For the higher-velocity tests, the deposition rates were similar for periods up to 100 h. Significant increases were recorded at test times of 300, 400, and 500 h. At a wall temperature of 450 K (350°F), for example, the deposition rate after 500 h was over 20 times greater than that at 100 h; the corresponding rate was \sim 4 times greater at a wall temperature of 505 K (450°F). Although the data were taken at a maximum wall temperature of 505 K, extrapolation of the results to higher temperatures indicated that the deposition-rate curves would merge at a temperature of \sim 533 K (500°F).

The long-term tests at a velocity of 0.076 m/s showed similar trends after 150 h, i.e., higher deposition rates at lower temperatures for the longer test times. For the low-velocity tests, however, data were taken at a higher wall temperature (533 K). At this temperature, the rates at 50 h and 150 h showed little variation. The general increase in deposition rates with time reported by Marteney [60], is consistent with earlier data for Jet A fuel obtained using the same apparatus [57].

The effect of dissolved copper on the deposition rate was determined at a fuel velocity of 0.3 m/s and a maximum wall temperature of 589 K (600°F). Small concentrations of copper are known to dramatically accelerate the oxidation rates of aviation fuels [10]. At concentrations

up to 100 ppb, the dissolved copper had little effect on the fuel deposition rates. At a concentration of 300 ppb, however, the deposition rates increased significantly with a maximum rate of $1500 \mu\text{g}/\text{cm}^2\text{-h}$, compared to $200 \mu\text{g}/\text{cm}^2\text{-h}$ for the baseline fuel. The addition of copper also resulted in lower oxygen levels along the length of the test tube. For copper concentrations of 50–100 ppb, the oxygen consumption was greater by up to 20%, although the deposition rates increased only slightly. At 300 ppb, however, it was speculated that the oxygen in the bulk fluid could have almost completely reacted by 589 K, leading to a significant increase in deposit formation.

Because of the long-term nature of these tests, substantial blockages of the small-diameter test tubes were observed under certain conditions. At a fuel velocity of 0.3 m/s, for example, the area reduction was less than 10% after 100 h. After 500 h, however, the tube blockage was approximately 60%. At a fuel velocity of 0.076 m/s, the area reduction was 84% after only 150 h of testing. The increasing deposit thickness was accompanied by greater numbers of fissures on the deposit surface. Very deep cracks were observed after hundreds of hours of testing. Based on results from an unsteady test included in the experimental program, it was concluded that thick deposits, when subjected to increased stresses from temperature and velocity transients, could be susceptible to spalling. In an actual fuel system, the resulting fragments would be carried downstream where they might obstruct other engine components. Several possible mechanisms that could be responsible for the removal of existing deposits are discussed in Sec. 2.4.

The results summarized in this section show that a significant number of tests on the thermal decomposition of aviation fuels have already been performed. Many of the experiments used small, electrically heated tubes and were conducted over time periods ranging from several hours to several hundreds of hours. These tests have served to identify the key factors affecting the rate of deposit formation, such as the temperature, dissolved-oxygen content, and levels of contaminants in the fuel (e.g., copper). They have also provided quantitative information on the deposition rates for specific fuels at various temperatures and flow rates. However, the mechanisms by which fuels react and subsequently form deposits on solid surfaces have still not been resolved. Because of the large number of variables in the heated-tube experiments, it is difficult to isolate the effects of fuel chemistry and transport processes on the results. Additional key variables, such as the oxygen concentration in ppm and the amount of deposits carried out of the tube, have not been measured in these tests. To begin to understand these mechanisms, additional experiments will probably be required to

effectively isolate the individual processes comprising both thermal decomposition and deposit formation. The nature of these proposed experiments is discussed in Sec. 6.0.

5.0 SOLUTION APPROACH AND RESULTS FROM THE PRESENT STUDY

5.1 Calibration of the Model for JP-5 Fuel

The thermal decomposition model described in Section 3.0 contains a number of unknown parameters. Because of a lack of understanding of the detailed mechanisms of fuel decomposition, these parameters cannot be determined directly from the properties of a particular fuel. Rather, the parameters must be obtained from experiments. Since the parameters are related to both fuel chemistry and transport processes, they should ideally be determined from well-controlled experiments that have isolated the individual mechanisms of the overall process. As noted in Section 4.0, however, data from such experiments are not currently available. The majority of thermal decomposition data have been obtained from heated-tube experiments, in which it is difficult to separate the various phenomena taking place. However, a large data base is available from the heated-tube experiments and, consequently, these data were used to obtain initial values for the unknown model parameters. The "calibration" procedure for the model involves the determination of these parameters for a particular fuel. Marteney and Spadaccini obtained thermal decomposition data for JP-5 fuel over a wide range of temperatures and flow rates [42,43]. These data were used to initially calibrate the model.

Marteney and Spadaccini conducted their experiments in long, thin tubes that were electrically heated (constant heat flux boundary condition). The tubes were either 1.22 m (4 ft) or 2.44 m (8 ft) in length, with a 3.17 mm (1/8 in.) O.D. and a 0.4 mm (16 mil) wall thickness. The tube I.D. was thus 2.36 mm, resulting in L/D ratios in the range of 500-1000 for the test sections. The test matrix for JP-5 fuel is shown in Table 5.1. Some properties of the test fuel are listed in Table 5.2. As shown in Table 5.1, tests were conducted at tube entrance Reynolds numbers of 400 (laminar flow), 3000 (transitional flow), and 21,000 (turbulent flow). Because of the large temperature differences throughout the test section, there is a significant variation in the fluid properties, particularly the viscosity. Thus, the fuel Reynolds numbers increase significantly along the length of the heated tube.

After each test, the tube was cut into a number of short segments (~5 cm long) and the accumulated deposit in each segment was reacted with oxygen. Based on an analysis of the product gases, the mass of carbon in the individual segments was calculated from a mass balance. The deposition data were reported as the mass of carbon deposited over the inside lateral surface area of each section during the test period, in units of $\mu\text{g}/\text{cm}^2\text{-h}$. The deposition

Table 5.1 Test Matrix (Nominal Conditions) for JP-5 Fuel [Ref. 43]

Test No.	Exit Pressure (MPa gage)	Tube Exit Temp (K)	Fuel Exit Temp (K)	Fuel Flow (kg/s)	Fuel Velocity (m/s)	Reynolds Number	Tube Length (m)	Test Duration (h)	Purpose
1-a	2.76	644	561	7.56×10^{-3}	2.1	3000	1.22	8	Shakedown
1-b	2.76	561	478	7.56×10^{-3}	2.1	3000	1.22	8	Lower T _{fuel}
1-c	2.76	575	491	7.56×10^{-3}	2.1	3000	1.22	8	Raise T _{fuel}
1-d	2.76	533	491	7.56×10^{-3}	2.1	3000	2.44	8	Increase Range in T _{wall}
51	1-e	2.76	589	533	7.56×10^{-3}	2.1	3000	2.44	8
	1-f	2.76	589	533	7.56×10^{-3}	2.1	3000	2.44	Increase Time 2x
	1-g	2.76	589	533	1.04×10^{-3}	0.3	400	2.44	8
	1-h	1.72	589	533	7.56×10^{-3}	2.1	3000	2.44	Laminar Flow
	1-i	2.76	589	533	7.56×10^{-3}	2.1	3000	2.44	Subcritical Pressure
	1-j	2.76	589	533	5.29×10^{-2}	14.9	21000	2.44	Increase Time 4x
	1-k	2.76	672	616	7.56×10^{-3}	2.1	3000	2.44	High Velocity
									High Exit Temperature

Table 5.2 Selected Properties of JP-5 Test Fuel [Ref. 43]

Aromatics	(vol %)	17
Olefins	(vol %)	0.8
Sulfur	(wt %)	0.008
Nitrogen	(ppm)	5
Hydrogen	(wt %)	13.7
Gravity (288 K)	(°API)	40.9
Viscosity (273 K)	(cS)	3.3
Distillation	(K)	
IBP		457
10%		472
20%		476
50%		489
90%		515
EP		534
JFTOT Thermal Stability Breakpoint Temperature	(K)	531

rates were typically plotted as a function of the initial tube wall temperature, i.e., the wall temperature measured prior to the accumulation of a significant deposit layer. Since there is a linear increase in the wall temperature for fully developed flow with a constant heat flux, this is equivalent to presenting the deposition data at various axial locations along the test section.

Prior to performing the model calibration, several input parameters for the model were fixed. The diffusion coefficients for the oxygen and deposit precursor transport equations were assumed to be represented by the self-diffusion coefficient of n-dodecane, as shown in Fig. 3.5. For lack of better data, the value of K in Eqn. 3.4 was initially set equal to a large number (10^{20}). This implies that all deposit precursors that reach the wall adhere and form a deposit. The initial oxygen concentration is another input value required by the model. Oxygen concentrations in the fuel were not reported in Refs. 42 and 43. For air-saturated Jet A fuel, oxygen concentrations of 45 wppm [55] and 55 wppm [57] have been reported. A baseline value of 50 wppm (mass fraction of 5.0×10^{-5}) was used in this study for the oxygen concentration of air-saturated JP-5 fuel.

As discussed in Section 3.0, the factor DPFRAC was not initially included in the formulation of the model. It had originally been assumed that all deposit precursors formed from the autoxidation reaction would be transported to the wall and form a deposit. This is equivalent to setting DPFRAC = 1. The initial calibration procedure therefore consisted of adjusting the chemistry parameters (preexponential constants and activation energies) for the wall and bulk reactions in order to match the experimental data. As discussed below, the failure of this procedure to adequately match the experimental data provided the rationale for introducing the parameter DPFRAC into the model.

Most of the data from Marteney and Spadaccini's tests (Table 5.1) were obtained at an inlet Reynolds number of 3000, corresponding to a fuel velocity of 2.1 m/s (7.0 ft/s). Test No. 1-k covers the widest range of fuel and wall temperatures and was the baseline test used for the initial calibration of the model. Data printouts were obtained for several of the tests [61]. The printouts contained measured values of fuel temperatures, wall temperatures, flow rates, and electrical power inputs. This information was used to set up the input data files for the code and to validate the predicted temperature profiles.

Because fuel decomposition involves chemical processes whose rates vary significantly with changes in temperature, it is important to accurately predict temperature profiles throughout the heated test section. The current code predicts two-dimensional profiles (axial

and radial) of the fuel temperature, as well as the other dependent variables (velocity, density, oxygen concentration, etc.). Wall temperatures are calculated by assuming a constant heat flux boundary condition, in conjunction with standard wall functions [62]. Although the inlet Reynolds number corresponding to a fuel velocity of 2.1 m/s is in the transitional range, the Reynolds number increases rapidly along the heated test section as the fuel viscosity decreases. These tests were thus modeled by assuming fully developed turbulent flow throughout the entire tube. Figures 5.1 and 5.2 show a comparison between the predicted and measured bulk fuel and wall temperatures for two different test conditions. The measured wall temperatures are the initial wall temperatures on the outside of the tube. The code predicts inside wall temperatures, which should be close to the outside wall temperatures because of the thin wall thickness. Even without a correction for the temperature drop through the tube wall, however, the code results are still in good agreement with the data, except in the entrance region. Data from the entrance region were only used for qualitative evaluations of the effects of large wall-to-bulk temperature differences on the deposition rates [43].

Deposition data from several tests at an inlet Reynolds number of 3000 are plotted against the inverse of the initial wall temperature in Fig. 5.3. As discussed in Section 3.0, these data fall into two distinct regimes. Below 533 K (500°F), the data are well fitted by an Arrhenius-type expression with an activation energy of 8–10 kcal/mole [43]. Activation energies of this magnitude are characteristic of wall-catalyzed heterogeneous reactions. Above 533 K, the data can be fitted with a second Arrhenius-type expression with a corresponding activation energy of 40 kcal/mole. This higher activation energy is more characteristic of homogeneous chemical reactions, such as those that might occur throughout the bulk liquid fuel [43]. This observed behavior provided the basis for including both a wall and a bulk reaction in the thermal decomposition model.

To initially calibrate the model, the activation energy for the wall reaction was fixed at 8 kcal/mole and the activation energy for the bulk reaction was fixed at 40 kcal/mole. The preexponential factors for the two reactions were then adjusted independently to match the data. The results are presented in Fig. 5.4 for $A_w = 4.0 \times 10^1 \text{ cm}^4/\text{mole}\cdot\text{s}$ and $A_b = 5.0 \times 10^{18} \text{ cm}^3/\text{mole}\cdot\text{s}$. Figure 5.4 shows calculated deposition rates for three cases: (1) deposits produced only from the heterogeneous wall reaction ($A_b = 0$), (2) deposits produced only by precursors that are formed in the bulk fluid and subsequently transported to the wall by turbulent diffusion ($A_w = 0$), and (3) deposits formed as a result of both wall and bulk reactions. Although the wall and bulk reactions are assumed to occur at all temperatures, each reaction becomes more important over a different temperature regime.

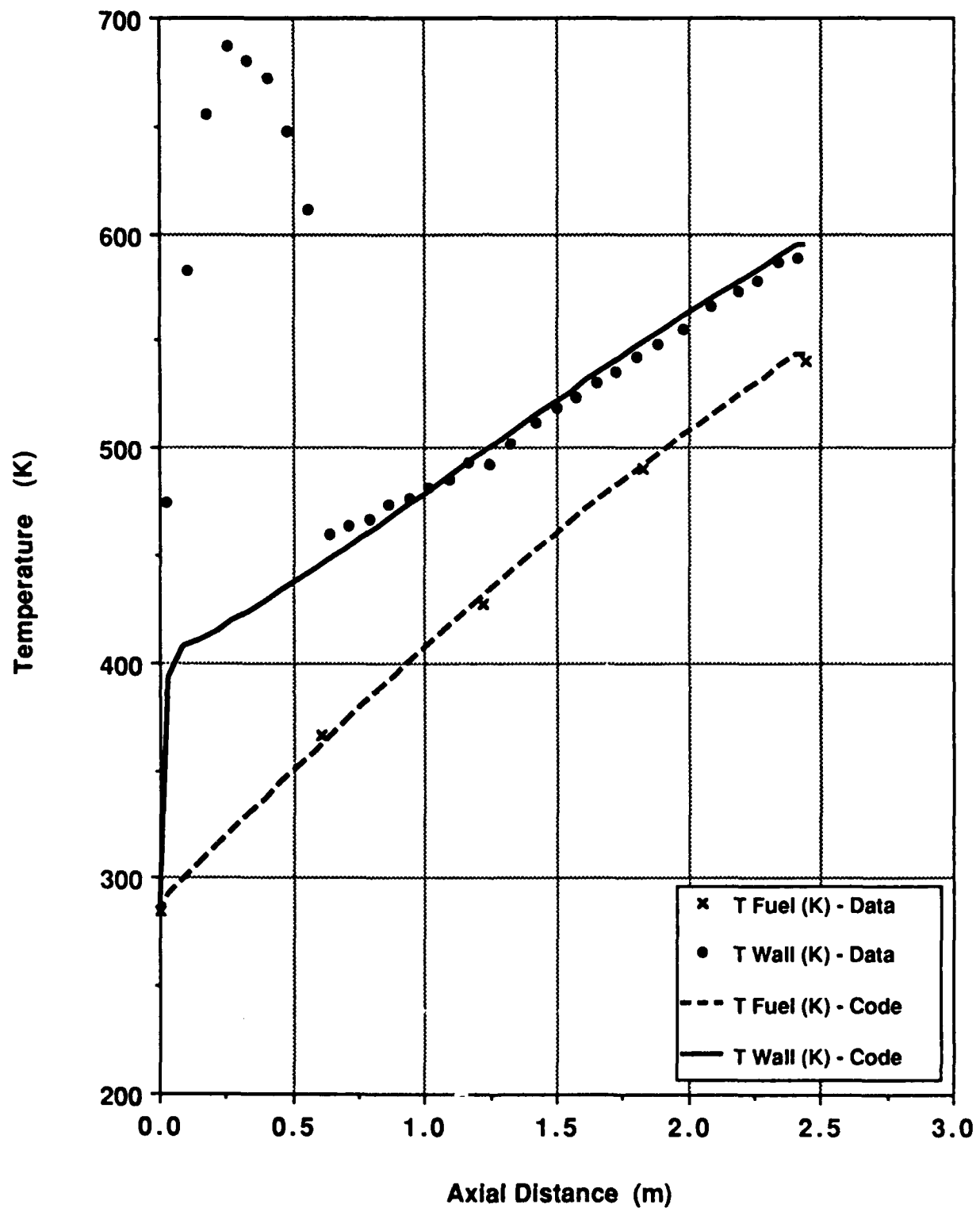


Fig. 5.1 Comparison of Predicted Temperature Profiles With Data for a Fuel Velocity of 2.1 m/s and Max $T_{wall} = 589$ K

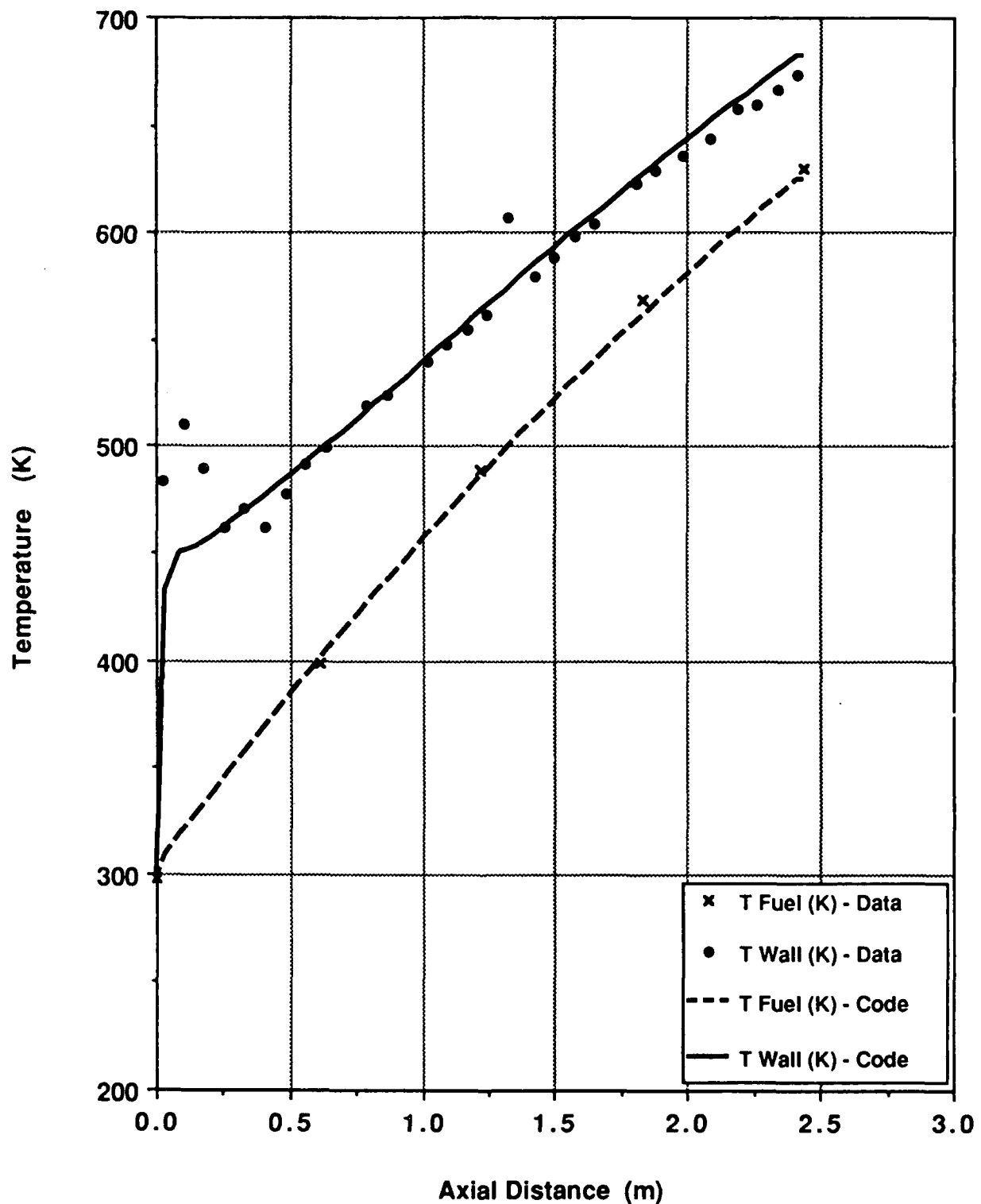


Fig. 5.2 Comparison of Predicted Temperature Profiles With Data for a Fuel Velocity of 2.1 m/s and Max $T_{wall} = 672$ K

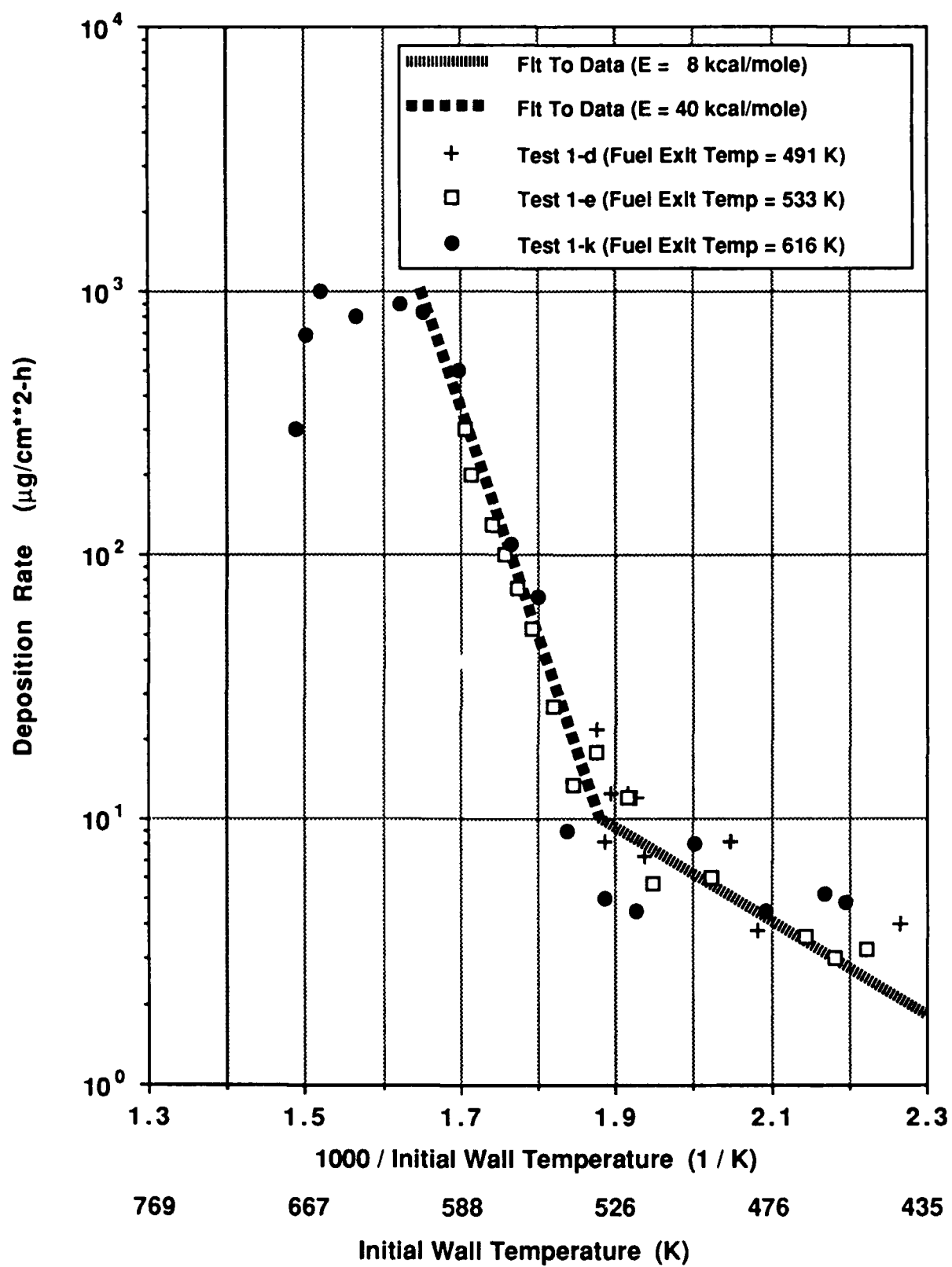


Fig. 5.3 Arrhenius Plot of JP-5 Deposition Rates for a Fuel Velocity of 2.1 m/s

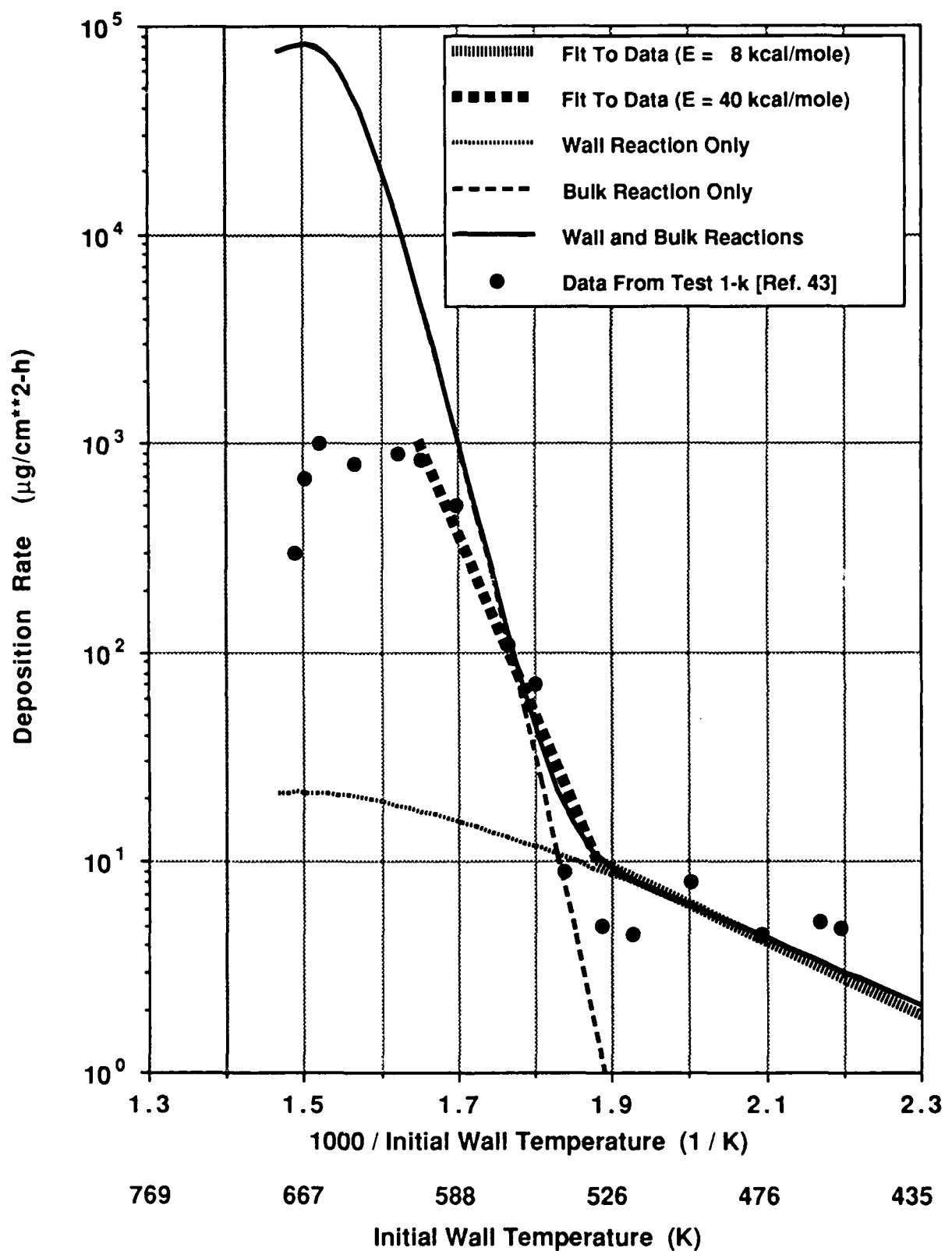


Fig. 5.4 Initial Calibration of the Chemistry Model

The preexponential factors could be adjusted to achieve a good match between the code results and the deposition data throughout most of the temperature range. However, the peak predicted deposition rates near the end of the heated tube were significantly higher (by almost two orders of magnitude) than the data. Possible reasons for this discrepancy include inadequacies in the transport model, incorrect values of the diffusion coefficient, and uncertainties in the adhesion process of precursors transported to the tube wall (represented by the parameter K). These factors were investigated in turn and the results are discussed below.

The present model assumes that deposit precursors are produced from the bulk fuel/oxygen reaction and subsequently transported to the wall, where they adhere and form a solid deposit. For turbulent flow, the transport equation for the deposit precursors uses wall functions similar to those used in the energy equation, with Pr replaced by Sc . In order to check this formulation for mass transfer, calculations were performed for a sample problem with wall deposition, but without chemical reaction. The selected sample problem stipulated that a known concentration of deposit precursors (100 wppm) flowed into a tube, where they could be transported to the wall and form a deposit. It was assumed that all precursors transported to the wall adhered and formed a deposit. This is the mass transfer equivalent of a heat transfer problem with a constant-temperature boundary condition. The tube dimensions were selected to be the same as those of the test section used by Marteney and Spadaccini [42].

To simplify the analysis of the code results, constant fluid properties were used for the calculations. The density (814 kg/m^3) and velocity (2.1 m/s) were the same as the inlet values for the transitional-flow case of Marteney and Spadaccini. (The product ρu is a constant for pipe flow.) The initial selected values of viscosity ($1.3 \times 10^{-4} \text{ kg/m-s}$) and the diffusion coefficient ($1.0 \times 10^{-8} \text{ m}^2/\text{s}$) were typical of those near the exit of the test section, where the fluid temperature is the highest. In addition, calculations were also performed with two lower values of the diffusion coefficient, so the code predictions could be checked over a range of Schmidt numbers.

The predicted results from the code were compared with the mass transfer correlation of Harriott and Hamilton [63]. Harriott and Hamilton performed mass transfer experiments in turbulent pipe flow. The rate of mass transfer was calculated from the weight loss of soluble pipe sections through which a liquid was circulated. The pipe walls were made of benzoic acid and the liquids used were water, glycerine-water solutions, and Methocel-water solutions [63]. Harriott and Hamilton fitted their data with the correlation

$$Sh = 0.0096 Re^{0.913} Sc^{0.346} \quad (5.1)$$

Here Sh is the Sherwood number (equivalent to the Nusselt number for mass transfer) and the data were fitted over the range $10^4 \leq Re \leq 10^5$ and $4.3 \times 10^2 \leq Sc \leq 1.0 \times 10^5$. This correlation fit the data with an average deviation of 5.4% and a maximum deviation of 13.2%.

The code results are compared with the predicted values from Eqn. 5.1 in Table 5.3. Fully developed turbulent flow was assumed throughout the tube. The deposition rates are proportional to the product of a mass transfer coefficient and the precursor concentration in the bulk fluid. When $Sc = 16$, the diffusion coefficient (and mass transfer coefficient) are high, resulting in a low precursor concentration at the tube exit. When $Sc = 1600$, the precursor concentration at the tube exit is high, but the mass transfer coefficient is low. The product of these two quantities is a maximum at the intermediate Schmidt number ($Sc = 160$) and so the deposition rates are the highest in this case.

The precursor concentration at the tube exit was calculated from the equation

$$C_{Pre}(L) = \frac{C_{Pre}(\text{inlet})}{\exp\left(\frac{4 \bar{h}_m L}{D u}\right)} \quad (5.2)$$

Here \bar{h}_m is the average mass transfer coefficient in the tube, as obtained from

$$Sh = \frac{\bar{h}_m D}{\mathcal{D}} \quad (5.3)$$

when Sh was calculated from Eqn. 5.1. Equation 5.2 has the same form as the equation for the axial distribution of the mean temperature in tube flow with a constant temperature boundary condition [64]. Table 5.3 shows that the code results are in reasonable agreement with values calculated from the correlation of Harriott and Hamilton, even for cases where the Schmidt numbers are lower than the minimum value (430) over which the correlation was developed. The largest differences between the code and the correlation are still much less than the observed discrepancy of nearly two orders of magnitude shown in Fig. 5.4. Thus, other possible causes for the high predicted deposition rates were investigated.

Table 5.3 Comparison of Code Results With Mass Transfer Correlation of Harriott and Hamilton [Ref. 63]

Re	Sc	Deposition Rate at Tube Exit ($\mu\text{g}/\text{cm}^2\text{-h}$)		Precursor Concentration at Tube Exit (wppm)	
		Code	Correlation	Code	Correlation
3.1×10^4	1.6×10^1	3.53×10^3	2.85×10^3	10.0	7.2
3.1×10^4	1.6×10^2	4.47×10^3	4.90×10^3	60.8	55.8
3.1×10^4	1.6×10^3	1.23×10^3	1.71×10^3	91.2	87.9

A second possible explanation for the discrepancy between the maximum predicted deposition rates and the data shown in Fig. 5.4 is that the diffusion coefficients used in the model were too high. Lower diffusion coefficients would correspond to the case where agglomerates or small particles, rather than molecular species, would be diffusing to the wall and forming a deposit. Table 5.4 shows a comparison between diffusion coefficients calculated from the baseline correlation (Eqn. 3.12) and diffusion coefficients obtained from the Stokes-Einstein equation. The Stokes-Einstein equation, which was derived for the case of large, spherical molecules diffusing in a dilute solution [26,65], is

$$D = \frac{k T}{3 \pi d \mu} \quad (5.4)$$

where k is the Boltzmann constant ($1.38 \times 10^{-23} \text{ J/K}$), d is the diameter of the solute (precursor) molecule, and μ is the solvent (fuel) viscosity. This relation would be valid for colloidal particles diffusing through liquids or high molecular weight species diffusing through a low molecular weight solvent.

For molecular-sized particles ($d = 10 \text{ \AA}^\circ$), the diffusion coefficients from the Stokes-Einstein equation are in the same range as those calculated for n-dodecane. For 1000 \AA° particles, the diffusion coefficients are much smaller. To determine the effect of the diffusion coefficient on the predicted deposition rates, the diffusion coefficients calculated from the baseline correlation were reduced by a factor of 100. (The factor 2.13×10^{-7} given in Fig. 3.5 was reduced to 2.13×10^{-9} .) The results of this calculation are shown in Fig. 5.5.

Three curves are included in Fig. 5.5. The first curve shows the predicted deposition rates using the baseline diffusion coefficient. The second curve shows the predicted deposition rates when the diffusion coefficient has been reduced by a factor of 100. The lower diffusion coefficient reduces not only the peak deposition rate, but also the deposition rates throughout the bulk-reaction region. To again match the data, the preexponential constant for the bulk reaction A_b must be increased. The third curve shows the predicted results with the lower diffusion coefficient and A_b increased from $5.0 \times 10^{18} \text{ cm}^3/\text{mole-s}$ to $1.0 \times 10^{20} \text{ cm}^3/\text{mole-s}$. This essentially corresponds to a "recalibration" of the model with the lower diffusion coefficient.

Changing the diffusion coefficient, even by a factor of 100, does not change the predicted results for the lower-temperature regime. In this regime, the deposition rate appears to be controlled by the heterogeneous surface reaction. In the current model, the same diffusion

Table 5.4 Comparison of Diffusion Coefficients for Molecules and Particles

T (K)	Self-Diffusion Coefficient for n-dodecane (Eqn. 3.12) (m ² /s)	Diffusion Coefficients From the Stokes-Einstein Equation (Eqn. 5.4)	
		(m ² /s)	°
	d = 10 Å	d = 1000 Å	
293	7.84 x 10 ⁻¹⁰	2.19 x 10 ⁻¹⁰	2.19 x 10 ⁻¹²
473	6.62 x 10 ⁻⁹	2.46 x 10 ⁻⁹	2.46 x 10 ⁻¹¹
673	1.86 x 10 ⁻⁸	1.25 x 10 ⁻⁸	1.25 x 10 ⁻¹⁰

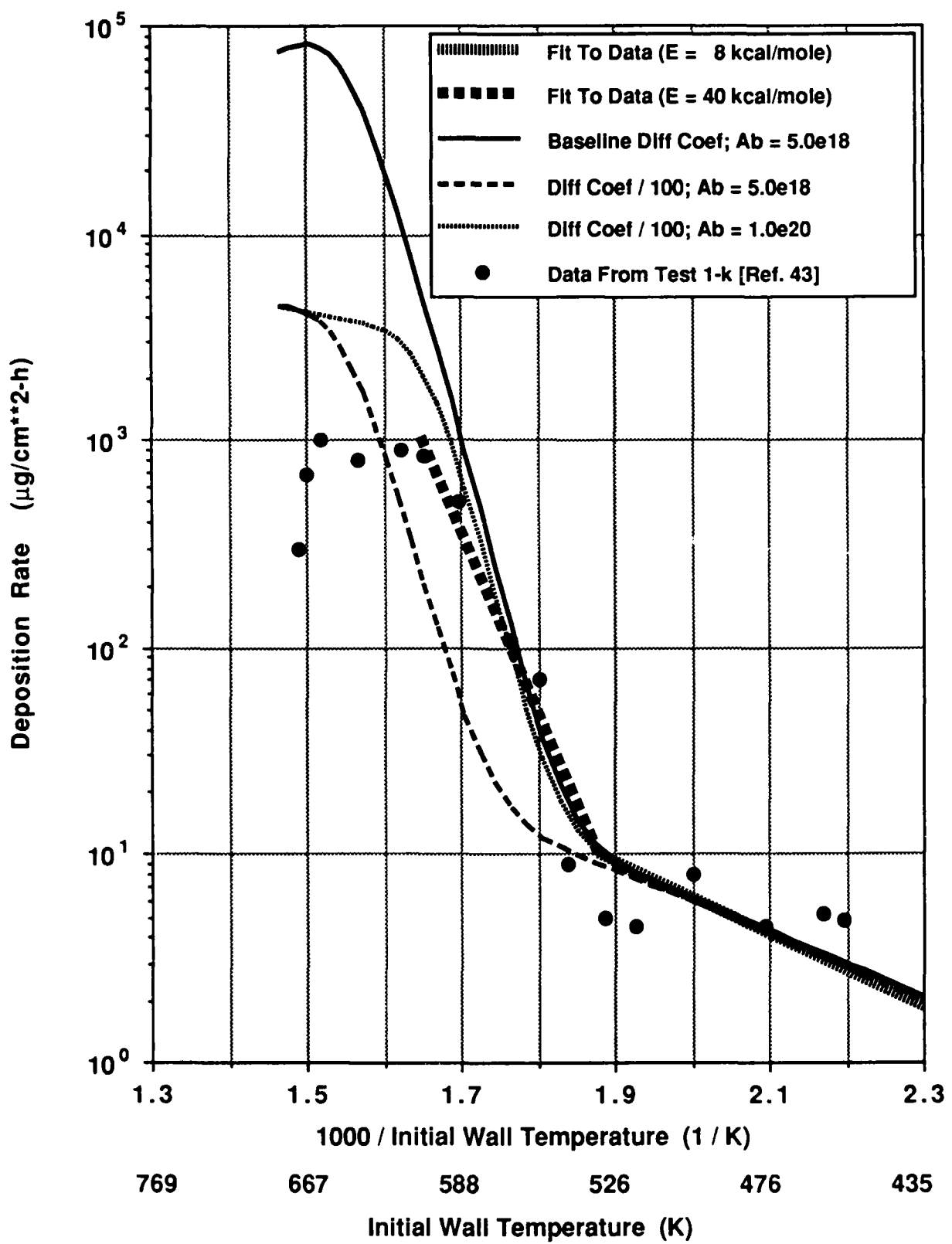


Fig. 5.5 Effect of the Diffusion Coefficient on the Predicted Deposition Rates

coefficient is used in the transport equation for both dissolved oxygen and the deposit precursors. Consequently, it is unclear as to which diffusion coefficient has a greater effect on the results. For turbulent flow at the lower temperatures, the overall surface reaction rate may be controlled by the kinetics of the reaction, rather than the rate of transport of oxygen molecules to the surface.

Although the diffusion coefficient can be reduced to provide better agreement with the peak deposition rate, the model predictions do not match the trend in the data at the high wall temperatures near the tube exit. As shown in Fig. 5.3, the measured deposition rates reach a maximum value of approximately $1000 \text{ } \mu\text{g}/\text{cm}^2\text{-h}$ and then start to decrease at higher temperatures. Although the exact cause of this behavior has not been identified, it may be related to a depletion of oxygen in the fuel, the decomposition of hydroperoxides known to occur at elevated temperatures, or to competing mechanisms in which different chemical reactions become the rate-limiting steps at higher temperatures [42]. The calculations with the baseline diffusion coefficient in Fig. 5.5 do show a slight drop-off in predicted deposition rates beyond the peak value. With the present model, this decrease appears to correspond to the depletion of dissolved oxygen in the fuel. Beyond this point the predicted deposition rates decrease, since existing deposit precursors are being transported to the wall, but new precursors are not being produced by the autoxidation reaction. With the diffusion coefficient reduced by a factor of 100, however, the predicted deposition rates do not decrease near the tube exit. Rather, the deposition rates continue to slowly increase at the highest wall temperatures. In addition, the diffusion coefficient would have to be reduced by more than a factor of 100 to match the maximum measured deposition rate of $1000 \text{ } \mu\text{g}/\text{cm}^2\text{-h}$. Thus, simply reducing the diffusion coefficient does not appear to improve the agreement between the model and the data.

A third possible explanation for the high predicted deposition rates with the original model is the uncertainty in the value of K , the parameter given in Eqn. 3.4. The baseline model assumes that all precursors transported to the wall adhere and form a deposit. This boundary condition is enforced by setting K equal to a very large number (arbitrarily selected as 10^{20}). This effectively sets the precursor concentration at the wall (C_w) equal to zero, as seen from Eqn. 3.6. However, if only a portion of the deposits stick to the wall, or if part of an existing deposit layer is subsequently removed, then this boundary condition would need to be modified.

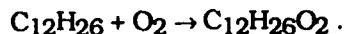
The wall boundary condition can be modified by using lower values of K . From Eqn. 3.6, K should be of the same order of magnitude as D/δ to significantly reduce the deposition

rates. If $K \gg D/\delta$, $C_w \rightarrow 0$ and all precursors stick to the surface. If $K \ll D/\delta$, then $C_w \rightarrow C_0$ and the deposition rate approaches zero. As shown in Table 5.4, the diffusion coefficient is on the order of $10^{-8} \text{ m}^2/\text{s}$ at high temperatures. The magnitude of δ in Eqn. 3.6 is much less than the pipe radius (10^{-3} m) for turbulent flow. For $\delta = 10^{-5} \text{ m}$, this suggests that K should be on the order of $10^{-8}/10^{-5} = 10^{-3} \text{ m/s}$ or less to substantially impact the wall deposition rate.

Figure 5.6 shows the predicted deposition rates for several values of the wall parameter K . Setting K equal to a very large number (10^{20}) forces the precursor concentration in the liquid fuel to be zero at the wall. Smaller values of K result in a finite (nonzero) precursor concentration at the wall, thereby lowering the deposition rate by reducing the precursor concentration gradient. Values of K in the range of 10^{-4} – 10^{-5} m/s are needed to match the peak experimental deposition rate of $\sim 1000 \text{ }\mu\text{g/cm}^2\text{-h}$.

As discussed in Section 3.0, an additional factor, DPFRAC, was included in the model. This factor accounts for the experimental observation that the deposit-forming chemistry does not appear to be in the main reaction sequence involving the formation and decomposition of oxygenated precursor species (e.g., hydroperoxides) [8]. The initial assumption that the precursors formed from the bulk reaction were directly transported to the wall could have caused the high deposition rates predicted by the model (Fig. 5.4). For example, the maximum hydroperoxide concentration measured in decomposition experiments with n-dodecane was approximately 200 mg/L or $2.0 \times 10^{-1} \text{ kg/m}^3$ [8]. At a fuel density of 814 kg/m^3 , this concentration corresponds to a hydroperoxide mass fraction of $2.0 \times 10^{-1}/8.14 \times 10^2 = 2.5 \times 10^{-4}$. Only two-thirds of the available oxygen, however, was accounted for in the hydroperoxide concentration [7].

The present model assumes that precursors are formed from the bulk reaction



At an initial oxygen mass fraction of 5.0×10^{-5} (50 wppm), the maximum predicted precursor (e.g., hydroperoxide) mass fraction would be

$$5.0 \times 10^{-5} \left(\frac{\text{MW}_{\text{Pre}}}{\text{MW}_{\text{O}_2}} \right) \text{ or}$$

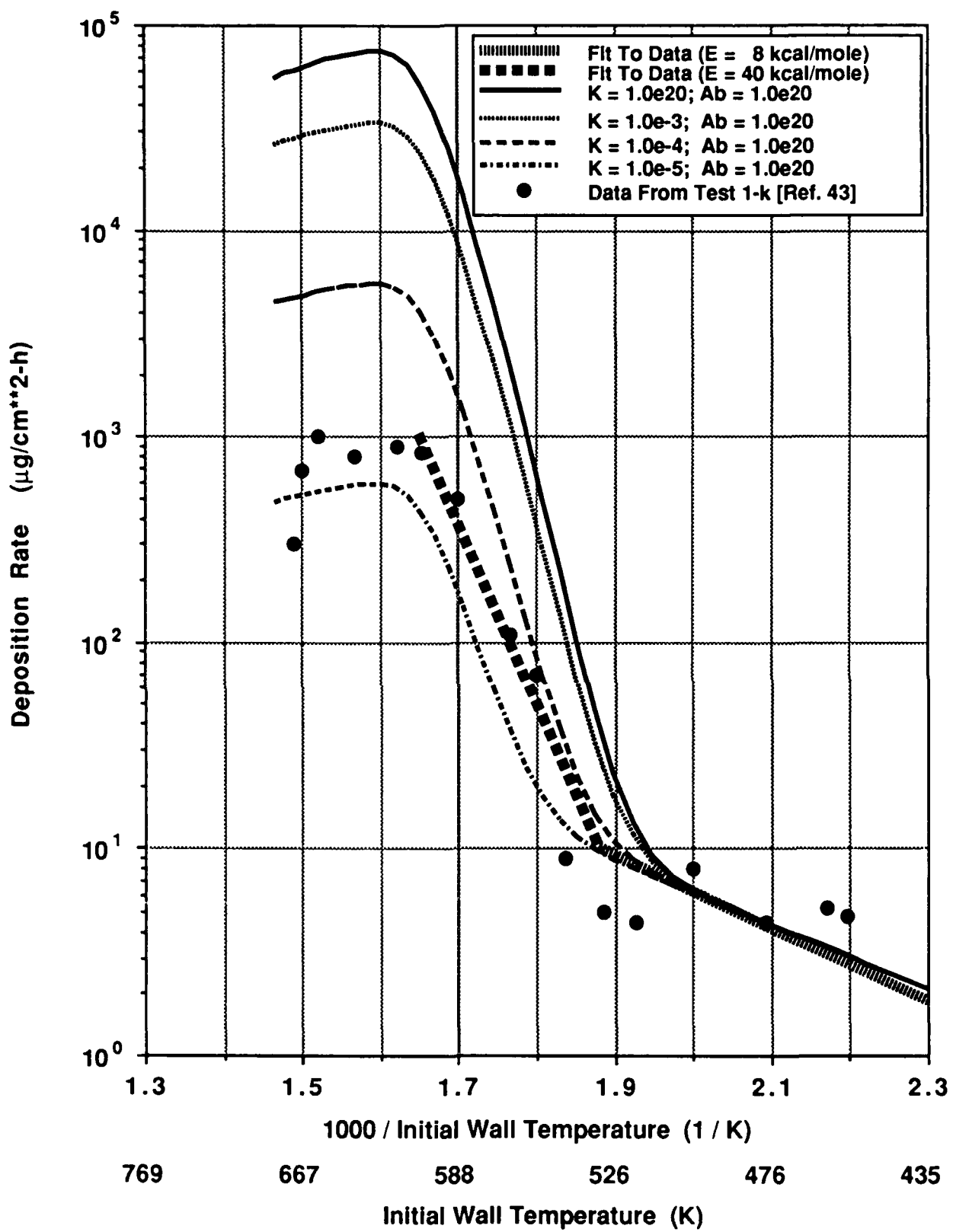


Fig. 5.6 Effect of the Wall Parameter K on the Predicted Deposition Rates

$$5.0 \times 10^{-5} \left(\frac{202}{32} \right) = 3.16 \times 10^{-4}.$$

(The present model assumes that all the available oxygen can react to form hydroperoxides. If only two-thirds of the oxygen was allowed to form hydroperoxides, the maximum hydroperoxide mass fraction would be 2.1×10^{-4} , in line with the above value of 2.5×10^{-4} obtained from n-dodecane decomposition experiments.) The Harriott/Hamilton mass transfer correlation [63] was used to predict the wall deposition rate for turbulent flow with a hydroperoxide (precursor) mass fraction of 3.16×10^{-4} . With $Sc = 16$ and $Re = 3.1 \times 10^4$, the predicted deposition rate was $1.25 \times 10^5 \mu\text{g}/\text{cm}^2\text{-h}$. This value is comparable to the maximum deposition rate obtained during the initial calibration of the model (shown in Fig. 5.4), but is two orders of magnitude higher than the maximum value of $\sim 1000 \mu\text{g}/\text{cm}^2\text{-h}$ measured by Marteney and Spadaccini [42].

The initial model also predicted that the maximum deposition rate would occur at the location of the maximum precursor concentration. The data of Hazlett, however, show that the tube deposit rating (a qualitative measure of the deposit thickness) increases as the hydroperoxide concentration decreases [8]. The hydroperoxides decompose into a variety of different products, eventually leading to the formation of solid deposits. The mechanism by which these insoluble materials are formed is not well understood. Given the uncertainty regarding the details of the reaction chemistry, together with the need to modify the model predictions to bring them into line with the deposition data, it was decided to introduce an additional empirical factor into the model.

The deposition rates resulting from the transport of precursors from the bulk fluid to the wall were subsequently modified by multiplying them by the dimensionless factor DPFRAC, which ranges from 0 to 1. This factor effectively changes the concentration of the deposit-forming species used to calculate the deposition rates. As better information is obtained on the chemistry of the thermal decomposition process, it is expected that the parameter DPFRAC will be replaced with an improved description of the kinetics governing the formation of deposit-forming species in the fuel.

The wall deposition rates predicted by the model can be modified through either the wall parameter K or the parameter DPFRAC. These two parameters are compared in Fig. 5.7. The values of $2.0 \times 10^{-5} \text{ m/s}$ for K and 1.5×10^{-2} for DPFRAC were chosen to obtain maximum

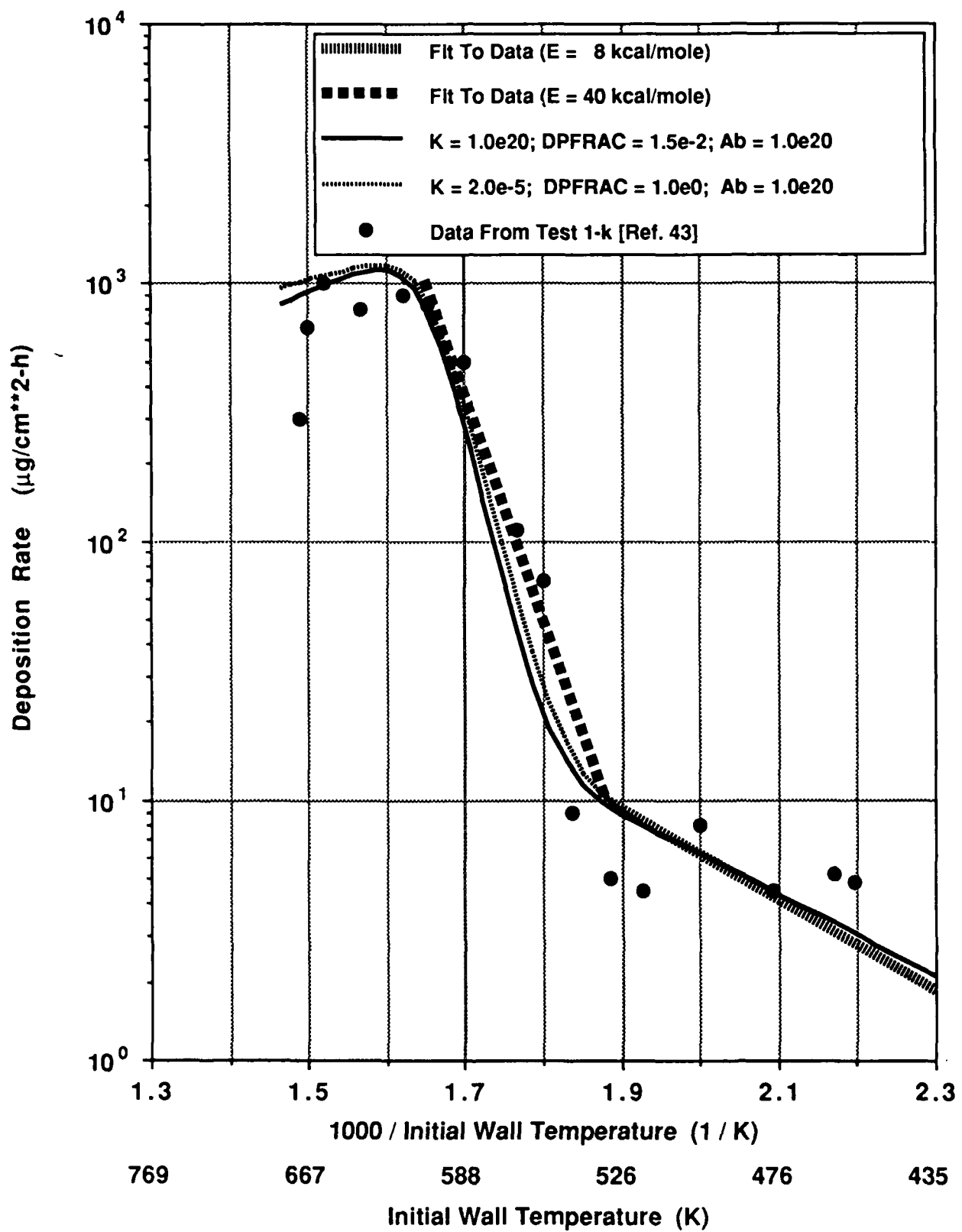


Fig. 5.7 Comparison of the Parameters K and DPFRAC on the Predicted Deposition Rates

deposition rates of $\sim 1000 \text{ }\mu\text{g}/\text{cm}^2\text{-h}$. The results are similar, although the curve for $\text{DPFRAC} = 1.5 \times 10^{-2}$ shows a somewhat higher drop-off in the deposition rates beyond the maximum value.

In addition to the reaction kinetics, there are also many uncertainties in the adhesion mechanisms occurring at the wall. Because of these uncertainties, together with the recognition that the actual concentration of deposit-forming species is probably much smaller than the maximum hydroperoxide concentration, it was decided to use the parameter DPFRAC for the final model calibration. As discussed in the following section, modifying the model with this parameter also gave a better comparison with the deposition data for laminar flow than did use of the parameter K. For the calculations presented below, the value of K was fixed at 1.0×10^{20} .

Calibration of the model now requires the determination of three parameters: the preexponential constant for the wall reaction, the preexponential constant for the bulk reaction, and DPFRAC. In the low-temperature region below 533 K (500°F), the deposition rates resulting from the bulk reaction are much smaller than the deposition rates resulting from the wall reaction. In this region, the model can be calibrated by adjusting only the preexponential constant for the wall reaction A_w . At higher temperatures where the deposition rate resulting from the bulk reaction becomes important, changes in the magnitude of DPFRAC have a greater effect on the predicted results. In this region, both DPFRAC and the preexponential constant for the bulk reaction, A_b , must be adjusted to calibrate the model.

Figure 5.8 shows predicted deposition rates for several values of DPFRAC, with $A_b = 2.0 \times 10^{19} \text{ cm}^3/\text{mole-s}$. These calculations used the same value of $A_w (4.0 \times 10^1 \text{ cm}^4/\text{mole-s})$ that was used in the initial attempt to calibrate the model shown in Fig. 5.4. Changing the value of DPFRAC alters the predicted deposition rates at high temperatures, although the peak deposition rate occurs at the same initial wall temperature. A value of $\text{DPFRAC} = 1.5 \times 10^{-2}$ gives a good match to the maximum measured deposition rate of $\sim 1000 \text{ }\mu\text{g}/\text{cm}^2\text{-h}$.

The effect of varying the preexponential constant for the bulk reaction A_b is shown in Fig. 5.9. The three cases shown in this figure all have approximately the same maximum deposition rates, but the location of the maximum value occurs at different temperatures. A value of $A_b = 1.0 \times 10^{20} \text{ cm}^3/\text{mole-s}$ provides a better fit to the data throughout most of the temperature regime. The maximum measured deposition rate of $1000 \text{ }\mu\text{g}/\text{cm}^2\text{-h}$ occurred at an initial wall temperature of 645 K [42]. Since $1000/645 \text{ K} = 1.55 \text{ K}^{-1}$, a value of $A_b = 2.0 \times 10^{19}$

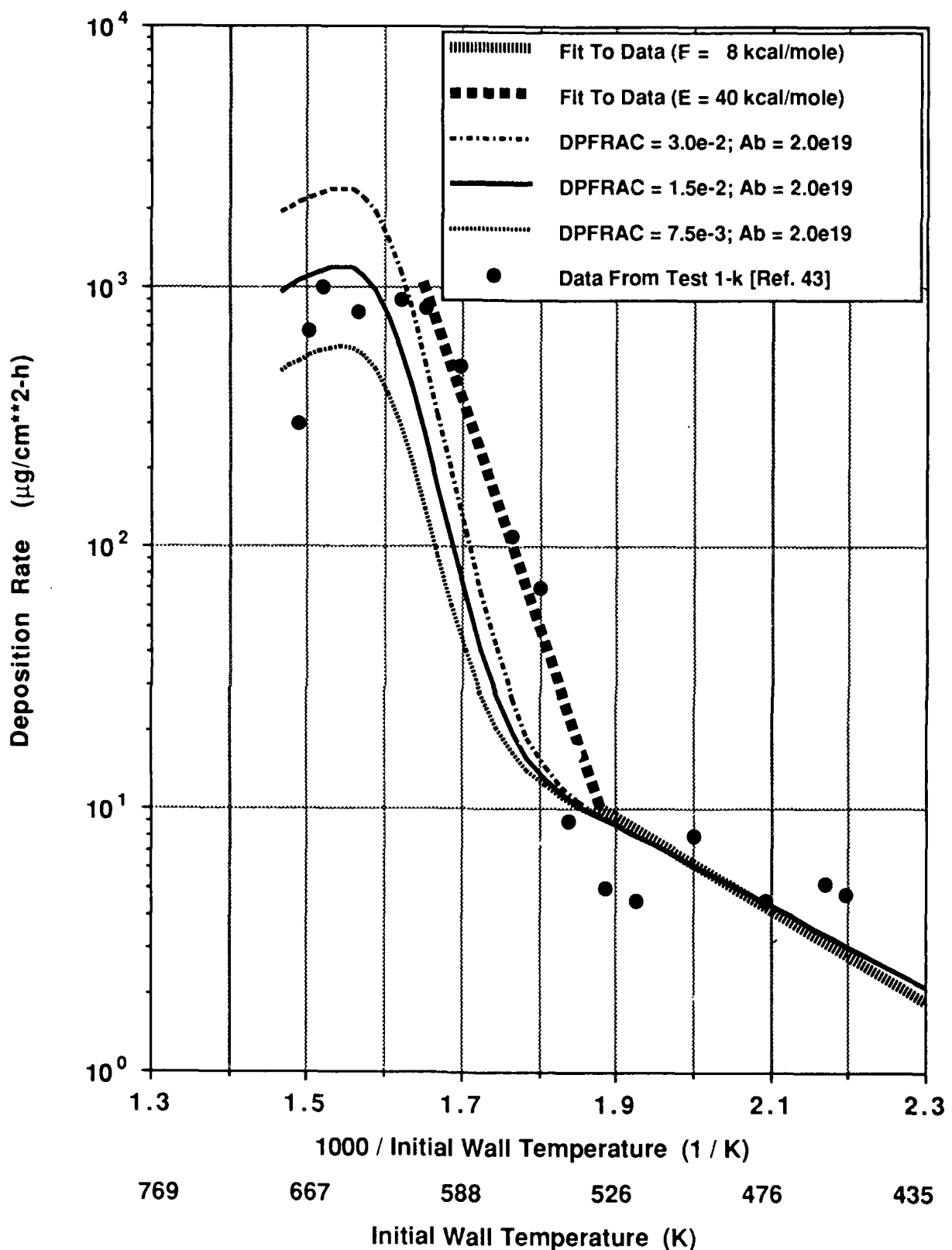


Fig. 5.8 Effect of the Parameter DPFRAC on the Predicted Deposition Rates

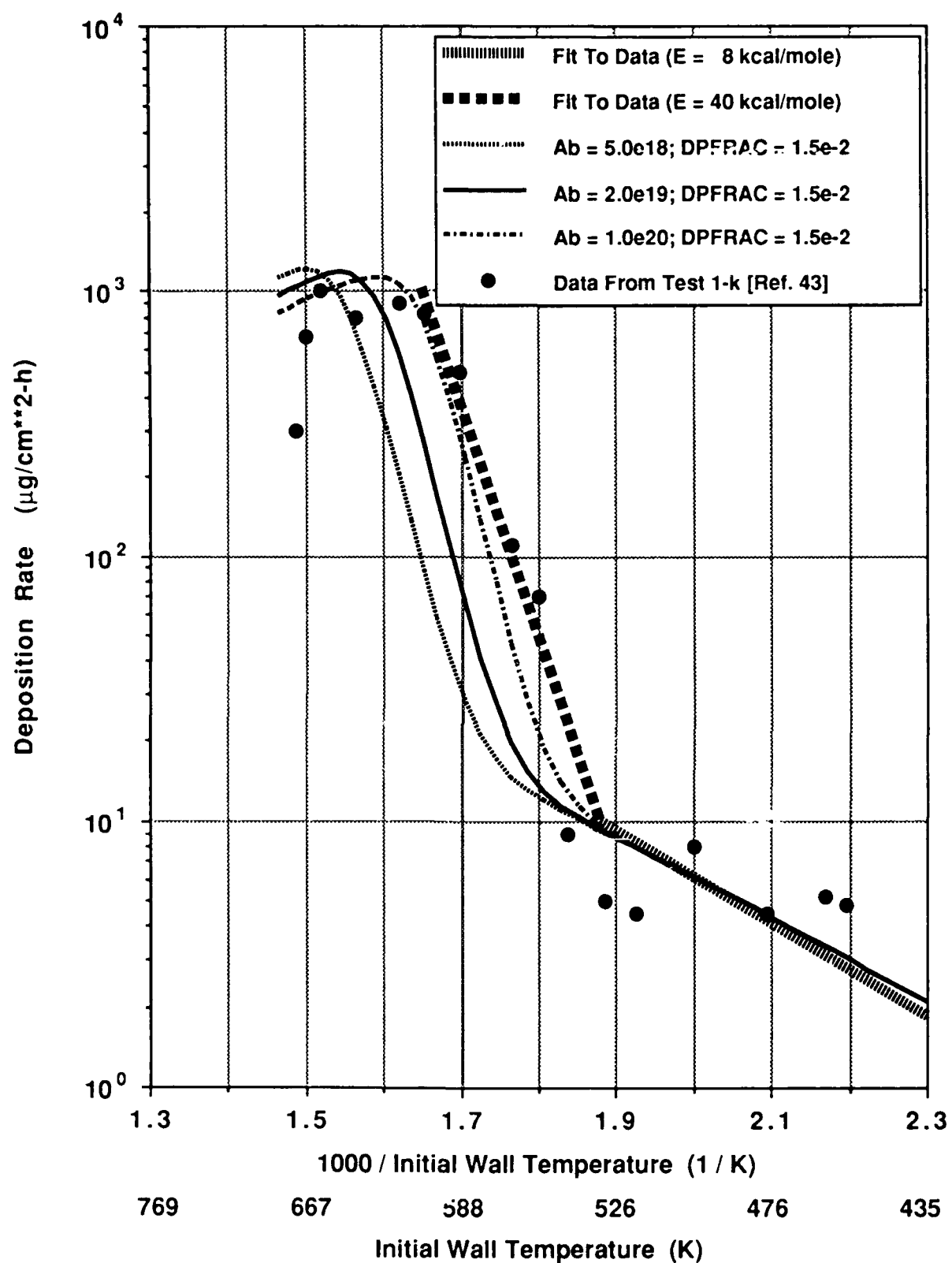


Fig. 5.9 Effect of the Preexponential Constant for the Bulk Reaction on the Predicted Deposition Rates

$\text{cm}^3/\text{mole-s}$ would provide a better match to the location of the peak deposition rate. Since the location of this peak value is not precisely known, however, it was decided to use a value of $A_b = 1.0 \times 10^{20} \text{ cm}^3/\text{mole-s}$ as the baseline preexponential constant for the bulk reaction.

The baseline values of the parameters DPFRAC, A_b , and A_w for the calibrated model were thus taken as follows: DPFRAC = 1.5×10^{-2} , $A_b = 1.0 \times 10^{20} \text{ cm}^3/\text{mole-s}$, and $A_w = 4.0 \times 10^1 \text{ cm}^4/\text{mole-s}$. Comparison of the calibrated model with additional deposition data is discussed in the following section.

5.2 Sample Calculations With the Calibrated Model

The calibration procedure discussed in Section 5.1 was performed using data from a test case with an inlet Reynolds number of 3000. For these calculations, fully developed turbulent flow was assumed to exist throughout the test section. In order to test the effects of the fuel velocity on the predicted deposition rates, it would be desirable to compare the model predictions with data for a laminar flow. A laminar flow test (Test 1-g in Table 5.1) was included in the test matrix of Marteney and Spadaccini's experimental program. The reported inlet Reynolds number for this test was 400. As discussed earlier, however, large temperature variations in the heated-tube experiments result in significant changes in fluid properties, particularly the viscosity. The inlet fuel temperature for Test 1-g was 286 K (54°F) and the fuel exit temperature was 533 K (500°F), with a maximum wall temperature of 589 K (600°F). The viscosity of JP-5 fuel changes by a factor of 10 over this temperature range [44]. Since the fuel exit temperature for Test 1-g was 533 K, the exit Reynolds number could be on the order of 4000, which is in the transitional flow regime.

This test was initially modeled by assuming laminar flow in the test section. However, the predicted temperature profiles were significantly different from the measured values. The reason for this discrepancy can be illustrated by the following sample calculations. For laminar pipe flow, the entry length required to obtain thermally fully developed flow is given by [64]

$$\left(\frac{x_{fd,t}}{D} \right) \approx 0.05 \text{ Re Pr.} \quad (5.5)$$

The product of the Reynolds number and the Prandtl number is the Péclet number

$$Pe = \frac{\rho u C_p D}{k}. \quad (5.6)$$

The product ρu is a constant for pipe flow, whereas the thermal conductivity of JP-5 is approximately 0.1 W/m-K over the temperature range 286–533 K [44]. The liquid specific heat, C_p , increases from about 1800 J/kg-K at 286 K to about 3100 J/kg-K at 533 K. Using an average value of 2450 J/kg-K, the thermal entrance length calculated from Eqn. 5.5 is 1.72 m, which is more than half the length of the 2.44-m test section. Assuming fully developed laminar flow at the exit of the test section, the Nusselt number for a constant wall heat flux is 4.36. Based on the measured wall heat flux (3.742×10^4 W/m²) and the thermal conductivity (8.4×10^{-2} W/m-K) at the bulk fuel exit temperature of 533 K, the calculated wall temperature was 774 K. This is significantly higher than the specified value of 589 K listed in Table 5.1.

The above calculation was repeated by assuming fully developed turbulent flow at the test section exit and using the Dittus-Boelter correlation [64]

$$Nu = 0.023 Re^{0.8} Pr^{0.4} . \quad (5.7)$$

In this case, the calculated wall temperature at the tube exit was 567 K, which was within 5% of the specified value of 589 K.

The calibrated model was used to predict the wall deposition rates for the case with an inlet Reynolds number of 400, corresponding to an inlet fuel velocity of 0.3 m/s (1.0 ft/s). For this calculation, however, fully developed turbulent flow was assumed to exist throughout the test section. The predicted bulk fuel and wall temperatures at the exit of the test section were 552 and 590 K, respectively, compared with the values of 533 and 589 K given in Table 5.1. The predicted fuel and wall temperatures are shown in Fig. 5.10, together with the measured values.

The corresponding deposition rates from the calibrated model are compared with the deposition data in Fig. 5.11. The magnitude of the peak deposition rate predicted by the model is in good agreement with the data, although the calculated value occurs at a lower temperature. The data points shown in Fig. 5.11 were not tabulated values, but were read from a semilog plot in Ref. 42. Thus, their locations on the graph should be regarded as approximate.

The results of long-duration, thermal decomposition tests conducted with JP-5 have been reported by Marteney [60]. These tests were performed at inlet fuel velocities of 0.3 m/s (1.0 ft/s) and 0.076 m/s (0.25 ft/s). The inlet Reynolds number for the 0.076 m/s test was only 70, so the flow presumably should remain laminar throughout the test section. Both short-duration (25 h) and long-duration (150 h) tests were performed at the low inlet velocity. The

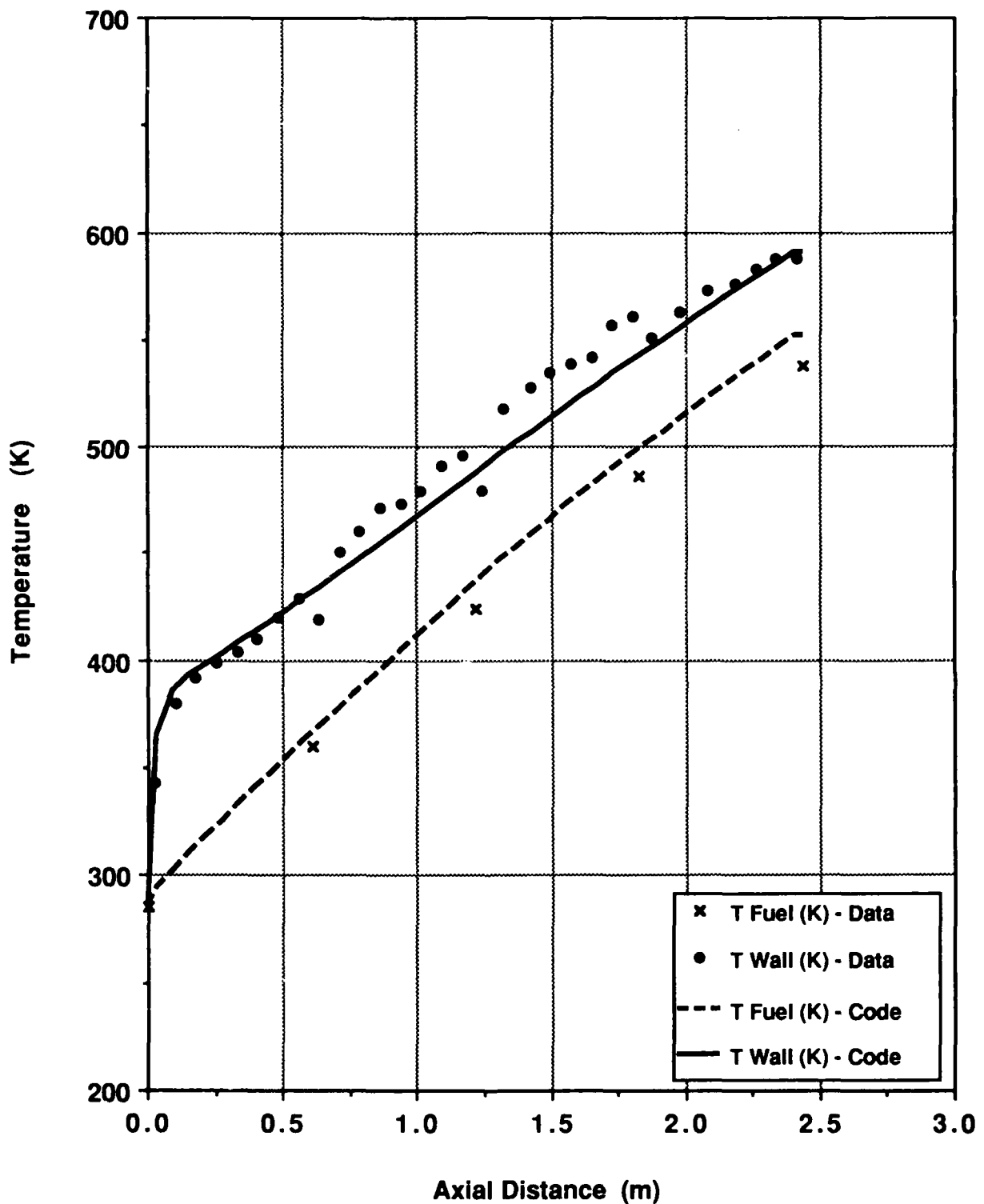


Fig. 5.10 Comparison of Predicted Temperature Profiles With Data for a Fuel Velocity of 0.3 m/s and Max $T_{wall} = 589$ K

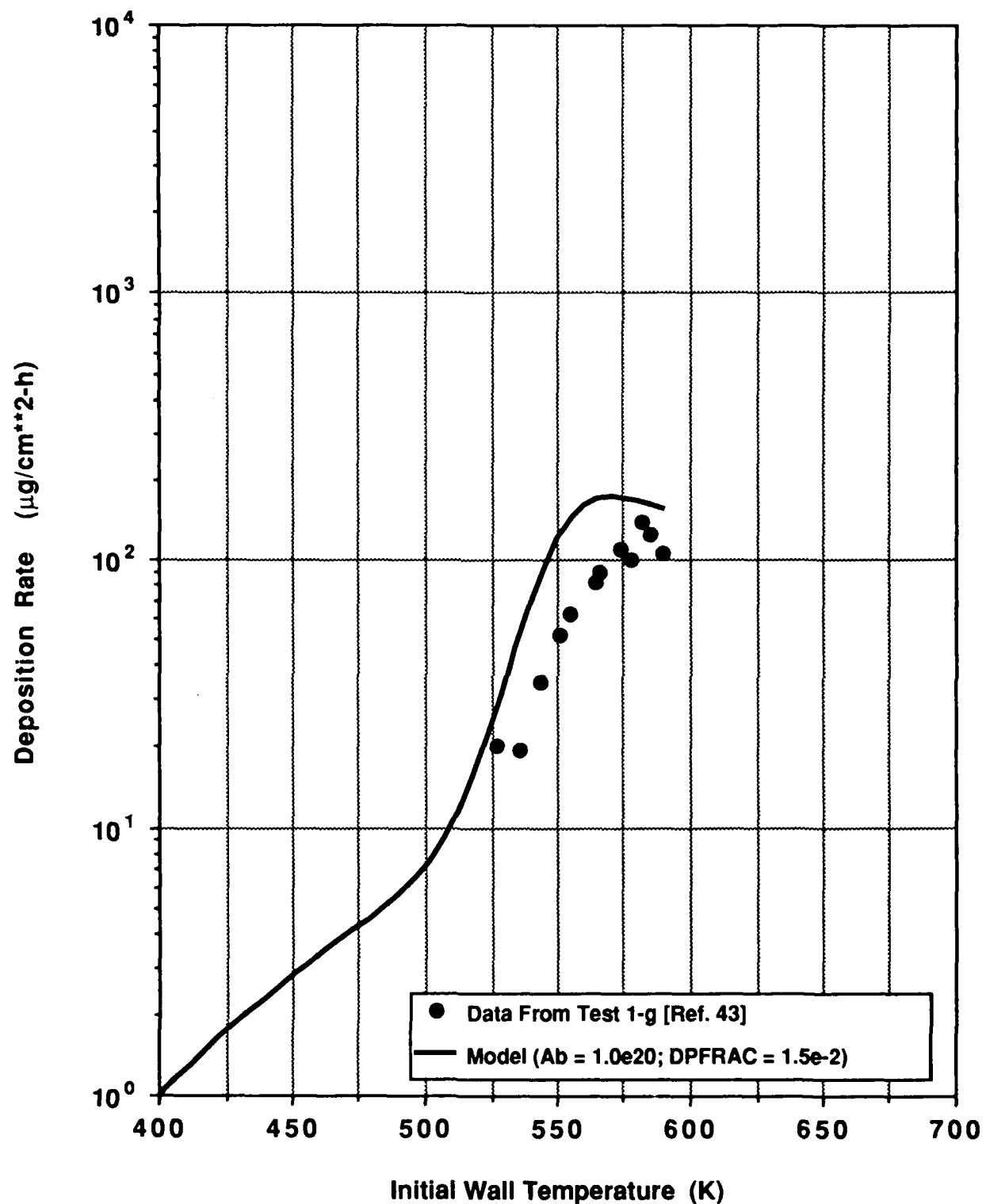


Fig. 5.11 Comparison of the Calibrated Model With the Data of Marteney and Spadaccini for a Fuel Velocity of 0.3 m/s

maximum wall temperature for the short-duration test was 589 K (600°F). Heat inputs for the tests were not reported in Ref. 60. The low-velocity test was modeled by assuming laminar flow and adjusting the input value of the heat flux to give a maximum wall temperature of 589 K. The corresponding outlet fuel temperature predicted for this case was 489 K (420°F).

The results from the calibrated model are compared with the deposition data in Fig. 5.12. Model predictions are shown for two values of the preexponential constant A_b . The figure shows that the agreement between the model predictions and the deposition data is not as good as that obtained for the higher-velocity case shown in Fig. 5.11. In particular, the peak predicted deposition rates in Fig. 5.12 are a factor of 3 lower than the data. In addition, the data show a sharp drop-off in deposition rates beyond the maximum value, whereas the model predicts a much slower drop-off. If the parameter K rather than DPFRAC is used in the calibrated model, the agreement is even worse. Using values of 2.0×10^{-5} m/s for K and 1.0 for DPFRAC (the same values shown in Fig. 5.7), the peak predicted deposition rate was 890 $\mu\text{g}/\text{cm}^2\text{-h}$, which is much higher than the measured value shown in Fig. 5.12.

The concentration of dissolved oxygen in the fuel was also measured during the experimental program. These tests were conducted in a separate heated-tube assembly not designated for deposit analysis. For these tests, the heat input to the tube was varied to achieve the desired outlet fuel temperatures. The results are shown in Fig. 5.13, along with the corresponding predictions from the calibrated model. The average oxygen concentrations were calculated in a similar manner to the bulk fuel temperatures, i.e.,

$$\bar{Y}_{O_2} = \frac{\sum_{i=1}^{i=n \text{ cell}} \rho_i A_i u_i Y_{O_2i}}{\sum_{i=1}^{i=n \text{ cell}} \rho_i A_i u_i} \quad (5.8)$$

where \bar{Y}_{O_2} is the average oxygen concentration. The summations are carried out over the total number of radial computational cells at each axial location. The denominator in Eqn. 5.8 is the total mass flow.

Using a preexponential constant of 1.0×10^{20} $\text{cm}^3/\text{mole-s}$, the model underpredicts the dissolved-oxygen concentrations for most outlet fuel temperatures. Lowering the preexponential constant to 2.0×10^{19} $\text{cm}^3/\text{mole-s}$ improves the results slightly, but still

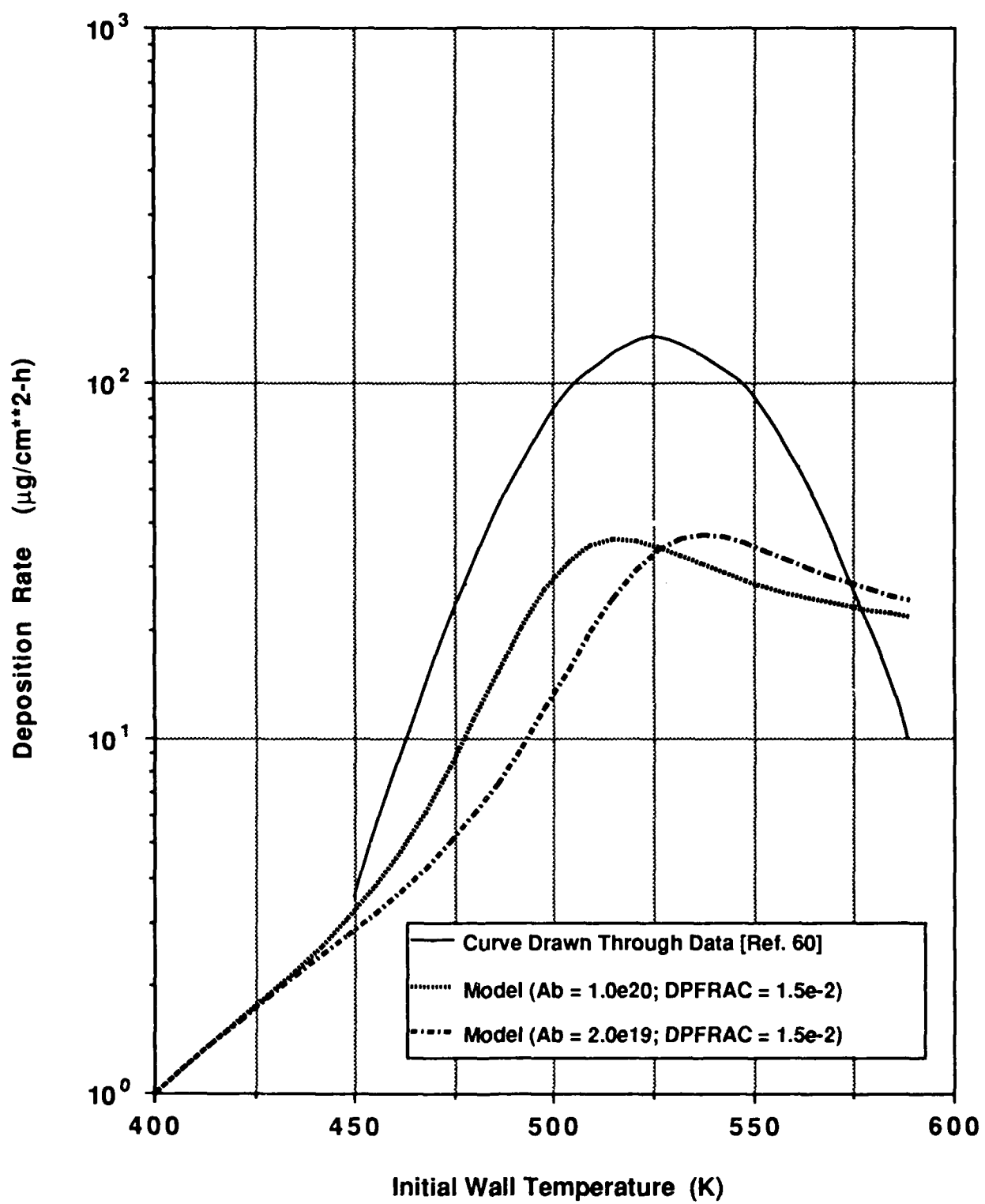


Fig. 5.12 Comparison of the Calibrated Model With Deposition Data for a Fuel Velocity of 0.076 m/s

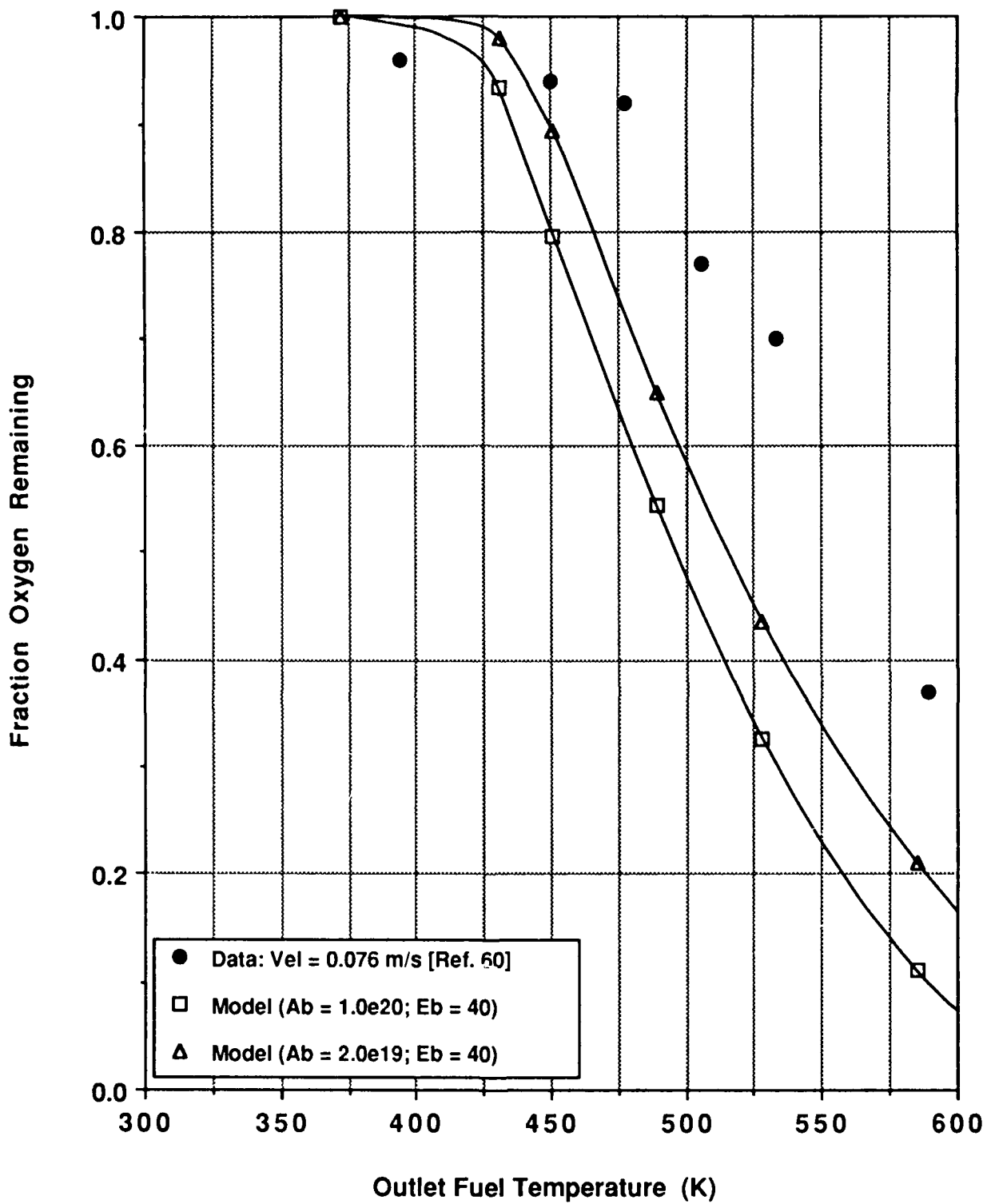


Fig. 5.13 Prediction of the Dissolved-Oxygen Concentration in Heated-Tube Tests

underpredicts the oxygen fractions at the exit of the test section. Using a preexponential constant lower than $2.0 \times 10^{19} \text{ cm}^3/\text{mole}\cdot\text{s}$ would improve the model comparison in Fig. 5.13. However, a lower preexponential constant (e.g., $5.0 \times 10^{18} \text{ cm}^3/\text{mole}\cdot\text{s}$) would result in poorer agreement with the data for the turbulent-flow case shown in Fig. 5.9. Increasing the diffusion coefficient would improve the agreement for the turbulent-flow case with a lower preexponential constant. Thus it may be possible that different combinations of DPFRAC, the precursor and oxygen diffusion coefficients, and the preexponential constant for the bulk reaction (A_b) could result in better agreement with the data sets for laminar and turbulent flow.

In performing the calculations described above, problems were observed with the density correlation at high temperatures. The thermophysical properties of JP-5 were curve-fitted over the temperature range of 273–673 K, as described in Section 3.0. The enthalpy and density values were fitted with third-order polynomials. At high enough temperatures, however, the density initially calculated from the correlation became negative. In the code, the minimum allowable fuel density was then set equal to 1.0. However, there remained a question as to how these artificial density values affected the calculated results.

The enthalpy and density property data compiled by the Shell Development Company [44] are shown in Figs. 5.14 and 5.15. Additional density data from the United Technologies Corporation, Pratt and Whitney Aircraft Group [54] are given in Fig. 5.15. The properties obtained from the Shell report were curve-fitted using second- and third-order polynomials. Curve-fit equations based on third-order polynomials were used for the calculations presented in this section. Figure 5.14 shows that the liquid enthalpies obtained from the second- and third-order curve-fits are almost identical over a temperature range of 250–850 K. The two density correlations, however, show significant differences at temperatures above the critical temperature of 685 K [44], a region where there is more uncertainty in the property data.

In order to compare the effects of the density and enthalpy correlations on the predicted results, the calculations used to obtain the dissolved-oxygen concentration were repeated at the highest fuel outlet temperature. The calculations using the third-order correlations from the baseline model were compared with results from second-order correlations obtained by ANL from J. A. Pearce [45]. The results from both cases were similar. With the third-order correlations and a preexponential constant of $1.0 \times 10^{20} \text{ cm}^3/\text{mole}\cdot\text{s}$, the predicted fuel outlet temperature was 605 K, the maximum wall temperature was 838 K, and the oxygen mass fraction at the tube exit was 3.15×10^{-6} . With the second-order correlations, the fuel outlet

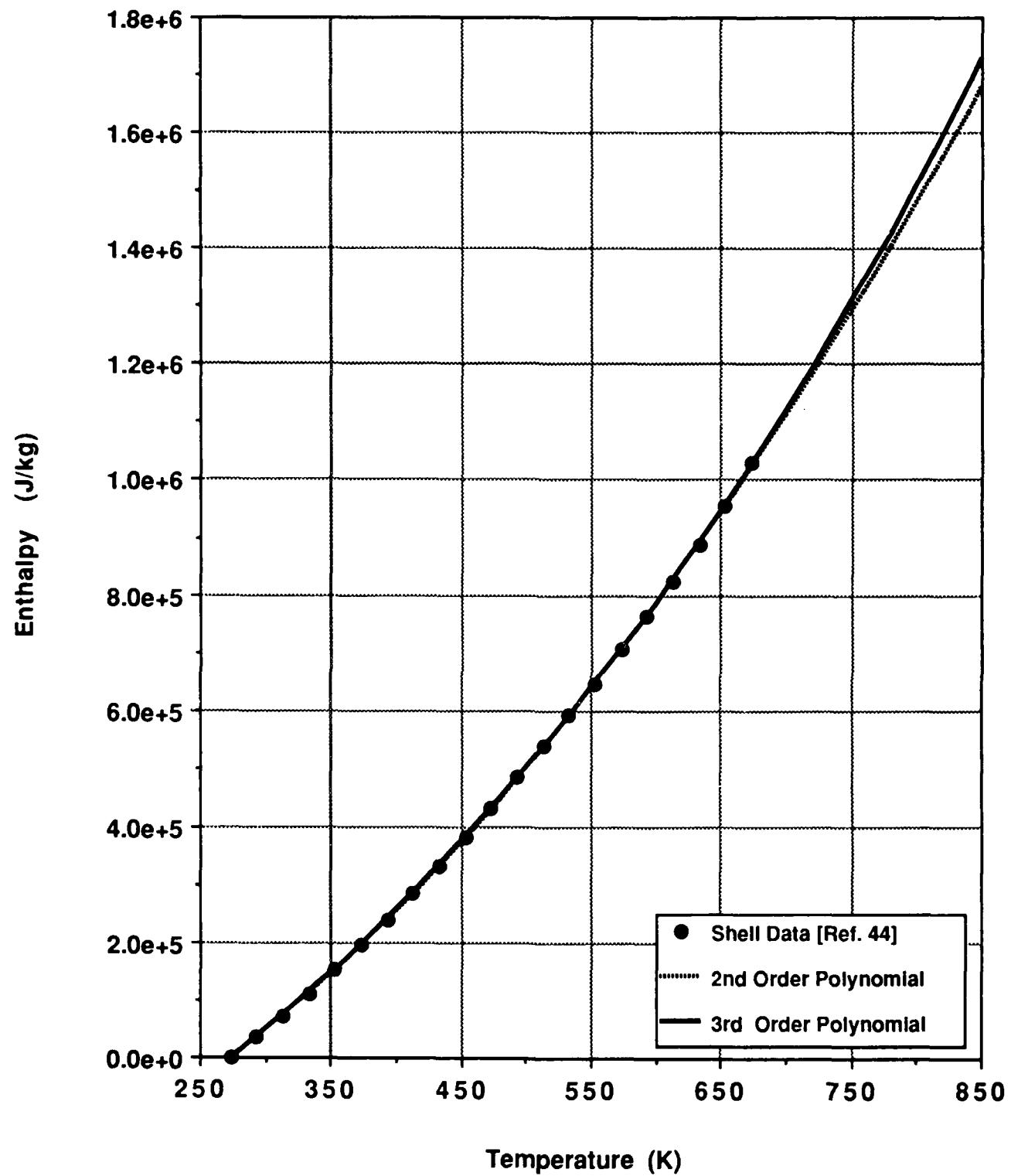


Fig. 5.14 Comparison of Enthalpy Curve-Fits for JP-5

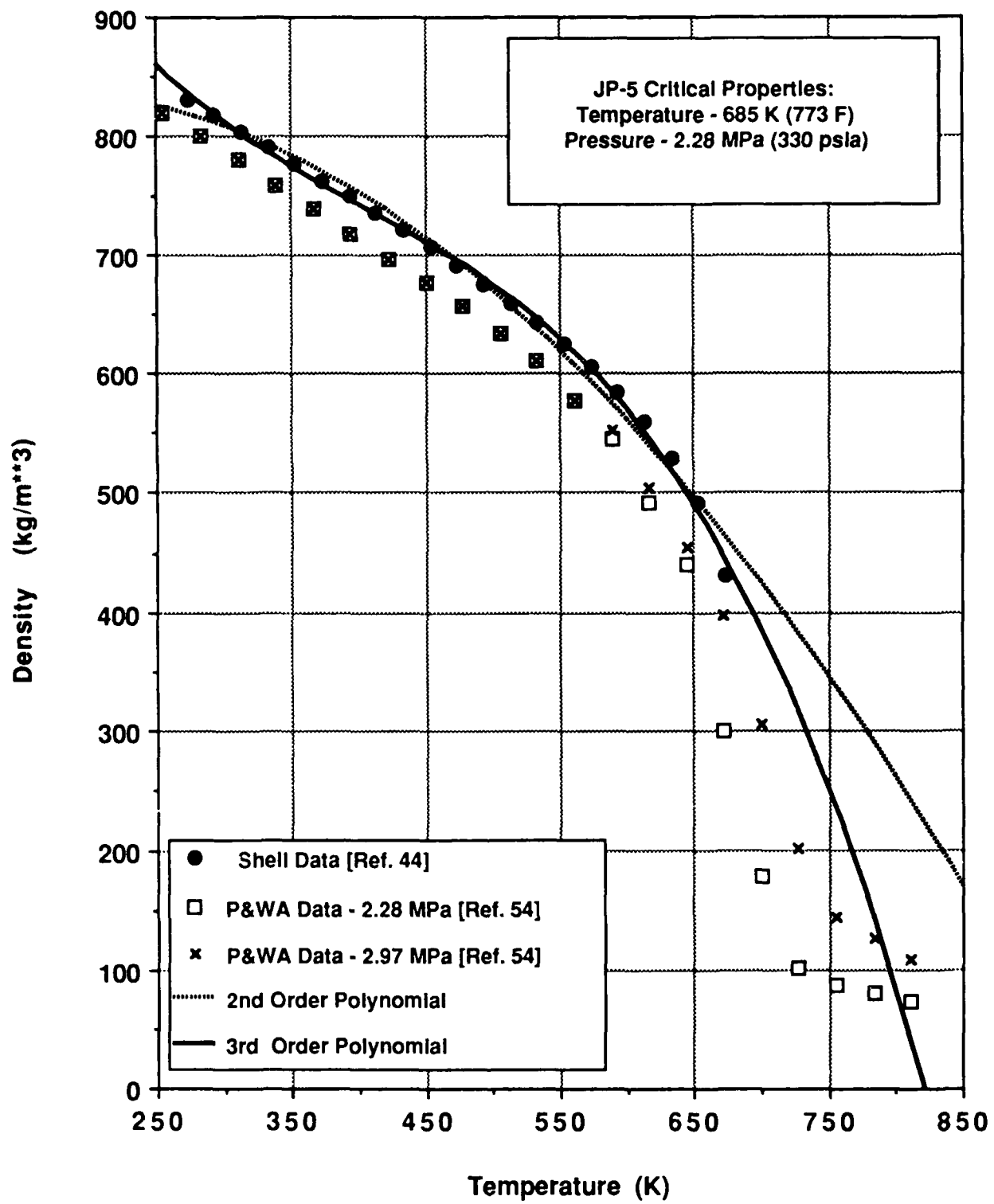


Fig. 5.15 Comparison of Density Curve-Fits for JP-5

temperature was 607 K, the maximum wall temperature was 825 K, and the oxygen mass fraction at the tube exit was 2.85×10^{-6} . The original enthalpy and density correlations were therefore used for the additional calculations with the calibrated model described below.

The final set of JP-5 deposition data used for comparison with the calibrated model was a series of earlier experiments conducted by TeVelde and Glickstein [54]. The apparatus for these tests was similar to that used by Marteney and Spadaccini [42,43]. However, the heat fluxes for the tests described in Ref. 54 were higher, resulting in fuel exit temperatures of 755 K (900°F) and initial surface temperatures up to 800 K (980°F). By contrast, the maximum bulk fuel and wall temperatures for Marteney and Spadaccini's tests (Table 5.1) were 616 and 672 K, respectively. The temperature profiles predicted by the model are compared with the data of TeVelde and Glickstein in Fig. 5.16. Again, the agreement is good except in the entrance region of the tube.

As discussed in Section 4.0, TeVelde and Glickstein conducted their experiments with two batches of JP-5 fuel: 400 gal obtained from the Naval Air Propulsion Center (NAPC) and 750 gal transferred from Pratt and Whitney Aircraft (P&WA) as residual Government property. Although laboratory analyses showed no dissimilarities between the two fuels, the P&WA fuel failed the JFTOT pressure drop criterion at 522 K (480°F), whereas the reported breakpoint temperature for the NAPC fuel was 544 K (520°F). Thus, the fuel batches were kept separate for the thermal stability tests.

The variables investigated during the JP-5 tests include the tube material (316 stainless steel and Inconel 600), fuel inlet pressure (2.76 MPa (400 psi) and 5.52 MPa (800 psi) gage), flow rate (5.67×10^{-3} to 9.45×10^{-3} kg/s (45–75 lb/h)), the test duration (1–20 h), and the fuel heating history (continuous heating or intermittent heating, i.e., 2 h of hot fuel, followed by 1 min of cold fuel). Fig. 5.17 shows a comparison between the calibrated model and deposition data for three test runs with JP-5 fuel. The three tests were conducted with the P&WA fuel batch under the following conditions: tube length – 2.44 m; tube material – 316 stainless steel; fuel pressure – 2.76 MPa gage; fuel exit temperature – 755 K; flow rate – 7.56×10^{-3} kg/s; and heating method – continuous. The only difference between the runs was the test duration, which ranged from 1.2 to 14.0 h.

As shown in Fig. 5.17, the maximum deposition rate predicted by the model lies within the scatter of the data. This peak deposition rate occurs at an initial wall temperature of 664 K, which is also in good agreement with the data. However, the model underpredicts the

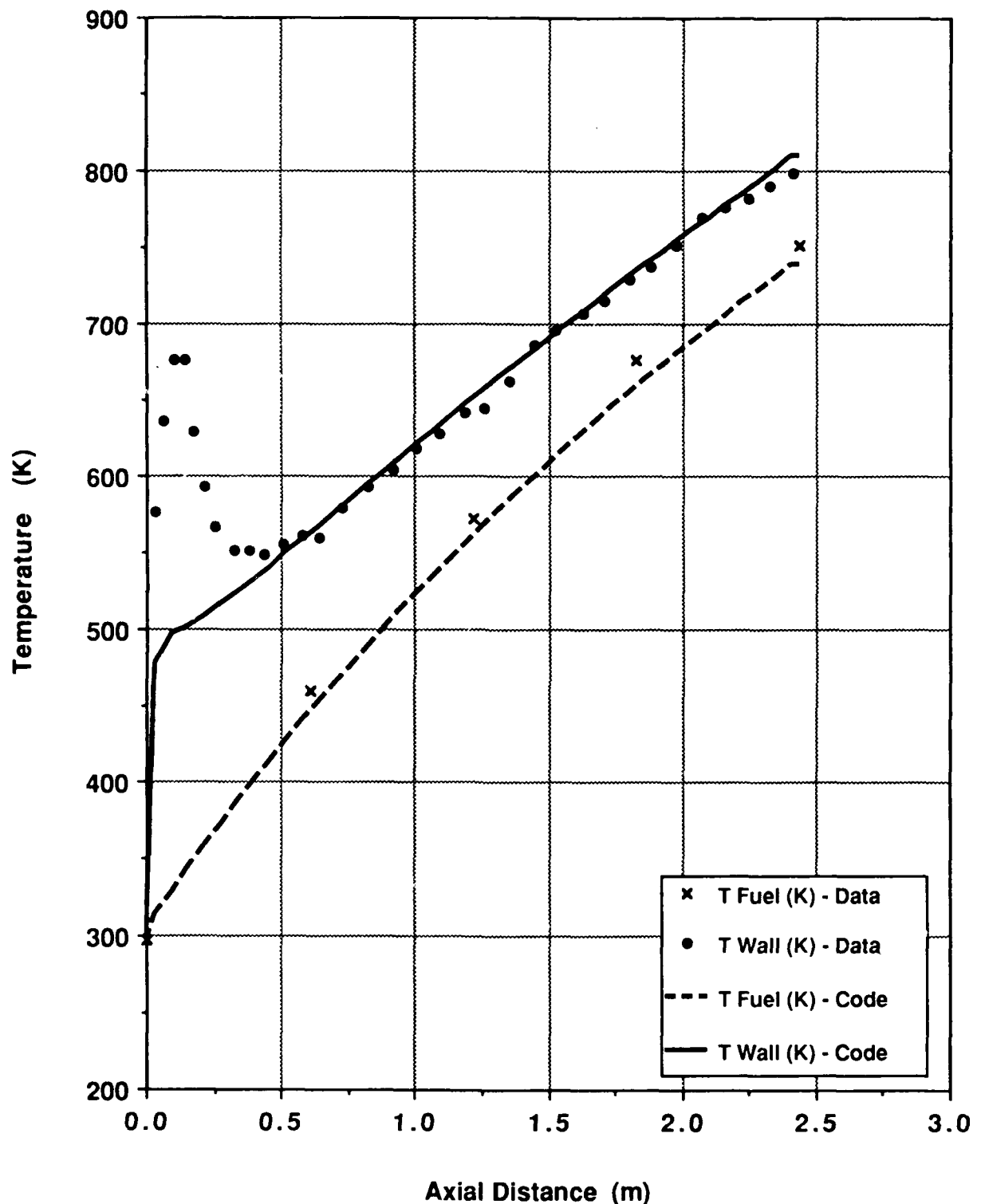


Fig. 5.16 Comparison of Predicted Temperature Profiles With the Data of TeVelde and Glickstein

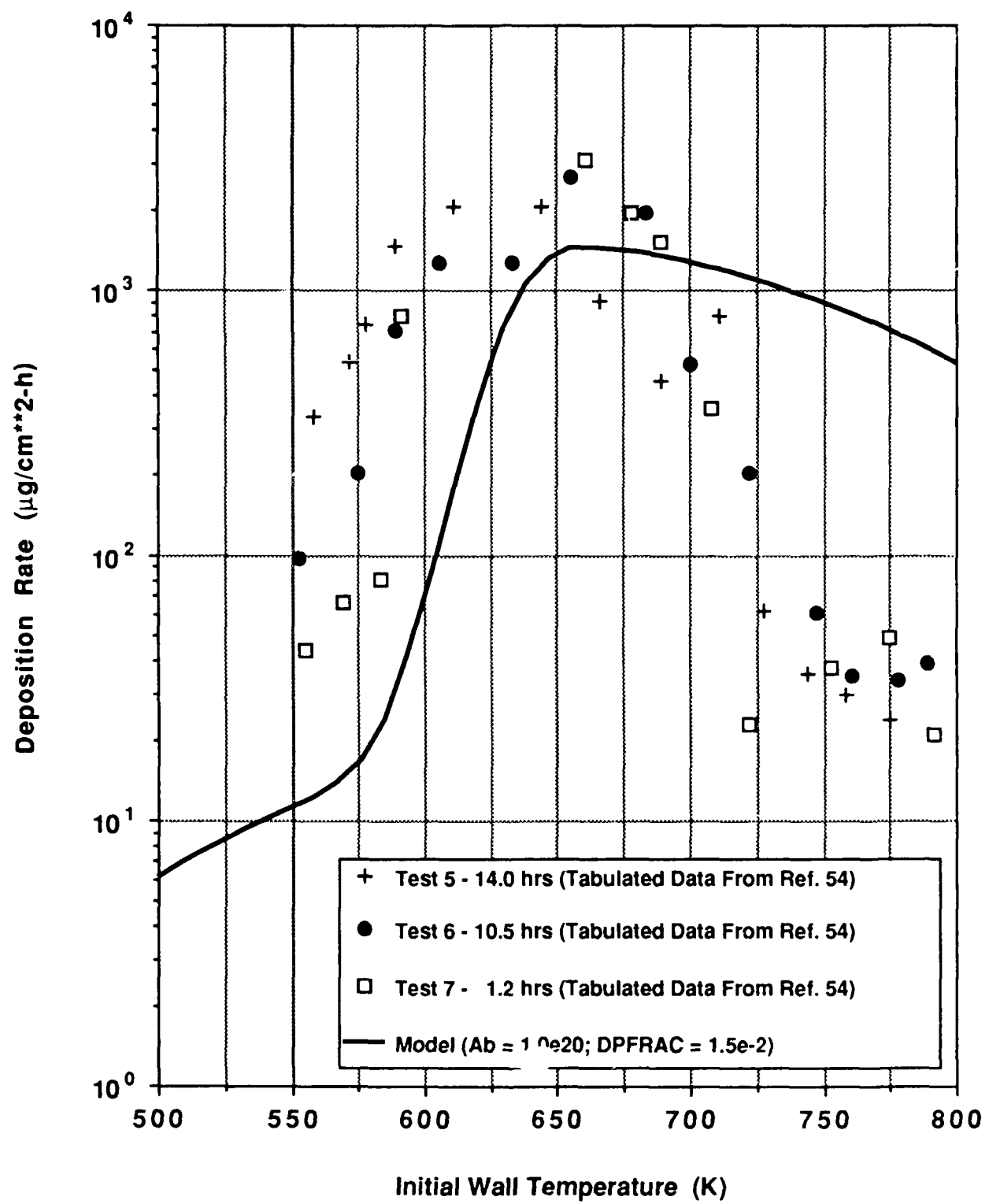


Fig. 5.17 Comparison of the Calibrated Model With the Data of TeVelde and Glickstein for a Fuel Velocity of 2.57 m/s

deposition rates at lower temperatures and overpredicts the deposition rates at higher temperatures. The data also show a steep drop-off in deposition rates following the peak value, whereas the model predicts a more gradual decrease. For the laminar-flow case shown in Fig. 5.12, the model also predicted a gradual decline in deposition rates at higher temperatures, whereas the data showed a sharper decline.

The primary objective of this section was to determine how well the calibrated model could predict deposit formation rates for JP-5 fuel over a range of flow rates and fuel temperatures. Calibration of the current model involved the determination of three parameters from experimental data: DPFRAC, the preexponential constant for the wall reaction, and the preexponential constant for the bulk fuel reaction. Comparison of the model with additional data sets indicated that the peak predicted deposition rates agreed reasonably well with the data for turbulent flow, but were too low (by a factor of 3) for laminar flow. In both cases, the data show a steep decline in deposition rates at high temperatures, whereas the model predicts a more gradual decline. Comparison of the predicted oxygen concentrations for laminar flow shows that the model overpredicts the rate of oxygen consumption at low flow rates. Because of uncertainties in the decomposition kinetics, diffusion coefficients, and wall adhesion mechanisms, it is difficult to identify the reasons for these discrepancies. Although the current model can be used to calculate trends in fuel deposition rates under different conditions, much more additional development will be required before it can be used to make reliable, quantitative predictions.

5.3 Sample Variable Profiles for Pipe Flow

The thermal decomposition model described in this report was incorporated into a two-dimensional version of a multigrid computer code developed at ANL [48]. Computational fluid dynamic and chemistry codes such as this provide a wealth of information about the characteristics of various flow fields. Validation of these calculations, however, requires detailed measurements of temperatures, species concentrations, and other variables throughout the flow field. Since such detailed measurements are often unavailable, code calibration frequently relies on comparisons with global measurements such as overall pressure drops and average temperatures.

Detailed, two-dimensional temperature and species profiles have not been measured in the heated-tube, thermal decomposition experiments. As an illustration of the type of information that can be obtained from the present two-dimensional model, Figs. 5.18 through 5.20 show predicted temperature, oxygen, and deposit precursor profiles along the length of a

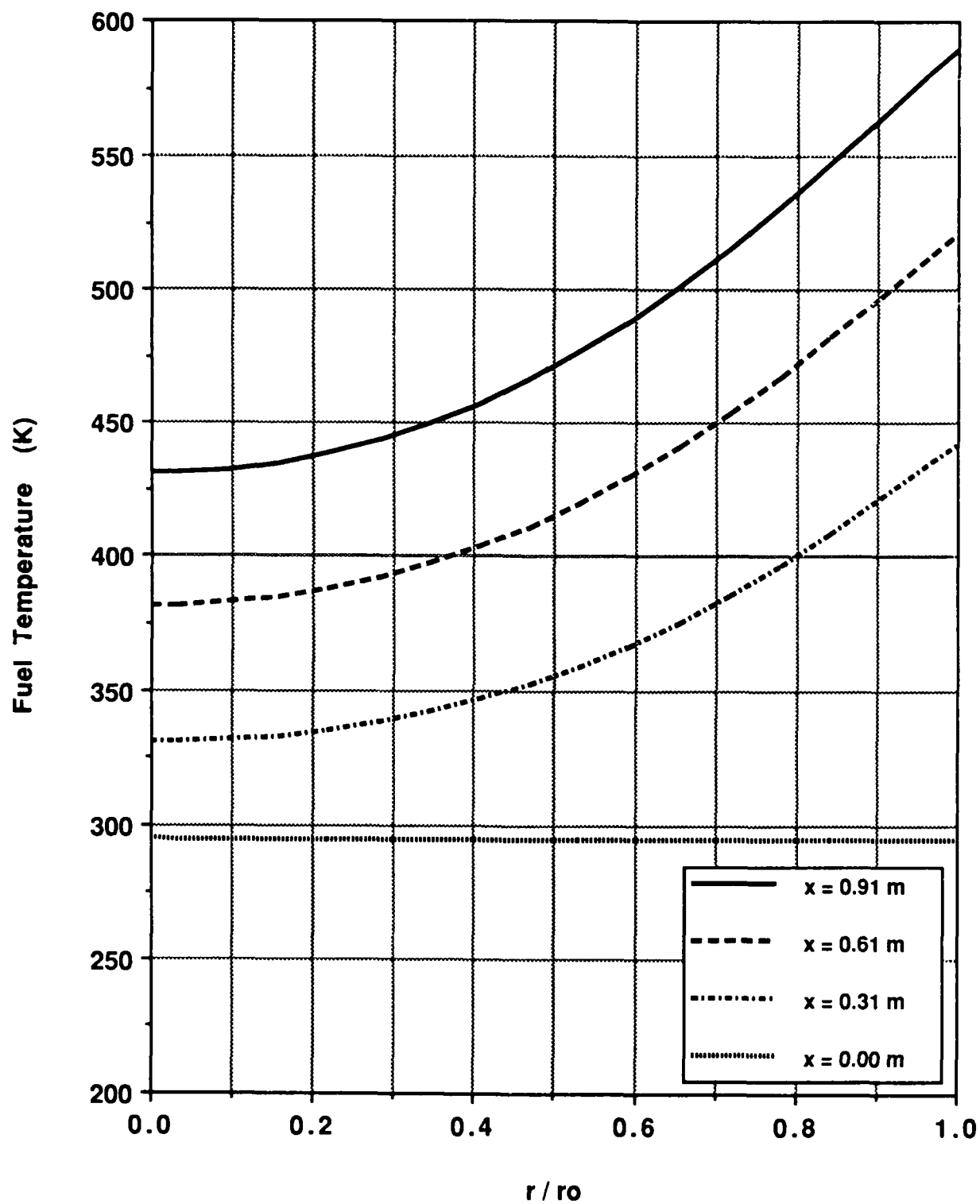


Fig. 5.18 Predicted Temperature Profiles for Laminar Flow

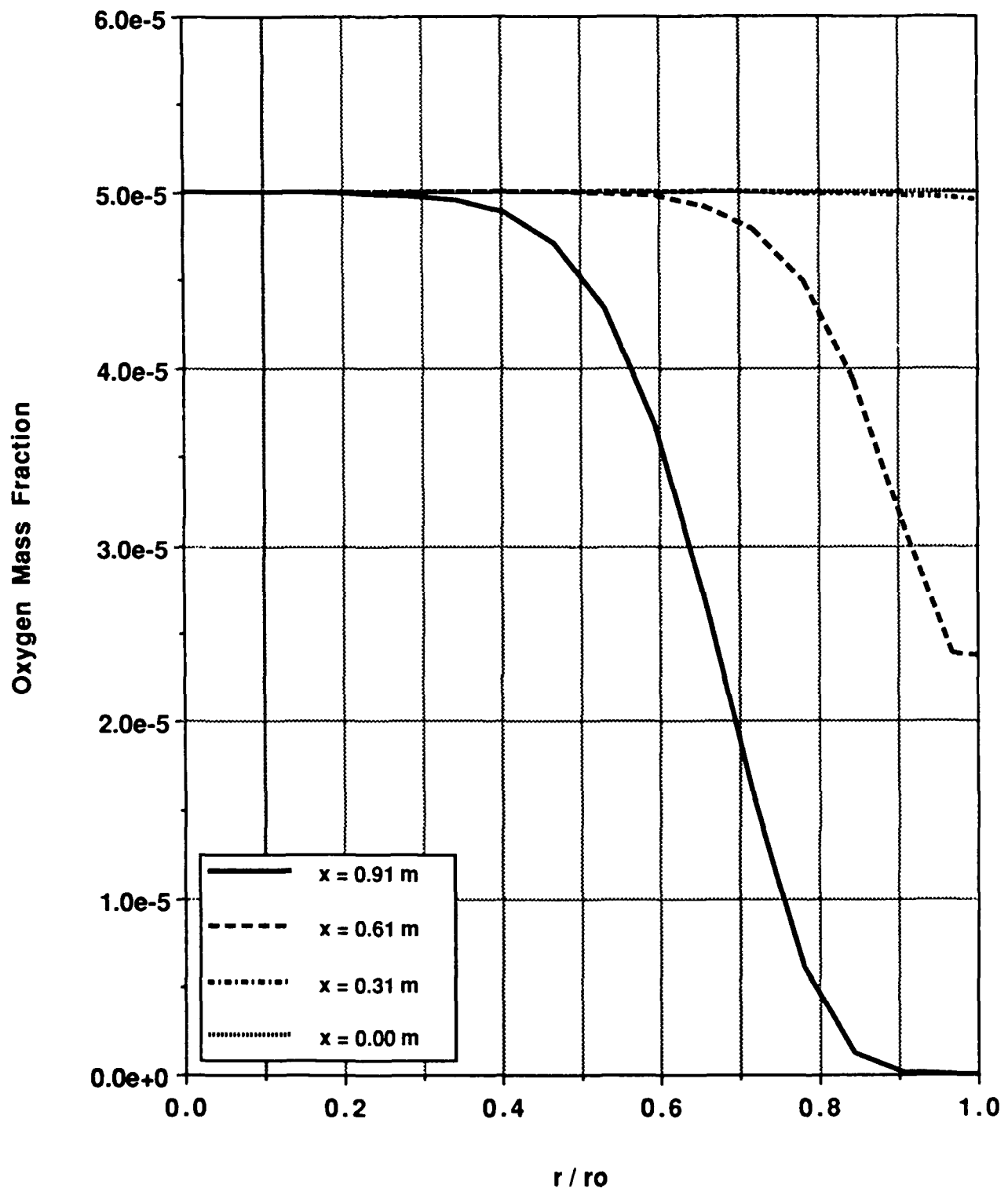


Fig. 5.19 Predicted Oxygen Profiles for Laminar Flow

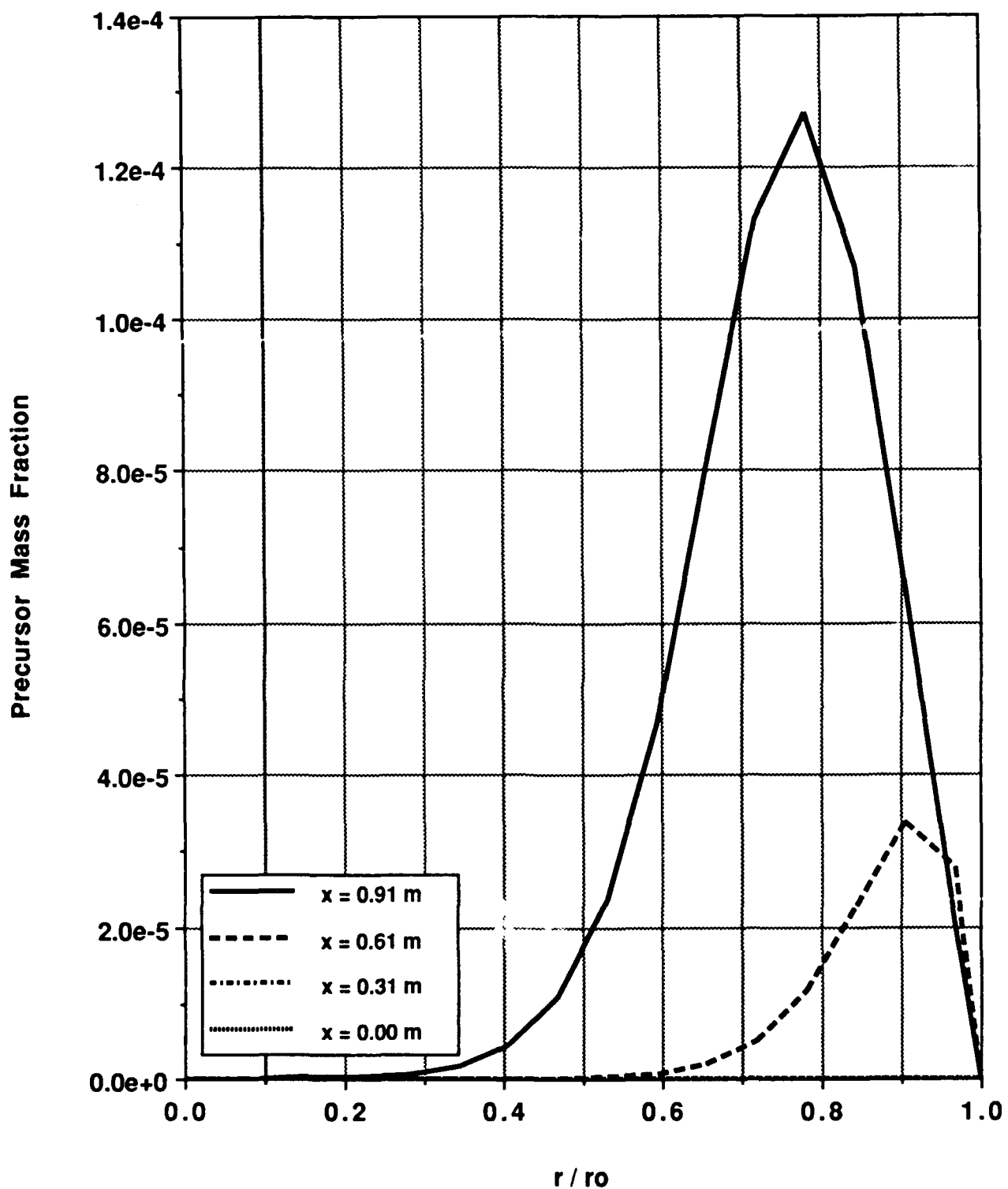


Fig. 5.20 Predicted Deposit Precursor Profiles for Laminar Flow

heated tube. The calculations were performed for the laminar-flow case discussed in Section 5.2 with an inlet flow velocity of 7.6×10^{-2} m/s. The preexponential factor for the bulk reaction was 2.0×10^{19} cm³/mole-s. The figures show radial profiles of the variables at the tube inlet ($x = 0.0$ m), tube exit ($x = 0.91$ m), and two intermediate axial locations. The flow was assumed to be axisymmetric and the calculations were performed over one-half of the tube diameter, with the tube center being treated as a symmetry line.

At an axial location of 0.31 m, the model predicts very little reaction of the dissolved oxygen. The maximum fuel temperature at this point is less than 450 K. As the fuel temperature increases, oxygen is depleted near the tube wall and the concentration of deposit precursors increases. At the tube exit, the model predicts that the dissolved oxygen has been depleted near the wall, but a significant concentration of oxygen still remains in the center of the tube. These profiles result from the large radial temperature differences across the tube in laminar flow.

The deposit precursor concentration shows a peak between the tube wall and the tube centerline. Near the center of the tube, very little oxygen has reacted and thus the precursor mass fraction is small. Near the tube wall, the precursor concentration goes to zero because of the imposed boundary condition that all deposit-forming species that reach the wall will adhere and form a deposit. At each axial location, the predicted deposition rate is proportional to the product of the precursor diffusion coefficient and the precursor concentration gradient at the tube wall.

The above calculations were performed using the multigrid solution algorithm with three computational grids. The finest grid consisted of 40 cells in the axial direction and 16 cells in the radial direction. As shown in Fig. 5.20, the precursor concentration gradients are quite steep near the tube wall. Since the predicted deposition rates depend on the magnitude of these concentration gradients, it is important that the deposit precursor mass fractions are calculated with sufficient accuracy, particularly near the tube wall. In order to insure that the calculated results did not vary significantly with the mesh size, the above calculations were repeated using four grids. In this case, the finest grid consisted of 80 cells in the axial direction and 32 cells in the radial direction. The predicted radial profiles using four grids are compared with the corresponding calculations for three grids in Figs. 5.21 through 5.23. As shown, there is very little difference between the two sets of calculations. Figures 5.24 and 5.25 show corresponding comparisons for the axial temperature profiles and the predicted deposition rates. Again, there are only small differences between the calculations.

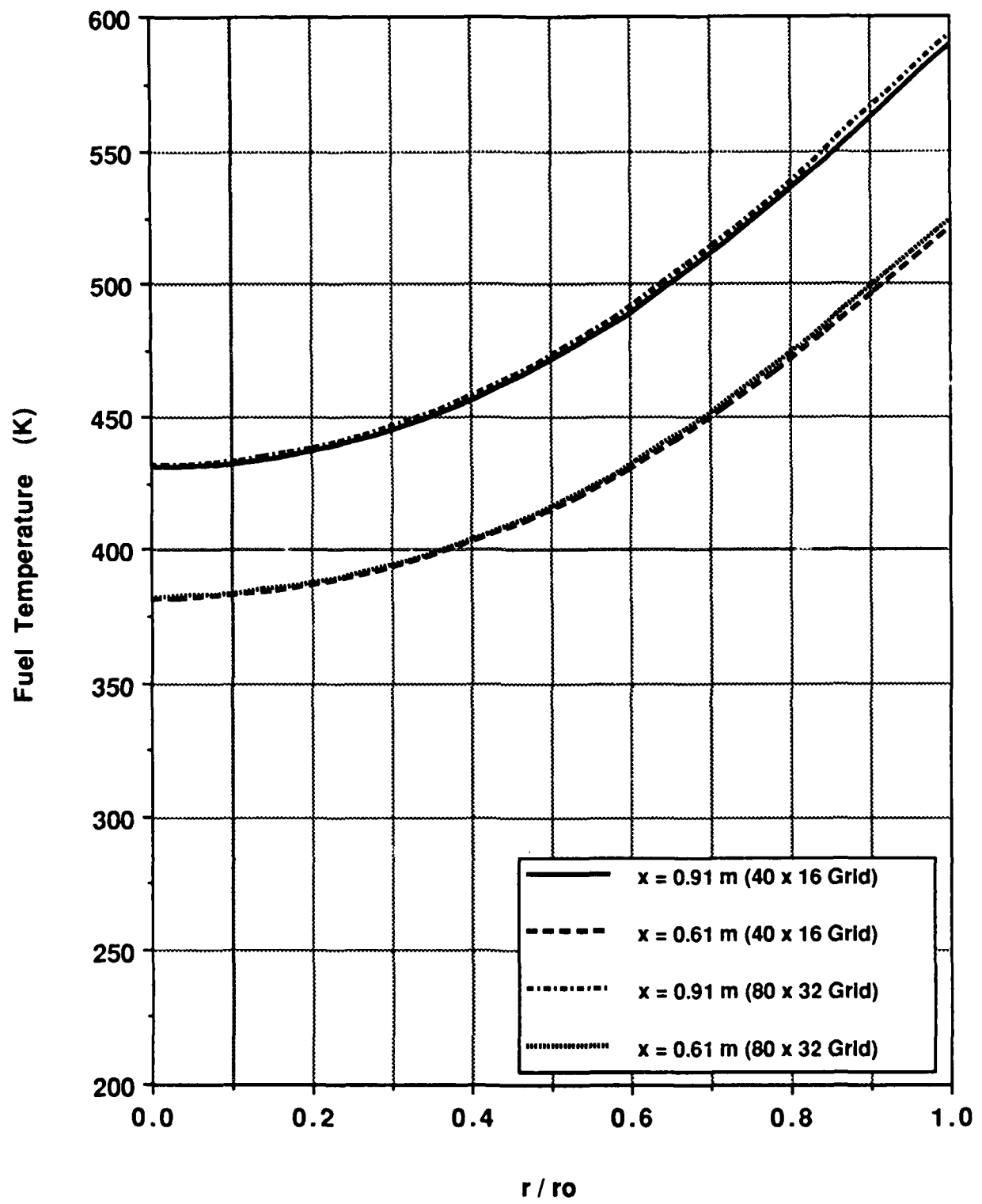


Fig. 5.21 Predicted Temperature Profiles (Grid Comparison)

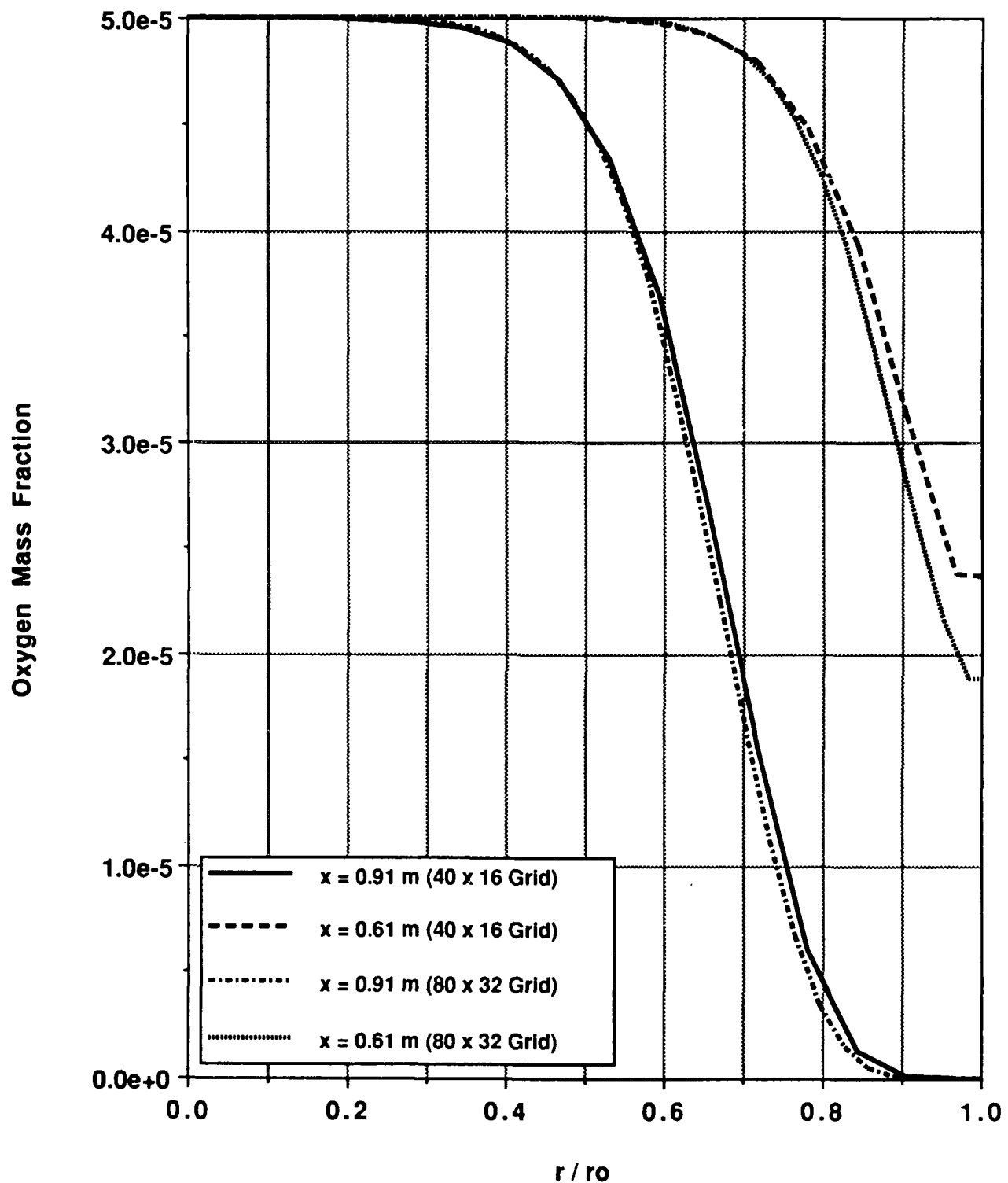


Fig. 5.22 Predicted Oxygen Profiles (Grid Comparison)

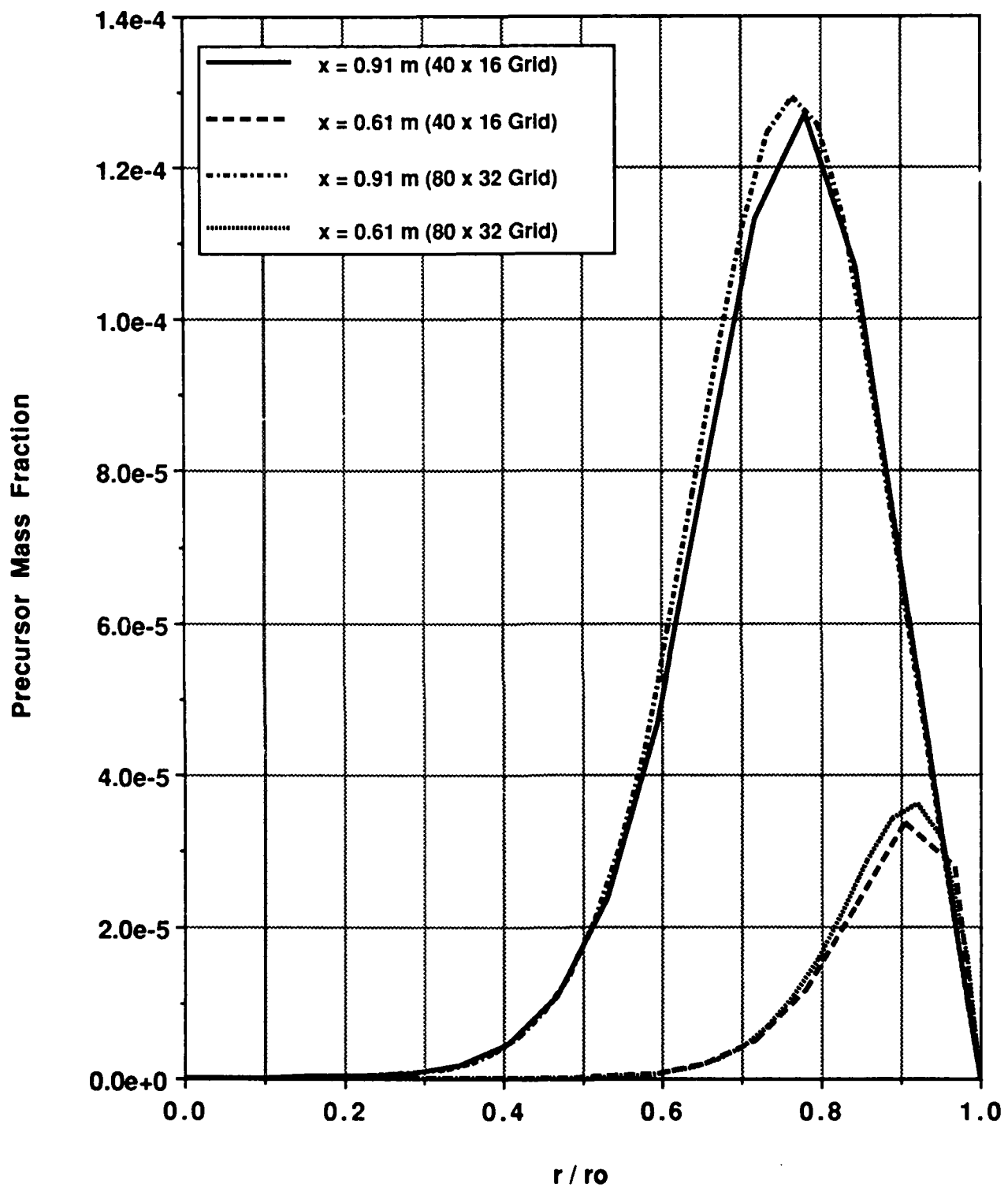


Fig. 5.23 Predicted Deposit Precursor Profiles (Grid Comparison)

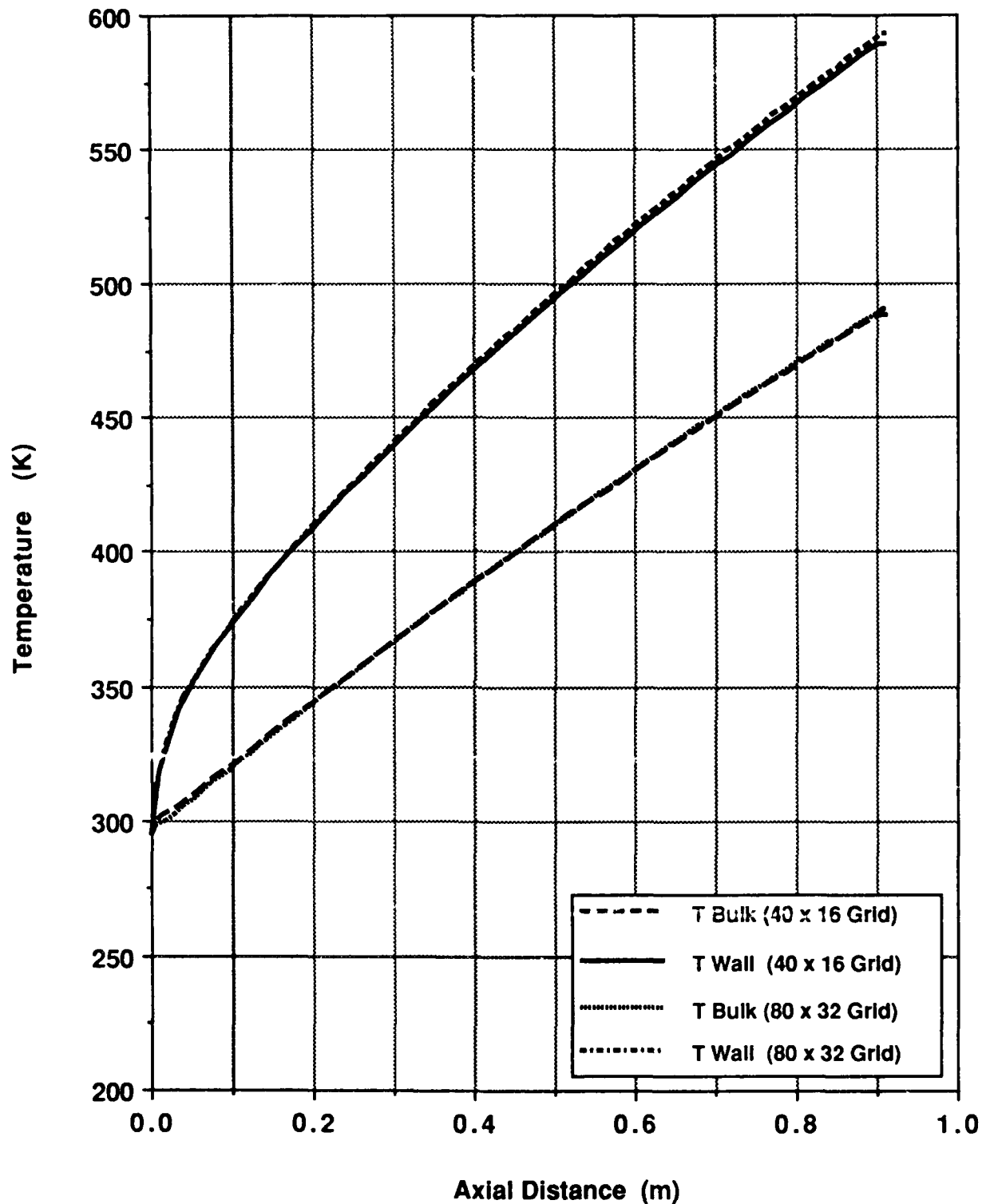


Fig. 5.24 Predicted Axial Wall and Bulk Fuel Temperatures (Grid Comparison)

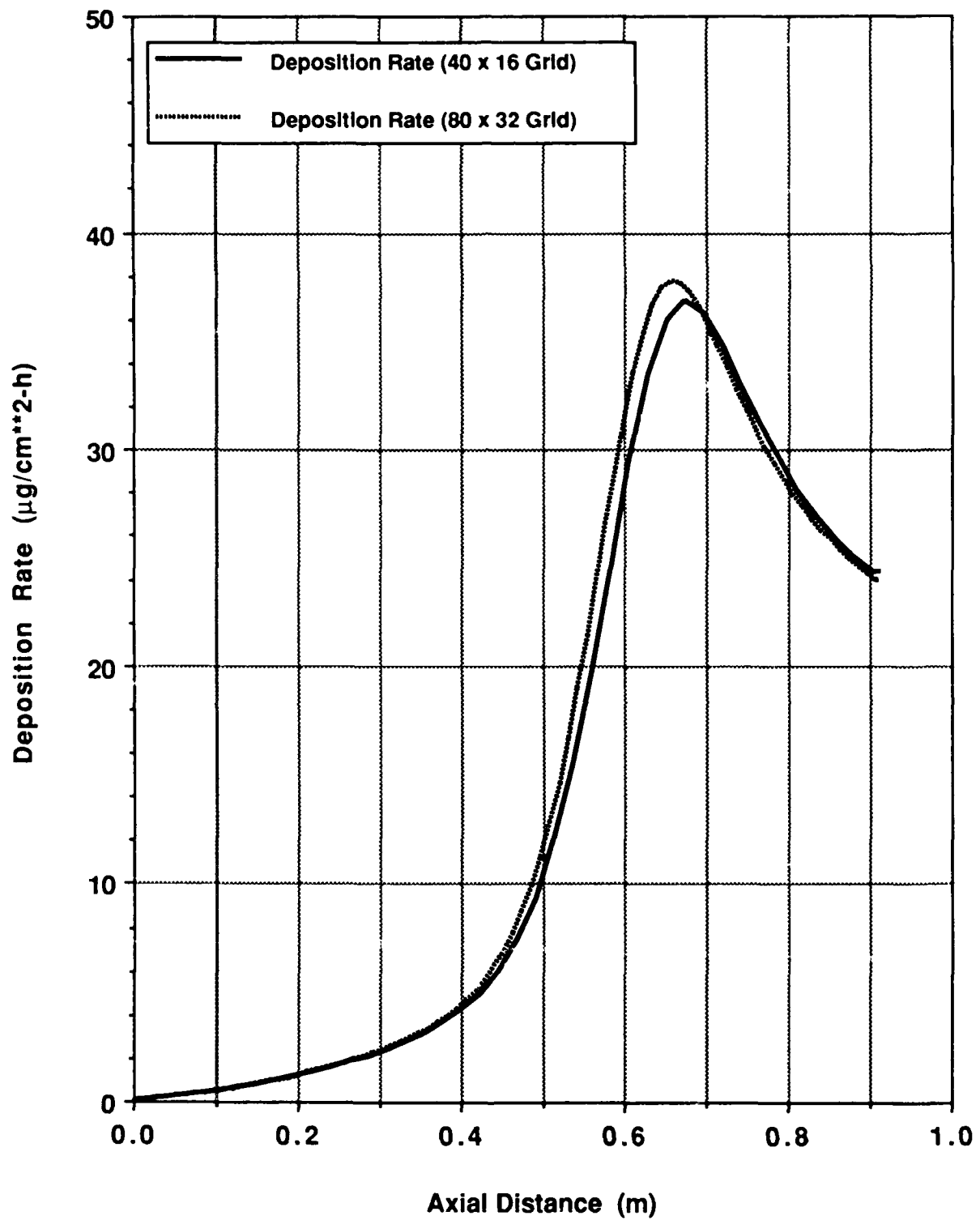


Fig. 5.25 Predicted Deposition Rates (Grid Comparison)

These sample results illustrate some of the detailed information that can be obtained from computational fluid dynamics and chemistry models. Initial validation of such models needs to be performed in simple flow fields, such as pipe flows. Once the models are validated, they can be used to predict fuel decomposition and deposit formation in more complex flow fields, such as flow in a heat exchanger. However, the current simplified model can still be used to perform parametric studies of the different factors affecting deposit formation, thereby helping to understand the interactions between the various individual mechanisms in the overall process.

5.4 Modification of the Chemical Kinetics Model

Comparison of the initial calibrated model with JP-5 deposition data indicated that the model could predict trends in wall deposition rates. However, quantitative agreement between the model and the data for oxygen consumption, deposition rates for laminar flow, and deposition rates for turbulent flow could not be obtained with the same set of calibration parameters. Although the peak predicted deposition rates agreed reasonably well with the data for turbulent flow, they were too low (by a factor of 3) for the laminar-flow case. The data for JP-5 also showed a steep decline in deposition rates downstream of the peak values, whereas the model predicted a more gradual decrease. In addition, the model overpredicted the rate of oxygen consumption at low flow rates.

Based on these differences, an effort was made to determine whether relatively simple changes in the kinetics model could improve the calculated results. In the original model, it was assumed that deposit precursors were produced from the bulk autoxidation reaction and transported to the wall, where they formed a solid deposit. An additional empirical factor, DPFRAC, was required to bring the peak predicted deposition rate into agreement with the data for turbulent flow. Using the same value of DPFRAC, however, the model could not match the peak deposition rate for laminar flow.

One of the major areas of uncertainty in the original model involved the values of the precursor and oxygen diffusion coefficients. Prior to modifying the chemical kinetics model, these diffusion coefficients were changed in an attempt to improve the model predictions. For lack of better information, the diffusion coefficient for dissolved oxygen in JP-5 fuel was initially taken to be the same as that for the deposit precursors. To examine the effect of this assumption on the model predictions, the original model was modified to allow for different oxygen and precursor diffusion coefficients. It was found that increasing the diffusion coefficient for the deposit precursors increased the predicted deposition rates. However, the

modified model still did not predict the steep drop-off in deposition rates near the tube exit. Increasing the oxygen diffusion coefficient increased the peak predicted deposition rates and also resulted in a more rapid decrease in deposition rates at higher temperatures. However, the calculations shown earlier in Fig. 5.13 indicate that the initial model overpredicted the rate of oxygen consumption for laminar flow. Increasing the oxygen diffusion coefficient would result in an even greater depletion of dissolved oxygen and worse agreement with the data. It thus did not appear that better agreement with the data could be achieved solely by adjusting the diffusion coefficients in the model. Consequently, the oxygen and precursor diffusion coefficients were fixed at their initial values and an attempt was made to modify the chemical kinetics model.

The wall deposition rates observed in heated-tube experiments typically show steep declines downstream of the peak values. These sharp decreases suggest the possibility that the phenomenon is associated with a chemical process, rather than a purely physical process such as diffusion. Although various chemical schemes could be postulated to account for these results, one possible mechanism involves an additional decomposition reaction for the deposit precursors in the bulk fuel. This reaction would serve as a sink for the deposit precursors at high temperatures, thereby preventing them from contributing to the wall deposition processes. Since the reaction would rapidly "consume" the precursors at high temperatures, fewer precursors would be transported to the walls and there would be a more rapid decline in the predicted deposition rates.

The initial chemistry model was thus modified by removing the empirical factor DPFRAC and adding an additional bulk reaction term for the deposit precursors. The deposit precursors can now either be transported to the wall, where they form a solid deposit as previously assumed, or be "consumed" by a homogeneous reaction in the bulk fluid. Since the nature of this reaction is unknown, the deposit precursors were assumed to undergo a simple first-order reaction. This reaction was included in the precursor transport equation by a sink term of the form

$$S_d = -A_{dc} \exp\left(\frac{-E_{dc}}{R T_b}\right) [Pre] \quad (5.9)$$

where A_{dc} is the preexponential constant for the decomposition reaction, E_{dc} is the activation energy, and $[Pre]$ is the precursor concentration. Several initial calculations were also performed using the assumption of a second-order decomposition reaction between precursor and fuel molecules, as assumed in Ref. 66. Since the concentration of dissolved oxygen in the

heated fuel is very small (50 wppm), however, the fuel concentration in the heated-tube experiments is essentially constant. The predicted deposition rates assuming a second-order reaction were therefore similar to those obtained using a first-order reaction. Consequently, a first-order decomposition reaction was assumed in the model.

Calibration of the modified model now requires a determination of the preexponential constants and activation energies for the heterogeneous wall reaction, the bulk fuel autoxidation reaction, and the precursor decomposition reaction. For the wall reaction, the modified model uses the same values for the kinetic parameters ($A_w = 4.0 \times 10^1 \text{ cm}^4/\text{mole}\cdot\text{s}$ and $E_w = 8 \text{ kcal/mole}$) as the initial model. The laminar flow test of Marteney discussed earlier [60] includes both deposition data and oxygen consumption data (Figs. 5.12 and 5.13). This test was used to calibrate the two homogeneous reactions in the modified model.

Deposition data from several of Marteney and Spadaccini's tests are shown in Fig. 5.3 as a function of the initial wall temperature. Above 533 K, the data were fitted using an Arrhenius-type expression with a corresponding activation energy of 40 kcal/mole. For homogeneous reactions in the bulk fluid, however, the reaction rate is governed by the local fluid temperature rather than the wall temperature. When the deposition data in Fig. 5.3 were fitted with an Arrhenius-type expression based on the bulk fluid temperature, the corresponding activation energy appeared to be lower, in the range of 25-30 kcal/mole. Therefore, activation energies lower than 40 kcal/mole were examined in calibrating the modified model.

In order to calibrate the autoxidation reaction, deposition rates were calculated for several values of the activation energy, E_b . The results are presented in Fig. 5.26 together with the laminar flow data for a fuel velocity of 0.076 m/s and a maximum wall temperature of 589 K. The precursor decomposition reaction was neglected in these calculations ($A_{dc} = 0$). To obtain these results, a value of E_b was initially assumed and the preexponential constant A_b was then adjusted until the predicted oxygen concentration at the tube exit matched the data shown earlier in Fig. 5.13. All three combinations of parameters given in Fig. 5.26 thus result in good agreement with the oxygen consumption data. The parameters $A_b = 1.0 \times 10^{14} \text{ cm}^3/\text{mole}\cdot\text{s}$ and $E_b = 30 \text{ kcal/mole}$ also result in good agreement with the low-temperature deposition data shown in Fig. 5.26. Consequently, these values were selected for the autoxidation reaction in the modified model. The predicted oxygen concentrations in Fig. 5.27 show the improvement obtained with the modified model.

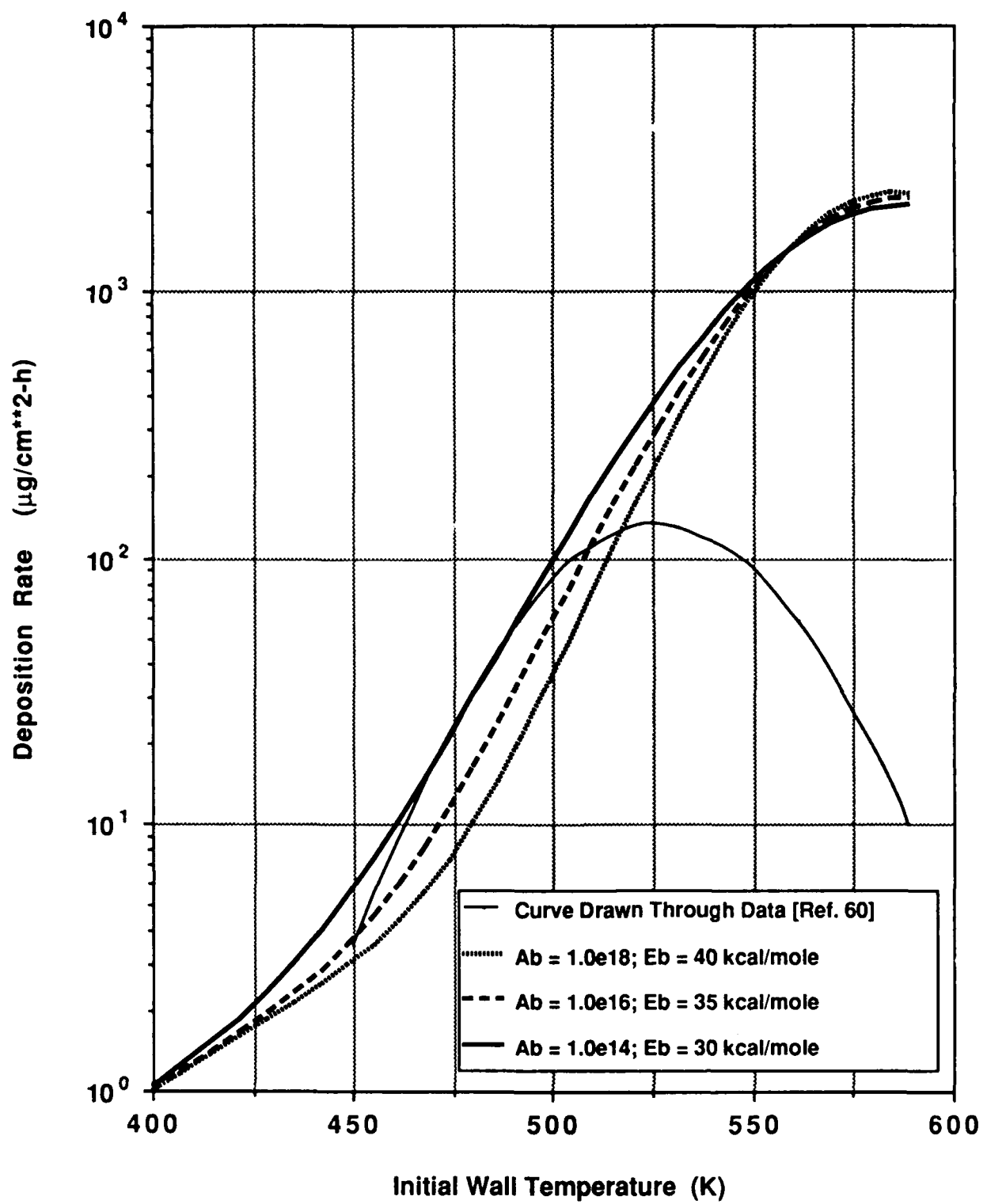


Fig. 5.26 Calibration of the Autoxidation Reaction for a Fuel Velocity of 0.076 m/s (No Precursor Decomposition)

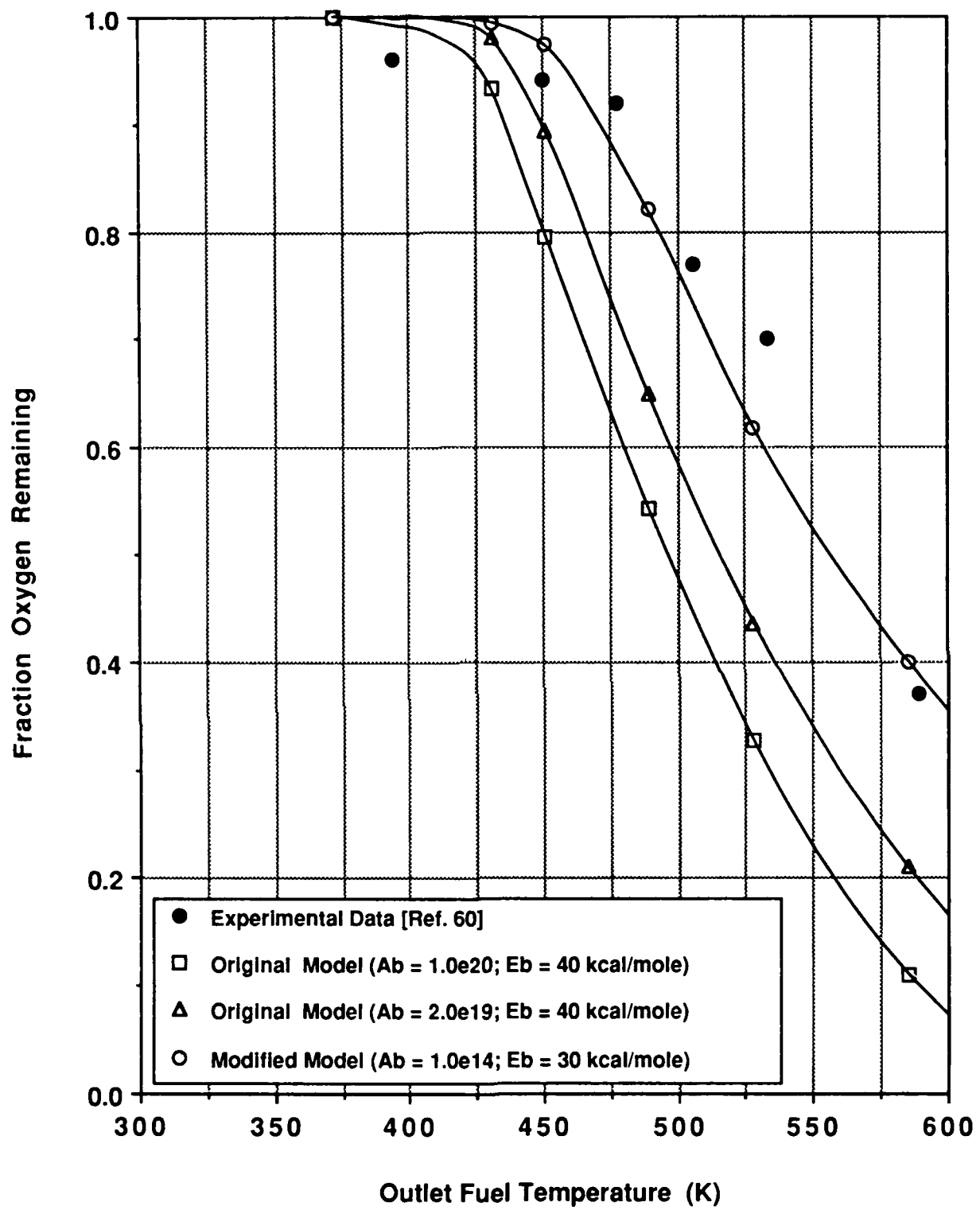


Fig. 5.27 Prediction of the Dissolved-Oxygen Concentration With the Modified Model for a Fuel Velocity of 0.076 m/s

Using the selected values of the preexponential constant and activation energy for the autoxidation reaction, the corresponding parameters for the precursor decomposition reaction (Eqn. 5.9) were determined by a comparison with both laminar and turbulent deposition data. From Fig. 5.26 it appears that the rate of decrease of the measured deposition rates beyond the peak value is similar in magnitude to the rate of increase at lower temperatures. Therefore, the activation energy E_{dc} was also varied over the range of 30–40 kcal/mole. For each selected value of E_{dc} , the preexponential constant A_{dc} was adjusted in an attempt to match the peak deposition rates for both laminar and turbulent flows. The results of this calibration procedure are shown in Fig. 5.28 for the laminar-flow case and Fig. 5.29 for the turbulent-flow case. As shown in Fig. 5.28, the calculated deposition rates are greater than the laminar-flow data at higher temperatures. Unlike the original model, however, the modified model now predicts the rapid decrease in deposition rates following the peak value. For the turbulent-flow case in Fig. 5.29, the modified model provides a somewhat better match to the higher-temperature data fitted by the $E = 40$ kcal/mole line. In the temperature range above ~645 K where the deposition rates start to decrease, the predicted deposition rates for the three values of E_{dc} all fall within the scatter of the data. For comparison with additional data sets, values of $3.0 \times 10^{15} \text{ s}^{-1}$ and 35 kcal/mole were selected for A_{dc} and E_{dc} , respectively.

Figure 5.30 shows the predicted deposition rates from the calibrated model for $A_b = 1.0 \times 10^{14} \text{ cm}^3/\text{mole-s}$, $E_b = 30$ kcal/mole, $A_{dc} = 3.0 \times 10^{15} \text{ s}^{-1}$, and $E_{dc} = 35$ kcal/mole. Also shown are the deposition rates calculated by assuming only a heterogeneous wall reaction ($A_b = 0$ and $A_{dc} = 0$) and the deposition rates calculated by assuming only homogeneous bulk reactions ($A_w = 0$). As seen from Fig. 5.30, the selected set of parameters in the calibrated model provides a good match to the turbulent-flow data throughout the entire range of initial wall temperatures.

Using the above set of parameters, the modified model was compared with two additional data sets that were used to test the original model. The first data set corresponded to a test case of Marteney and Spadaccini [43] at a fuel velocity of 0.3 m/s (Test 1-g in Table 5.1). The reported inlet Reynolds number for this test was 400. As discussed in Section 5.2, however, reductions in the fuel viscosity can significantly increase the Reynolds number over the length of the heated tube. In order to achieve a reasonable match with the temperature data, this test was again modeled by assuming fully developed turbulent flow throughout the test section. The results are presented in Fig. 5.31. As indicated in the figure, the predicted deposition rates from the modified model show somewhat worse agreement with the data than those from the original model. The general trends in the data, however, are still predicted reasonably well.

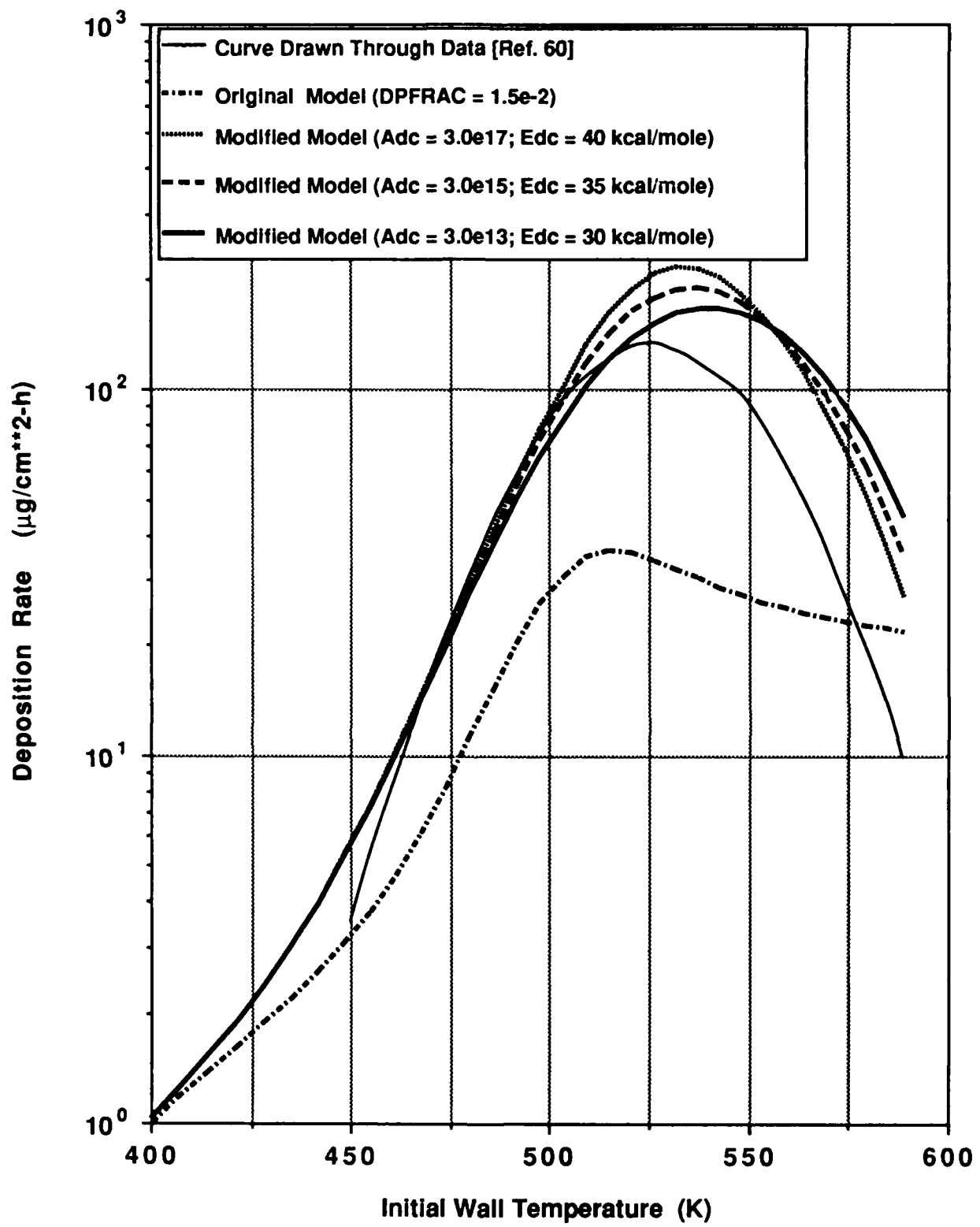


Fig. 5.28 Calibration of the Precursor Decomposition Reaction for a Fuel Velocity of 0.076 m/s

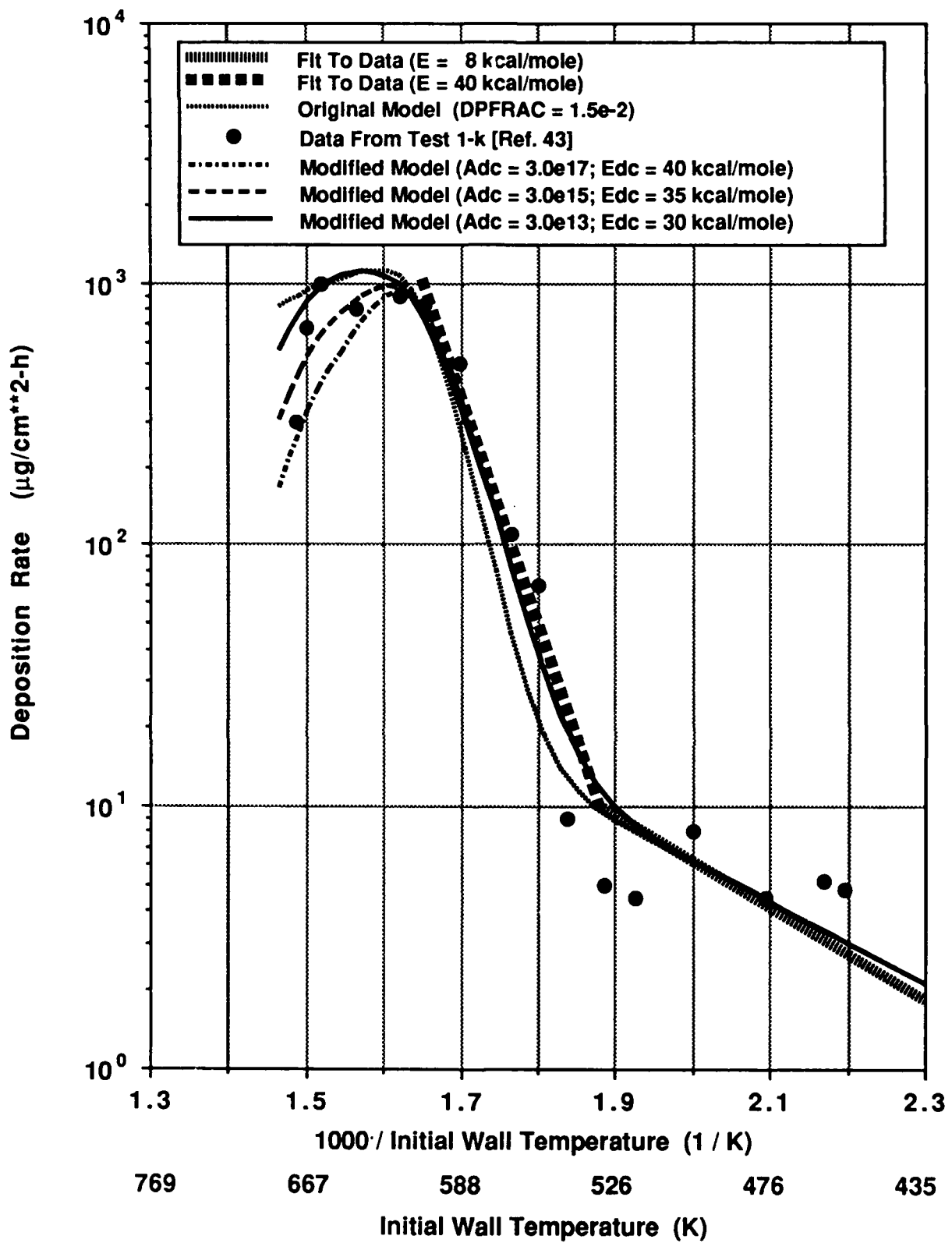


Fig. 5.29 Calibration of the Precursor Decomposition Reaction for a Fuel Velocity of 2.1 m/s

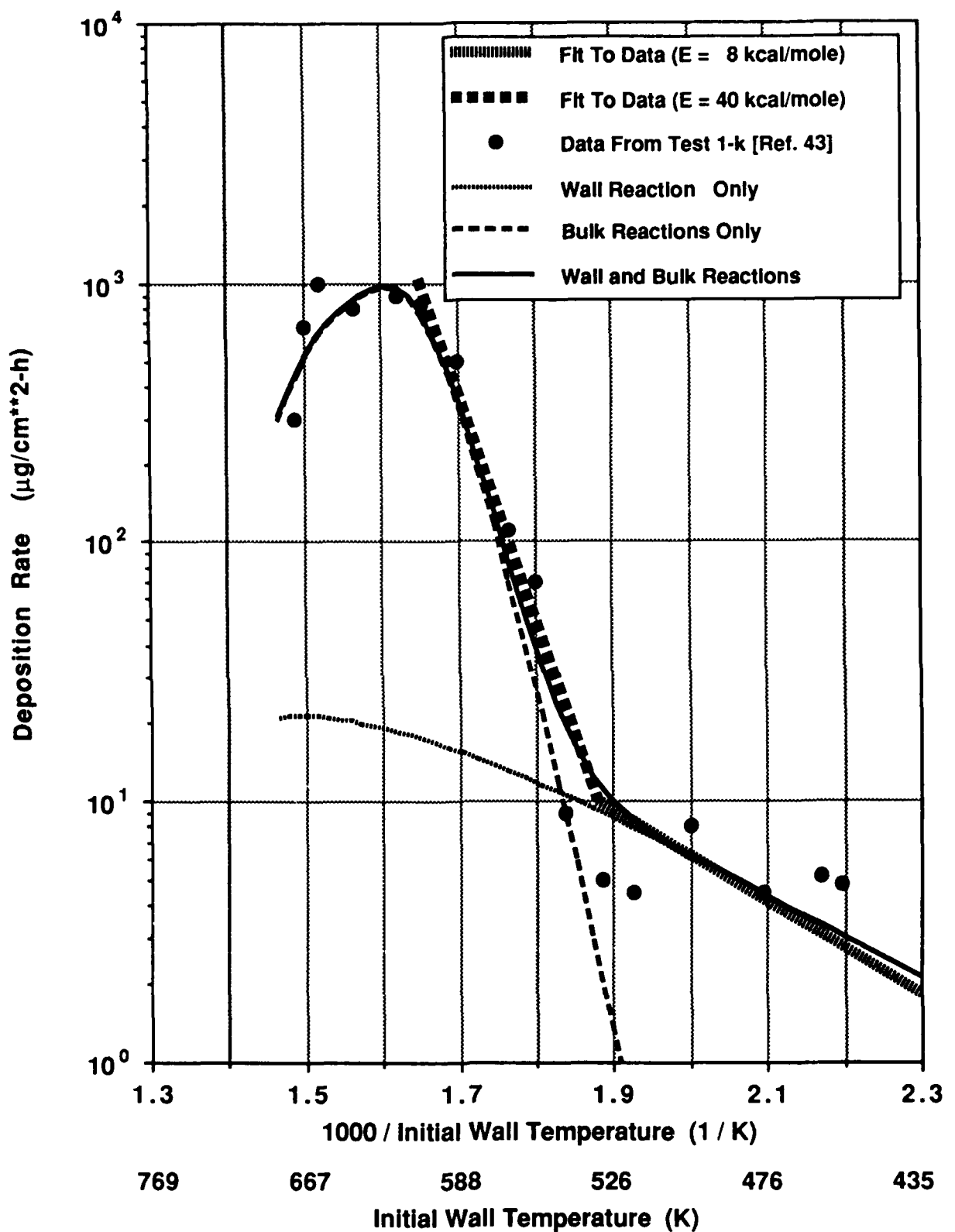


Fig. 5.30 Effect of the Wall and Bulk Reactions on the Predicted Deposition Rates for a Fuel Velocity of 2.1 m/s

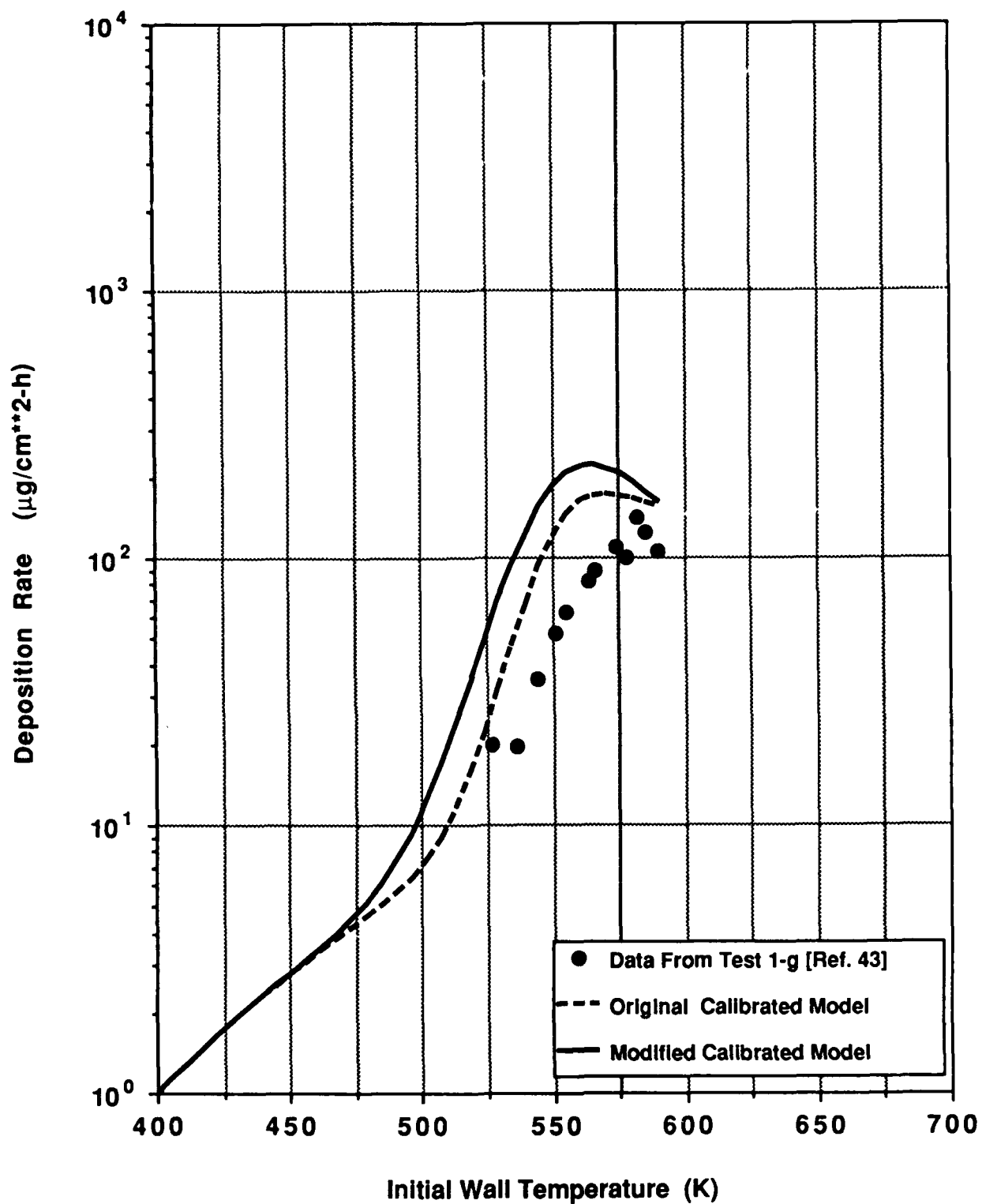


Fig. 5.31 Comparison of the Modified Calibrated Model With Deposition Data for a Fuel Velocity of 0.3 m/s

The discrepancy between the predicted and measured deposition rates may be partly due to the assumption of fully developed turbulent flow, since the fuel may have been in the laminar and transitional flow regimes throughout much of the test section.

The second set of JP-5 deposition data used to test the modified model was the data of TeVelde and Glickstein [54]. The deposition rates predicted by the modified model are compared with their data in Fig. 5.32. At lower temperatures, the results from the modified model are similar to those from the original model. At higher temperatures, the modified model shows better agreement with the data and predicts the sharp drop-off in deposition rates following the peak value. At initial wall temperatures above 750 K, the measured deposition rates appear to level off. Beyond this temperature, other data have shown an eventual increase in deposition rates with increasing wall temperature [8]. These increasing deposition rates could be due to fuel pyrolysis, which becomes significant at temperatures above 755 K or 900°F [7,8]. The current thermal decomposition model does not include the effects of fuel pyrolysis reactions.

The calculations presented in this section illustrate that the inclusion of a precursor decomposition reaction results in substantial improvements in the predicted deposition rates. The current global chemistry model appears to include many of the qualitative features of the JP-5 deposition data for both laminar and turbulent flows. Further development and validation of this model should be coordinated with well-controlled experiments that can be used to test proposed mechanisms of fuel decomposition and wall deposition. For example, the precursors formed from the autoxidation reaction could participate in an additional series of reactions that eventually produce solids in the bulk fuel. These solid particles could be carried out of the heated tube or be transported to the wall and contribute to the wall deposition processes. Additional experiments are needed to evaluate the importance of such processes in the formation of solid deposits and to help guide the continued development of the fuel decomposition model.

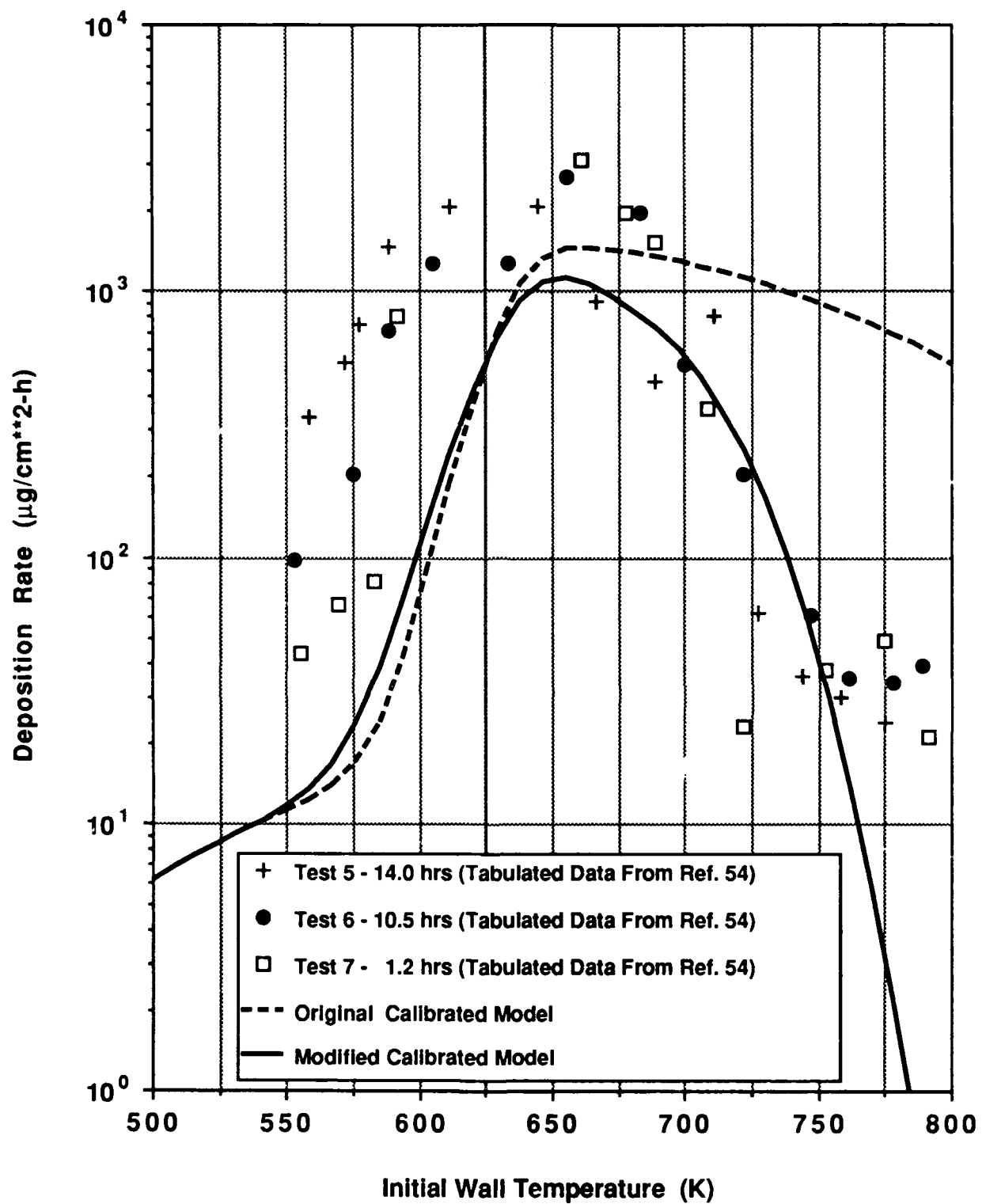


Fig. 5.32 Comparison of the Modified Calibrated Model With Deposition Data for a Fuel Velocity of 2.57 m/s

6.0 PROPOSED EXPERIMENTS TO SUPPORT FURTHER MODEL DEVELOPMENT

Much of the existing data base for fuel decomposition consists of results from tests with electrically heated tubes. In the Jet Fuel Thermal Oxidation Tester (JFTOT), the test fuel flows in a narrow annulus over a heated aluminum tube for 2 1/2 hours. This test yields the breakpoint temperature of the fuel, which corresponds to the maximum heater tube temperature at which the amount of deposits on the wall or the measured pressure drop across a filter do not exceed specified limits. No quantitative information is provided on the wall deposition rate or the amount of decomposition products that are formed in the test section, but carried downstream.

Deposition experiments have also been conducted in long, thin tubes for time periods ranging from several hours to several hundreds of hours. Although these experiments provide quantitative information on the wall deposition rates, the deposit-forming species carried out of the test section are not generally measured. Because of large temperature variations in these tests, the transport processes and fuel chemistry can change considerably along the length of the tube. Such experiments are useful in comparing the relative performance of various fuels and do yield some global, quantitative information on fuel decomposition. However, they do not provide much insight into the fundamental physicochemical mechanisms of the decomposition process.

In order to obtain such fundamental information, it is necessary to systematically study each aspect of the problem. This will require a series of experiments that can effectively isolate each of the many variables that impact the decomposition process. Three general types of experiments will be discussed here: property measurements, chemistry experiments, and experiments on transport processes and deposit adhesion mechanisms. It is not the intent here to develop detailed test plans for the proposed experiments. Rather, the experimental needs will be discussed in a general qualitative manner, with some references given to earlier related work.

Accurate fuel property data are needed, of course, in order to reliably calculate fuel decomposition rates over a wide range of pressures and temperatures. One specific property which is not well known is the diffusion coefficient. Diffusion coefficients are needed in the transport equations for the deposit precursors and for dissolved oxygen. For lack of better information, the current model uses the same diffusion coefficient for both the deposit precursors and dissolved oxygen. Accurate values of the diffusion coefficient are particularly important for the precursor transport equation, since they affect the rate of transport of

deposit-forming species to the walls. Initially, the nature of the deposit-forming species produced from the bulk fuel autoxidation reaction needs to be better defined. The diffusion coefficient will change considerably depending upon whether individual molecules or larger colloidal particles are being formed in the bulk and transported to the wall. The diffusion coefficients for these species then need to be determined over the range of temperatures and pressures encountered in the heated-tube experiments. A generalized correlation over the complete fluid region, including the compressed liquid state, has been developed for predicting self-diffusivities for a variety of substances [47]. Similar correlations are needed for the diffusion coefficients of deposit precursors and dissolved oxygen in aviation fuels.

Experiments are also required to better understand the chemistry of fuel decomposition. The present simplified model requires values for the preexponential constant and activation energy of the wall and bulk reactions. As more complex kinetic schemes are developed, rate constants will also be needed for the various intermediate reactions. Such information cannot be extracted from the existing heated-tube data. The activation energies shown in Fig. 5.3 were obtained by plotting the measured deposition rates versus the tube wall temperatures. Reactions in the bulk fluid, however, will proceed at a rate determined by the local fluid temperature, rather than the wall temperature. In addition, at low fuel velocities certain reactions may be controlled by diffusional processes, rather than pure chemistry. There is thus a need to conduct experiments at known, well-controlled conditions (temperatures, oxygen concentrations, containment materials, etc.) to obtain reliable kinetic data.

Reaction rates of various processes have previously been measured under both static and dynamic conditions. Stability tests on refrigerant materials were conducted with sealed, static capsules that were maintained at fixed temperatures for various periods of time [67,68]. The effects of air, water, and oil on the fluid stability were measured during the tests. Metal coupons were inserted into the glass tubes to determine the effects of various materials on refrigerant stability. Using such capsules allowed a large number of individual tests to be conducted simultaneously.

Liquid autoxidation reactions have been studied using reaction vessels with various configurations [10,69,70]. These reactions were designed to ensure good mixing of oxygen and the test fluid, to minimize oxygen mass transfer effects, and to maintain the liquid at a uniform temperature. Kinetic information on the rapid reactions occurring during the oxidation of gaseous hydrocarbons was obtained from a turbulent, adiabatic flow reactor [14].

By maintaining fully developed turbulent flow in the test section, the fluid mechanics could be described as a one-dimensional plug flow with nearly uniform properties (temperature, velocity, etc.) at each axial location of the cylindrical test section. Distances along the reactor could thus be readily converted to times for the development of kinetic rate expressions.

Experiments such as those mentioned above will be needed to help develop kinetic schemes that describe the thermal decomposition process. System variables such as the temperature, oxygen content, copper and sulfur concentrations, wall material, and other pertinent factors will need to be separated out to quantitatively determine their individual effects on fuel decomposition.

In addition to the decomposition chemistry, the formation of deposits on a solid surface is also influenced by the fluid mechanics of the system. If deposit-forming species are formed in the bulk fluid, they must be transported to a solid surface prior to forming a deposit layer. Once at a surface, a particle may or may not adhere, depending on the interaction forces between the surface and the approaching particle. As a deposit layer builds up, changes in the surface roughness and subsequent variations in the near-wall turbulence could affect the rate of wall deposition. Long-term deposition tests have shown an increase in the deposition rate with time, as the deposit layer builds up on the tube surface [57,60]. Fragments of existing deposit layers can also break off and be carried downstream, where they can redeposit or clog small passages elsewhere in the fuel system.

In order to acquire additional information on these and other aspects of deposit formation, additional experiments are needed to examine the fluid mechanics of the process. Ideally, these experiments would be conducted without chemical reactions, in order to study the effect of fluid mechanics on the overall deposition process. Harriott and Hamilton, for example, conducted mass transfer experiments using soluble pipe sections that were dissolved by a circulating liquid [63]. Bowen and Epstein performed deposition experiments in parallel-plate channels under laminar flow conditions [28]. By seeding the fluid with radioactively tagged silica particles, they could measure the particle accumulation rates on a wall with a collimated detector. Particle release measurements were also made by monitoring the activity of radioactive material accumulated on the wall, while a nonradioactive particle suspension flowed through the test section. Crittenden et al. used a dilute solution of styrene in kerosene as a model fluid to study chemical reaction fouling [71]. Styrene polymerizes to polystyrene upon heating and the polystyrene forms deposits on the tube walls. Because of a good understanding of the mechanism of styrene polymerization, the mass transfer aspects of the

fouling problem could be studied with reasonably well-defined chemical kinetics [71]. If a substance could be found to represent the deposit-forming species produced during the decomposition of aviation fuels, mass transfer experiments could then be conducted by doping a test fluid with known concentrations of the material.

Experiments such as those described in this section will be needed to better understand the individual mechanisms of fuel decomposition. The information obtained from such tests will also be required to develop more realistic models of deposit formation. The models, in turn, can be used to guide the experiments and help establish appropriate test conditions, so that the effects of key parameters on fuel decomposition can be effectively measured.

7.0 CONCLUSIONS AND RECOMMENDATIONS

This report describes the development of a mathematical model for predicting the thermal decomposition rates of aviation fuels. Because the mechanisms of the decomposition process are not well understood, the decomposition chemistry was initially modeled by two global Arrhenius expressions. The deposition process was modeled by assuming that all deposit-forming species transported to the wall, adhered and formed a deposit. Calibration of the initial model required the determination of three parameters for a given fuel: (1) the parameter DPFRAC, (2) the preexponential constant for the wall reaction, and (3) the preexponential constant for the bulk reaction. Replacing the parameter DPFRAC by a precursor decomposition reaction was found to give better agreement with the deposition data and oxygen consumption data for JP-5 fuel. The current model is restricted to the temperature range in which fuel decomposition is initiated primarily by an autoxidation reaction with dissolved oxygen.

Comparison of the calibrated model with experimental data indicates that the current model can characterize trends in fuel deposition rates. The model is also a useful tool that can be employed to help understand the coupling between the chemistry, fluid mechanics, and heat-transfer processes that occurs during fuel decomposition. Much additional work is needed, however, before the model can be utilized to make reliable quantitative predictions of wall deposition rates under various flow conditions. The individual fuel constituents known to affect fuel decomposition, such as the concentrations of sulfur and copper, are not explicitly accounted for in this initial model. Consequently, the model needs to be recalibrated for fuels other than JP-5, or for batches of JP-5 whose compositions differ significantly from the fuel used in the initial model calibration. In addition, the current model does not consider the impact of deposit build-up on the heat-transfer and fluid-transport processes. Consequently, the model is restricted to short periods of time where such effects are not important.

Further development of the model is hindered by a lack of data from well-controlled experiments that have isolated the various phenomena in the overall decomposition process. Much information has already been obtained from heated-tube experiments. However, these tests involve large temperature variations throughout the fuel, in which it is difficult to separate out the effects of chemistry and the transport processes on the deposition rates. The tests also frequently involve Reynolds numbers in the transitional flow regime, where there are more uncertainties in the transport models. Consequently, additional experiments are needed that can isolate these various factors and provide the required input data for the model.

Three general classes of proposed experiments were discussed in this report. These involve experiments to better characterize the deposit-forming species and acquire more reliable liquid diffusivity data, decomposition chemistry experiments conducted at well-controlled temperatures to help decipher the decomposition kinetics, and wall deposition experiments conducted under isothermal conditions (without the decomposition chemistry) to further understand the transport processes and adhesion mechanisms of deposit-forming species. These experiments need to be coordinated with further model development to ensure that the measurements provide the type of information required to improve and validate the model. Examples of the types of information needed by the model include:

- Chemical kinetic data (activation energies, preexponential constants) obtained at well-controlled temperatures,
- Measurements of oxygen concentrations throughout the heated fuel,
- Better identification of those species that actually form the solid deposits,
- Measurements of the amount of insoluble material being carried out of the test section, compared with the mass depositing on the walls, and
- Diffusion coefficients for dissolved oxygen and deposit-forming species as functions of temperature.

Computational fluid dynamic codes in general can supply a large amount of information about a particular flow field. The code used in this study, for example, provides two-dimensional profiles of temperatures, velocities, species concentrations, and other variables throughout the domain of interest. Such codes are not only valuable research tools but, after sufficient development and testing, can be used to obtain design information for individual system components, such as heat exchangers. The model described in this report represents an initial, simplified description of the thermal decomposition process. The decomposition model was coupled with models describing the fluid mechanics and heat transport. The present framework thus provides a foundation that can be used to develop and test more comprehensive models of fuel decomposition and deposit formation.

8.0 REFERENCES

1. Somerscales, E. F. C. and Knudsen, J. G., eds., Fouling of Heat Transfer Equipment, Hemisphere Publishing Corporation, New York (1981).
2. Epstein, N., "Fouling in Heat Exchangers," Sixth International Heat Transfer Conference, Vol. 6, pp. 235-253, Toronto (Aug. 7-11, 1978).
3. Coordinating Research Council, "CRC Literature Survey on the Thermal Oxidation Stability of Jet Fuel," CRC Report No. 509 (Apr. 1979).
4. Taylor, W. F. and Wallace, T. J., "Kinetics of Deposit Formation From Hydrocarbon Fuels at High Temperatures," Industrial and Engineering Chemistry Product Research and Development, Vol. 6, No. 4, pp. 258-262 (1967).
5. Taylor, W. F., "Kinetics of Deposit Formation From Hydrocarbons—Fuel Composition Studies," Industrial and Engineering Chemistry Product Research and Development, Vol. 8, No. 4, pp. 375-380 (1969).
6. Taylor, W. F., "Deposit Formation From Deoxygenated Hydrocarbons. I. General Features," Industrial and Engineering Chemistry Product Research and Development, Vol. 13, No. 2, pp. 133-138 (1974).
7. Hazlett, R. N., Hall, J. M., and Matson, M., "Reactions of Aerated N-Dodecane Liquid Flowing Over Heated Metal Tubes," Industrial and Engineering Chemistry Product Research and Development, Vol. 16, No. 2, pp. 171-177 (1977).
8. Hazlett, R. N., "Free Radical Reactions Related to Fuel Research," Frontiers of Free Radical Chemistry, W. A. Pryor, ed., Academic Press, New York, pp. 195-223 (1980).
9. Fabuss, B. M., Smith, J. O., and Satterfield, C. N., "Thermal Cracking of Pure Saturated Hydrocarbons," Advances in Petroleum Chemistry and Refining, Vol. IX, pp. 157-201 (1964).
10. Kendall, D. R. and Mills, J. S., "Thermal Stability of Aviation Kerosines: Techniques to Characterize Their Oxidation Properties," Industrial and Engineering Chemistry Product Research and Development, Vol. 25, No. 2, pp. 360-366 (1986).
11. Mayo, F. R. and Lan, B. Y., "Gum and Deposit Formation From Jet Turbine and Diesel Fuels at 130°C," Industrial and Engineering Chemistry Product Research and Development, Vol. 25, No. 2, pp. 333-348 (1986).
12. Mayo, F. R. and Lan, B. Y., "Gum and Deposit Formation From Jet Turbine and Diesel Fuels at 100°C," Industrial and Engineering Chemistry Research, Vol. 26, No. 2, pp. 215-220 (1987).
13. Westbrook, C. K. and Dryer, F. L., "Simplified Reaction Mechanisms for the Oxidation of Hydrocarbon Fuels in Flames," Combustion Science and Technology, Vol. 27, pp. 31-43 (1981).
14. Hautman, D. J. et al., "A Multiple-Step Overall Kinetic Mechanism for the Oxidation of Hydrocarbons," Combustion Science and Technology, Vol. 25, pp. 219-235 (1981).

15. Wells, A. C. and Chamberlain, A. C., "Transport of Small Particles to Vertical Surfaces," British Journal of Applied Physics, Vol. 18, pp. 1793-1799 (1967).
16. Douglas, P. L. and Illas, S., "On the Deposition of Aerosol Particles on Cylinders in Turbulent Cross Flow," Journal of Aerosol Science, Vol. 19, No. 4, pp. 451-462 (1988).
17. Walker, K. L., Homsy, G. M., and Geyling, F. T., "Thermophoretic Deposition of Small Particles in Laminar Tube Flow," Journal of Colloid and Interface Science, Vol. 69, No. 1, pp. 138-147 (1979).
18. Rosner, D. E., Eisner, A. D., Liang, B., and Castillo, J. L., "Experimental and Theoretical Studies of Coal Mineral Matter Deposition From Combustion Gases," Proceedings of the Second Annual Heat Engines Contractors Meeting, DOE Report No. DOE/METC-85/6023, pp. 181-186 (May 1985).
19. Ruckenstein, E. and Prieve, D. C., "Rate of Deposition of Brownian Particles Under the Action of London and Double-Layer Forces," Journal of the Chemical Society: Faraday Transactions II, Vol. 7, pp. 1522-1536 (1973).
20. Spielman, L. A. and Friedlander, S. K., "Role of the Electrical Double Layer in Particle Deposition by Convective Diffusion," Journal of Colloid and Interface Science, Vol. 46, No. 1, pp. 22-31 (1974).
21. Davies, C. N., "Deposition of Aerosols From Turbulent Flow Through Pipes," Proceedings of the Royal Society: Series A, Vol. 289, pp. 235-246 (1966).
22. Sehmel, G. A., "Particle Diffusivities and Deposition Velocities Over a Horizontal Smooth Surface," Journal of Colloid and Interface Science, Vol. 37, No. 4, pp. 891-906 (1971).
23. Beal, S. K., "Deposition of Particles in Turbulent Flow on Channel or Pipe Walls," Nuclear Science and Engineering, Vol. 40, pp. 1-11 (1970).
24. Lin, C. S., Moulton, R. W., and Putnam, G. L., "Mass Transfer Between Solid Wall and Fluid Streams," Industrial and Engineering Chemistry, Vol. 45, No. 3, pp. 636-640 (1953).
25. Friedlander, S. K. and Johnstone, H. F., "Deposition of Suspended Particles From Turbulent Gas Streams," Industrial and Engineering Chemistry, Vol. 49, No. 7, pp. 1151-1156 (1957).
26. Reid, R. C., Prausnitz, J. M., and Sherwood, T. K., The Properties of Gases and Liquids, McGraw-Hill Book Company, New York (1977).
27. Bowen, B. D., Levine, S., and Epstein, N., "Fine Particle Deposition in Laminar Flow Through Parallel-Plate and Cylindrical Channels," Journal of Colloid and Interface Science, Vol. 54, No. 3, pp. 375-390 (1976).
28. Bowen, B. D. and Epstein, N., "Fine Particle Deposition in Smooth Parallel-Plate Channels," Journal of Colloid and Interface Science, Vol. 72, No. 1, pp. 81-97 (1979).
29. Visser, J., "Measurement of the Force of Adhesion Between Submicron Carbon-Black Particles and a Cellulose Film in Aqueous Solution," Journal of Colloid and Interface Science, Vol. 34, No. 1, pp. 26-31 (1970).

30. Beal, S. K., "Correlations for the Sticking Probability and Erosion of Particles," Journal of Aerosol Science, Vol. 9, pp. 455-461 (1978).
31. Browne, L. W. B., "Deposition of Particles on Rough Surfaces During Turbulent Gas-Flow in a Pipe," Atmospheric Environment, Vol. 8, pp. 801-816 (1974).
32. Montgomery, T. L. and Corn, M., "Aerosol Deposition in a Pipe With Turbulent Airflow," Journal of Aerosol Science, Vol. 1, pp. 185-213 (1970).
33. Standards of Tubular Exchanger Manufacturers Association (TEMA), 6th Edition, New York, pp. 138-142 (1978).
34. McCabe, W. L. and Robinson, C. S., "Evaporator Scale Formation," Industrial and Engineering Chemistry, Vol. 16, No. 5, pp. 478-479 (1924).
35. Kern, D. Q. and Seaton, R. E., "A Theoretical Analysis of Thermal Surface Fouling," British Chemical Engineering, Vol. 4, pp. 258-262 (1959).
36. Taborek, J. et al., "Fouling: The Major Unresolved Problem in Heat Transfer," Chemical Engineering Progress, Vol. 68, No. 2, pp. 59-67 (1972).
37. Taborek, J. et al., "Predictive Methods for Fouling Behavior," Chemical Engineering Progress, Vol. 68, No. 7, pp. 69-78 (1972).
38. Cleaver, J. W. and Yates, B., "Mechanism of Detachment of Colloidal Particles From a Flat Substrate in a Turbulent Flow," Journal of Colloid and Interface Science, Vol. 44, No. 3, pp. 464-474 (1973).
39. Cleaver, J. W. and Yates, B., "A Sub Layer Model For the Deposition of Particles From a Turbulent Flow," Chemical Engineering Science, Vol. 30, pp. 983-992 (1975).
40. Cleaver, J. W. and Yates, B., "The Effect of Re-Entrainment on Particle Deposition," Chemical Engineering Science, Vol. 31, pp. 147-151 (1976).
41. Nallasamy, M., "Turbulence Models and Their Applications to the Prediction of Internal Flows: A Review," Computers & Fluids, Vol. 15, No. 2, pp. 151-194 (1987).
42. Marteney, P. J. and Spadaccini, L. J., "Thermal Decomposition of Aircraft Fuel," Journal of Engineering for Gas Turbines and Power, Vol. 108, pp. 648-653 (Oct. 1986).
43. Marteney, P. J. and Spadaccini, L. J., "Thermal Decomposition of Aircraft Fuels," Naval Air Propulsion Center Report No. NAPC-PE-143C (Dec. 1984).
44. Nixon, A. C., et al., "Vaporizing and Endothermic Fuels for Advanced Engine Application: Part III. Studies of Thermal and Catalytic Reactions, Thermal Stabilities, and Combustion Properties of Hydrocarbon Fuels," Vol. II, Air Force Aero Propulsion and Power Laboratory Report No. AFAPL-TR-67-114 (Feb. 1970).
45. Pearce, J. A., WRDC/Aero Propulsion and Power Laboratory, Wright-Patterson AFB, Personal Communication (1989).
46. Ertl, H. and Dullien, F. A. L., "Self-Diffusion and Viscosity of Some Liquids as a Function of Temperature," AIChE Journal, Vol. 19, No. 6, pp. 1215-1223 (Nov. 1973).

47. Lee, H. and Thodos, G., "Self-Diffusivity: A Generalized Correlation over the Complete Fluid Region Including the Compressed Liquid State." Industrial and Engineering Chemistry Research, Vol. 27, No. 6, pp. 992-997 (1988).
48. Vanka, S. P., "Analytical Studies of Three-Dimensional Combustion Processes," Air Force Aero Propulsion and Power Laboratory Report No. AFWAL-TR-88-2140 (1988).
49. Martel, C. R., "Military Jet Fuels, 1944-1987," Air Force Aero Propulsion and Power Laboratory Report No. AFWAL-TR-87-2062 (Nov. 1987).
50. American Society for Testing and Materials (ASTM), "Standard Test Method for Thermal Stability of Aviation Turbine Fuels." Standard No. D 1660-87, 1988 Annual Book of ASTM Standards, Vol. 05.01, pp. 657-671 (1988).
51. American Society for Testing and Materials (ASTM), "Standard Test Method for Thermal Oxidation Stability of Aviation Turbine Fuels (JFTOT Procedure)." Standard No. D 3241-85, 1988 Annual Book of ASTM Standards, Vol. 05.02, pp. 669-687 (1988).
52. Vranos, A. and Marteney, P. J., "Experimental Study of the Stability of Aircraft Fuels at Elevated Temperatures," NASA Report No. NASA CR-165165 (Dec. 1980).
53. Vranos, A., Marteney, P. J., and Knight, B. A., "Determination of Coking Rate in Jet Fuel," Fouling of Heat Transfer Equipment, E. F. C. Somerscales and J. G. Knudsen, eds., Hemisphere Publishing Corporation, New York, pp. 489-499 (1981).
54. TeVelde, J. A. and Glickstein, M. R., "Heat Transfer and Thermal Stability of Alternative Aircraft Fuels," Vols. I and II, Naval Air Propulsion Center Report No. NAPC-PE-87C (Nov. 1983).
55. Watt, J. J., Evans Jr., A., and Hibbard, R. R., "Fouling Characteristics of ASTM Jet A Fuel When Heated to 700°F in a Simulated Heat Exchanger Tube," NASA Report No. TN D-4958 (Sept. 1968).
56. Purvis, W. J., "Investigation of Thermal Coking Rates of Air Force Jet Fuels," Air Force Aero Propulsion and Power Laboratory Report No. AFWAL-TR-84-2004 (Mar. 1984).
57. Giovanetti, A. J. and Szetela, E. J., "Long Term Deposit Formation in Aviation Turbine Fuel at Elevated Temperature," AIAA Paper No. AIAA-86-0525, Presented at the AIAA 24th Aerospace Sciences Meeting, Reno, NV (Jan. 6-9, 1986).
58. CRC Handbook of Chemistry and Physics, 63rd Edition, CRC Press, Inc., Boca Raton, FL, p. F-1 (1982-1983).
59. Levenspiel, O., Chemical Reaction Engineering, John Wiley & Sons, Inc., New York (1972).
60. Marteney, P. J., "Thermal Decomposition of JP-5 in Long Duration Tests," Naval Air Propulsion Center Report No. NAPC-PE-201C (1989).
61. Marteney, P. J., United Technologies Research Center, East Hartford, CT, Personal Communication (1989).

62. Launder, B. E. and Spalding, D. B., "The Numerical Computation of Turbulent Flows." Computer Methods in Applied Mechanics and Engineering, Vol. 3, pp. 269-289 (1974).
63. Harriott, P. and Hamilton, R. M., "Solid-Liquid Mass Transfer in Turbulent Pipe Flow." Chemical Engineering Science, Vol. 20, pp. 1073-1078 (1965).
64. Incropera, F. P. and DeWitt, D. P., Fundamentals of Heat Transfer, John Wiley & Sons, Inc., New York (1981).
65. Gambill, W. R., "Predict Liquid Diffusivities," Chemical Engineering, pp. 113-116 (June 30, 1958).
66. Deshpande, G. V., Serio, M. A., Solomon, P. R., and Malhotra, R., "Modeling of the Thermal Stability of Aviation Fuels," Presented at the 198th National ACS Meeting, Symposium on the Chemical Aspects of Hypersonic Propulsion, Miami Beach, FL (Sept. 10-15, 1989).
67. Parmelee, H. M., "Sealed-Tube Stability Tests on Refrigeration Materials." ASHRAE Transactions, Vol. 71, pp. 154-161 (1965).
68. Walker, W. O., Rosen, S., and Levy, S. L., "Stability of Mixtures of Refrigerants and Refrigerating Oils." ASHRAE Journal, pp. 59-72 (Aug. 1962).
69. Jensen, R. K., Korcek, S., Mahoney, L. R., and Zinbo, M., "Liquid-Phase Autoxidation of Organic Compounds at Elevated Temperatures. 1. The Stirred Flow Reactor Technique and Analysis of Primary Products from n-Hexadecane Autoxidation at 120-180°C." Journal of the American Chemical Society, Vol. 101, No. 25, pp. 7574-7584 (Dec. 5, 1979).
70. Naidu, S. K., Klaus, E. E., and Duda, J. L., "Evaluation of Liquid Phase Oxidation Products of Ester and Mineral Oil Lubricants." Industrial and Engineering Chemistry Product Research and Development, Vol. 23, No. 4, pp. 613-619 (1984).
71. Crittenden, B. D., Hout, S. A., and Alderman, N. J., "Model Experiments of Chemical Reaction Fouling." Chemical Engineering Research & Design, Vol. 65, pp. 165-170 (Mar. 1987).